Ph.D. Dissertation of Energy Systems Engineering

Lithium recovery by solvent extraction : strategies to improve recovery from produced/flowback water containing impurities

용매 추출을 이용한 리튬 회수 : 불순물을 함유한 생산수/환류수로부터의 리튬 회수율을 향상 시키는 전략 분석

2023 August

Graduate School of Energy Systems Engineering

Seoul National University

Junbeum Lee

Lithium recovery by solvent extraction : strategies to improve recovery from produced/flowback water containing impurities

Academic Advisor Eunhyea Chung

Submitting a Ph.D. Dissertation of Engineering

2023 August

Graduate School of Engineering

Seoul National University

Energy Systems Engineering Major

Junbeum Lee

Confirming the Ph.D. Dissertation written by
Junbeum Lee

2023 August

Chair _____(Seal)
Vice Chair _____(Seal)
Examiner _____(Seal)
Examiner _____(Seal)
Examiner _____(Seal)

Abstract

Shale gas produced water and geothermal flowback water contains high concentrations of total dissolved solids that originated from various geochemical reactions between the fluid in the reservoir and the minerals in the rock. Marcellus shale gas produced and Soultz-sous-Forêts geothermal flowback contains a relatively high concentration of lithium, one of the important metals in various industries; as a result, there have been several studies on recovering lithium from the solutions. However, the produced/flowback water also includes impurities like organic compounds or silicate ions that can show a probable inhibitory effect on the recovery of lithium. In this study solvent extraction was used to recover lithium selectively. The effect of the impurities for each produced/flowback water was observed during the solvent extraction. Two consecutive stages of solvent extraction were used to separate the lithium from the produced/flowback water that contains different alkane chain or concentrations of organic compounds or different silicate ions respectively. In addition, selective removal of organic compounds (98.0%) or silicate ions (98.0%) that can inhibit the selective recovery of lithium was implemented to increase the lithium extraction efficiency. Many extractants were used to extract lithium from the produced water including D2EHPA 1M, D2EHPA 1M + TBP (0.3M, 0.5M, and 1.0M) and an ionic liquid was designed by using Cyphos IL 101 and D2EHPA and this was used as an extractant to recover lithium. The highest lithium extraction efficiency from synthesized shale gas produced water was measured 85.9% from the dilution ratio of 25 times by using a

synthesized ionic extracting agent [Cyphos IL 101][D2EHPA] (1 M).

Keywords : Lithium, Produced water, Flowback water, Solvent extraction, Organic compounds, Silicate ions

Student Number : 2017-21273

Table of Contents

List of Figures

List of Tables

Chapter 1. Introduction

1.1 Study background

Produced water and flowback water are classified as a wastewater that are generated during the process of oil and gas production or geothermal system. Both of these types of wastewater can have significant impurities that can cause environmental impacts and should be treated properly. This study focuses shale gas produced water and geothermal flowback water that was produced from USA, Marcellus and France, Soultz-sous-Forêts respectively which contain a high lithium concentration due to geochemical reactions.

Shale is a prolific gas-bearing stratum that can be exploited by hydraulic stimulation and fracturing. When shale gas is developed, a certain amount of water is generally injected for fracking in the rock formation. As such, a large amount of produced water is released from the gas wells after hydraulic stimulation or fracturing, while concentrations of major inorganic compounds in the produced water are significantly high (Akob et al., 2015). Produced water, a mixture of injection and in-situ formation water, typically shows a high concentration of salt, including metal, and a high level of organics (Gregory et al., 2011; Haluszczak et al., 2012). It was reported that the total produced water volumes in the major unconventional basins in US ranged from 1.72 to 14.32 million liters per well, and the shale gas produced water in Marcellus region was 3.94 million liters per well in average (Kondash et al, 2017).

Enhanced geothermal systems (EGSs) is one option of aa geothermal systems, to effectively generate electricity for human consumption (Olasolo et al., 2016). Despite natural fractures in the reservoir for the fluid pathway, hydraulic

stimulation is applied to increase the permeability of a fluid for the sustainable use of a geothermal system (Hofmann et al., 2014). Once the fracture network is created, water is injected through an injection well in the deep reservoir where the thermal energy is stored and comes out through the nearby pumping well containing thermal energy (Caulk et al., 2016). During the hydraulic stimulation, the chemical composition of the production fluid changes abruptly compared to that of the injection fluid. The composition changes usually take place due to the mixing of an indigenous fluid and an injected fluid or geochemical reactions between an injected water and the bedrock (Owen et al., 2020; Lee & Chung, 2020a). Through the hydraulic stimulation, the total dissolved solids (TDS) of the production fluid increase due to geochemical reactions. According to Clark et al. (2013), the initial geothermal fluid volume was reported approximately 500,000 m^3 before a year of the circulation test in Soultz-sous-Forêts EGS (Genter et al., 2012). Lithium ions are used in various industries, such as the manufacturing of glass, ceramics, catalysts, pharmaceuticals, rubber, and batteries. (Swain, 2017; Sonoc & Jeswiet., 2014; Vikström et al., 2013; Lee & Chung, 2020b). The number of electric vehicles is expected to increase to 145 million by 2030 so the demand of lithium continues to increase with applications in the battery field (An et al., 2012; Swain, 2017; Li et al., 2023). According to a market research firm for 2022, the global lithium market is valued at USD 7.49 billion and this will be forecasted to grow 12% from 2022 to 2030 (Li et al., 2023). There are several sources of lithium in the natural environment like spodumene($LiAl(SiO_3)_2$), petalite($LiAlSi_4O_{10}$), lepidolite($K(Li,Al)_3(Al,Si,Rb)_4O_{10}(F,OH)_2$), brine lake deposits and seawater (Harvianto et al., 2016; Sanjuan et al., 2022). It requires various processes for extracting lithium from various sources however the cost for selective lithium

extraction from rock is estimated to be about twice compared to solutions like brines (Toba et al., 2021). The average concentration of lithium ions in seawater is known to be 0.17 mg/L (Li et al., 2018; Harvianto et al., 2016). Despite a relatively low concentration, many studies were conducted to recover lithium ions from seawater as a function of its massive volume (Nishihama et al., 2011). Compared to lithium concentration in seawater (0.17 mg/L), the produced water of Marcellus shale gas (95 mg/L) and flowback water of Soultz-sous-Forêts EGS (150 mg/L) has a relatively high lithium content (Haluszczak et al., 2012; Scheiber et al., 2012). Table 1.1.1 shows several cationic concentrations in promising lithium sources such as shale gas produced water, geothermal flowback water, Li battery recycling solution, and salt lake brine. The Li concentration is about 1,919 mg/L in battery recycling plant wastewater, however, the amount of wastewater might not be comparable to the shale gas produced water or geothermal flowback water. The lithium enrichment of the produced water and flowback water is known as many factors like the influence of temperature, fluid salinity and mineralogy of the reservoir rocks during the dissolution of constituents by the geochemical reactions due to water injection in the reservoir (Sanjuan et al., 2022; Haluszczak et al., 2013).

Due to Maguire-Boyle and Barron. (2014), shale gas is planned to be projected to increase from 23% of US natural gas production in 2009 to 47% by 2035 and cumulative net water used in all shale in USA plays during the next 50 years totals over 1trillion gallons. In Marcellus region, 3,000,000-5,000,000 gallons of water is required to fracture each well (He et al., 2014).

The geothermal water is usually used as a circulated system during the EGS so it is relatively used in a smaller amount than the shale gas produced water. For the

EGS sites reviewed by Clark et al. (2013), maximum water requirements is reported as 91,000 m^3 (24,000,000 gal) for a multizone well stimulation at Newberry Volcano. The site that is targeted in this research (Soultz-sous-Forêts EGS) is injected 500,000 m^3 volume of geothermal water to the reservoir for the circulation test in Soultz-sous-Forêts EGS (Genter et al., 2012).

The shale gas produced water and geothermal flowback water needs treatment to the massive amount of produced and flowback water due to the high amount of impurities or scale inducer after the reaction between rock-fluid interactions (Amakiri et al., 2022; Putera et al., 2018; Gallup, 2007). Since shale gas produced water and flowback water is classified as an byproduct, this yields a great deal of economic advantage in selectively recovering lithium ions from the Marcellus shale gas produced water and Soultz-sous-Forêts flowback water before treatment process.

Table 1.1.1 Concentration of cations in various promising lithium sources (mg/L) (Haluszczak et al., 2012; Scheiber et al., 2012., 1992; He et al, 2018; Kim et al., 2018).

	Li	Si	Na	Ca	K	Mg	Ni	Fe
Shale Gas Produced Water (U.S., Pennsylvania)	4–202	N/A	1,100-44,100	204-14,800	8-1,010	22–1,800	N/A	14-59
Geothermal fluid (France, Soultz-sous-Forêts)	150-152	189–226	21,340-26,677	6,850-7588	3,200-3,540	124-155	0.01 >	0.01 >
Waster water from battery recycling plant (Korea, Gunsan)	1,919	N/A	42,450	N/A	N/A	N/A	522.5	N/A
Salt lake brine (China, Yiliping)	97.5	N/A	100,400	N/A	3,500	13,100	N/A	N/A

1.2 Research objectives

In this dissertation, shale gas produced water and geothermal flowback water was selected as a promising source of lithium. The shale gas produced water and geothermal flowback water is introduced as a promising source of lithium however these types of water shows a high existence of impurities that can hinder the recovery of lithium ions. The average total organic carbon (TOC) concentration is analyzed at 2,348 mg/L in the produced water of Marcellus shale gas (Maguire-Boyle and Barron, 2014). The composition of organic compounds is usually due to fracturing fluid composition or environmental pollution caused by petrol compositions (Szabó and Varga., 2020). Geothermal water has a high TDS, including silicate ions, which usually is produced by geochemical reactions of silicate minerals (Lee & Chung, 2021). A high concentration of silicate ions (130 – 409 mg/L) was reported for the GPK-2 production well of the Soultz-sous-Forêts EGS on different sampling dates (Sanjuan et al., 2006).

During the lithium recovery process from the solution, the organic compounds or silicate ions may affect the recovery efficiency, so it is important to know the influence of organics or silicate ions during lithium recovery. From previous research, it was found that the chain length of alkanes influences the extraction efficiency in solvent extraction. For example, in the experiment using [4empy][Tf2N]+[emim][DCA] as an ionic liquid solvent to extract toluene from three different lengths of alkane (hexane, octane, and nonane), the toluene/n-alkane selectivity increases with increasing the alkane length (Larriba et al., 2014). In an experiment using Ionic liquid [C8mim][BF4] as a solvent, extracting thiophene from aliphatic hydrocarbon (heptane, dodecane, and hexadecane) was implemented

with increased selectivity from the length of the alkane (Alonso et al, 2008). It was found that organic compounds could affect the recovery efficiency during removal of metal ions in the aqueous solutions (Jang and Chung, 2019; Zheng et al., 2019; Zhang et al., 2019). Many studies observe the influence during the adsorption of metal (Zheng et al., 2019; Zhang et al., 2019); however, the relationship between different types or concentrations of alkanes and the metal extraction efficiency in liquid extraction has not been fully discovered.

High concentration of silicate ions dissolved in the fluid have also been reported to possibly inhibit the extraction efficiency of metal ions (Hano et al., 1992). Accordingly, several studies have reported methods to remove dissolved silicate from solutions (Spitzmüller et al., 2021; Putera et al., 2018), the relationship between the existence of silicate ions and the specific metal extraction efficiency during solvent extraction has not been researched fully. Therefore, in this study, different types and concentrations of organics were tested in shale gas produced water and different concentrations of silicate ions were tested in the geothermal water to investigate their interaction and influence during lithium recovery from solvent extraction.

In the previous study, 2 steps of solvent extraction were implemented in the solution with no impurities to remove the divalent ions that can suppress the Li recovery in the first step (Jang et al., 2017). This method shows a high loss of Li (25%) in the first step and the Li recovery only showed a 41.2 % of extraction efficiency in the second step hence the overall Li recovery was measured only 30.8 % (Jang et al., 2017). In this study a method was developed to propose a strategy to improve Li recovery from produced/flowback water containing impurities. Due to the inhibit effect of the impurities like organic compounds and

silicate ions, high recovery of lithium was aimed by removing the impurities and divalent ions in the previous stage to recovery lithium with a high selectivity. To decrease the lithium loss, and increase the removal of impurities and divalent ions from the water samples, adsorption and chemical precipitation was chosen for an effective method. In addition, different concentrations of extractants (D2EHPA + TBP) were used to compare the Li recovery efficiency and a new combination of ionic liquid [Cyphos IL 101][D2EHPA] was verified as an extractant to extract Li effectively from the produced water.

Chapter 2. Literature review

2.1 Solvent extraction

In the shale gas produced water or geothermal water, many inorganic ions including monovalent and multivalent cations coexist. Many methods can recover lithium in an aqueous solution, with one being liquid extraction using an organic solvent. Significant organic solvent is used in the solvent extraction process, which can cause serious environmental contamination; however, using this method is a simple process with a short operation time (Jang et al., 2017; Yang et al., 2003). In other cases, solvent extraction can be an effective method to remove organic contaminants in soil, sediment, sludge, or water. Ions can be removed through one or through several extraction steps (Nardella et al., 1999), as these ions are extracted by a cross current stage (Khodadoust et al., 1999). Many researchers have used various solvents like esters, crown ethers, or alcohol, such as D2EHPA[Di-(2-ethylhexyl)phosphoric acid], Cyanex 272[bis(2,4,4-trimethylpentyl)phosphinic acid)], and Cyanex 301[Bis(2,4,4-trimethylpentyl)dithiophosphinic

acid] to extract specific metal ions from aqueous solutions (Sadakane et al., 1975; Umetani et al., 1987; Hano et al., 1992; Jang et al., 2017; Jafari et al., 2018). In previous research, D2EHPA was used to recover manganese from a solution based on lithium-ion batteries (Vieceli et al., 2021), and strontium was extracted from the leach liquor of ore by using a crown ether (18-crown-6) (Alamdar Milani et al., 2021). Due to different functional groups or properties of solvents, solute-solvent interactions and the distribution ratio can be affected, resulting in a different cation affinity (Kislik et al., 2003; Kislik & Eyal. 2003). Among the extractants, D2EHPA has greater affinity for divalent cations, such as calcium or magnesium, than monovalent cations (Hano et al., 1992). Marcellus produced water contains inorganic cations of Ca^{2+}, Sr^{2+}, Ba^{2+}, Mg^{2+}, Li^{+}, Na^{+}, and D2EHPA, which has an affinity in the order of $Ca^{2+} > Sr^{2+} > Ba^{2+} > Mg^{2+} > Li^{+} > Na^{+}$ (Jang et al., 2017; Haluszczak et al., 2012). As such, D2EHPA was chosen in previous research as a metal extractant for many studies (Hano et al., 1992; Jang et al., 2017; Nadimi et al., 2014). In this dissertation, D2EHPA(Di-(2-ethylhexyl)phosphoric acid, $C_{16}H_{35}O_4P$) was chosen as an extractant to recover lithium from a shale gas produced water and geothermal flowback water.

An extractant D2EHPA is chemically stable and has a good loading and a stripping characteristics, and has a low solubility in the aqueous phase (Ekberg et al., 2015). Chemical formula ($C_{16}H_{35}O_4P$) of D2EHPA and the deprotonation form is shown in equation (2.1.1), (Jang et al., 2017).

$$(C_8H_{17}O)_2\overset{\overset{O}{\|}}{P}\text{-}OH \leftrightarrow (C_8H_{17}O)_2\overset{\overset{O}{\|}}{P}\text{-}O^{-} + H^{+} \qquad (2.1.1)$$

The deprotonated D2EHPA is hydrophobic and creates a chelate in the aqueous phase and the metal/extractant complex transport back to the organic phase (Lee et al., 2011; Jang et al., 2017). D2EHPA exists predominantly as a dimer in a nonpolar solvent and thus the reaction between D2EHPA(HR) and metal ions can be described as equation (2.1.2), (Hano et al., 1992).

$$M^{n+} + \frac{(n+x)}{2} (HR)_2 \leftrightarrow MRn(HR)_x + nH^+ \qquad (2.1.2)$$

where M is abbreviated as metal cation, x is the solvation number of complex, n is the valent number of metal ion. In addition, the extraction equilibrium constant is described as equation (2.1.3).

$$Ke = \frac{[MR_n(HR)_x][H^+]^n}{[M^{n+}][(HR)_2]^{\frac{(n+x)}{2}}} = \frac{Dm\ [H+]^n}{[(HR)_2]^{\frac{(n+x)}{2}}} \qquad (2.1.3)$$

After changing the order of the equation (2), the formula can be used as equation (2.1.4).

$$\log D_m = \frac{(n+x)}{2} \log [(HR)_2] + \log \frac{Ke}{[H+]^n} \qquad (2.1.4)$$

Equation (4) shows the logarithmic distribution ratio (D_m) of metal ions in different D2EHPA concentrations. The separation factor(S), a cation separated to each other from one cation to another cation is known through the distribution ratio (D_m) that can be described as equation (2.1.5), (Jang et al., 2017).

$$S_{M2}^{M1} = \frac{D_{M1}}{D_{M2}} =$$

$$\frac{Ratio\ of\ M_1\ ion\ in\ the\ ion\ in\ the\ organic\ phase\ /\ M_1\ ion\ in\ the\ ion\ in\ the\ aqueous\ phase}{Ratio\ of\ M_2\ ion\ in\ the\ ion\ in\ the\ organic\ phase\ /\ M_2\ ion\ in\ the\ ion\ in\ the\ aqueous\ phase} \qquad (2.1.5)$$

As shown in equation (2.1.4), the solvation number x can be calculated by knowing the slope $\frac{(n+x)}{2}$ and n for valent of ion. For Li^+, n is considered to be 1, as the slope is analyzed by $\frac{(n+x)}{2}$ for the Li ion in the D2EHPA- Li reaction (Hano et al, 1992). The extraction efficiency of metal ions is calculated by the equation below,

$$\text{Extraction efficiency}(\%) = \frac{[C]_{in,aq} - [C]_{fin,aq}}{[C]_{in,aq}} \times 100 \qquad (2.1.6)$$

where $[C]_{in,aq}$ is the initial concentration of the ion in the aqueous phase and $[C]_{fin,aq}$ is the final concentration of the ion in the aqueous phase. (Jafari et al., 2018).

In this dissertation, TBP (Tributyl phosphate, $C_{12}H_{27}O_4P$) is used together with D2EHPA which acts as a synergistic additive in the loading reaction (Jang et al., 2017). TBP improves the enhancement of the extraction efficiency when D2EHPA and TBP is combined in a proper amount (Amani et al., 2017). The synergistic reaction of TBP-D2EHPA-metal ions (Li^+) is described as equation (2.1.7), (Hano et al, 1992).

$$LiR_x(HR) + TBP \leftrightarrow LiR_{(x-1)}HR(TBP) + HR \qquad (2.1.7)$$

In equation (6), Li-D2EHPA complex reacts with TBP and replaces one molecule of D2EHPA. D2EHPA that comes out to the production is able to react with other metal ions to increase the extraction efficiency. As TBP is added to the reaction of metal ion-D2EHPA complex to increase the distribution ratio of lithium, a decrease of metal ion extraction can appear as equation (2.1.8) (Hano et al., 1992).

$$HR + TBP \leftrightarrow HR(TBP) \quad (2.1.8)$$

When TBP concentration is excessed, reaction between D2EHPA and TBP appears directly to suppress the extractant of metal ions (Jang et al., 2017). Thus an appropriate amount of TBP is needed to extract a massive amount of lithium ions. Ionic liquid(IL) is known for a new class of extractants composed with bulky organic cations and anions and known for the favorable properties such as negligible vapor pressure, low flammability, and high thermal stability to be useful for the design of relevant solvent extraction systems (Kumari et al., 2016; Zante et al., 2020; Shi et al., 2017). There are many ionic liquids like [Aliquat 336][Cyanex272], [Aliquat 336][PC88A], [Cyphos IL 101][Cyanex 272], and [Aliquat 336][D2EAPA] that are used to extract specific ions (Zante et al., 2020; Kumari et al., 2016; Tran and Lee, 2020) however ionic liquid that is designed by using Cyphos IL 101 and D2EHPA to extract Li was not researched yet.

2.2 Lithium recovery methods

Several studies of selective lithium recovery from various solutions including geothermal flowback water or shale gas produced water have been reported, including adsorption, ion exchange, electrochemical extraction, and solvent extraction (Battistel et al., 2020; Yen et al., 2016; Jang & Chung., 2019; Han et al., 2014; Warren, 2021).

Many researchers applied the adsorption and the ion exchange methods to recover lithium ions from various solutions, and many of them showed significantly selective lithium recovery results (Warren, 2021; Braun et al., 2002;

Kumar et al., 2017; Goc et al., 2021; Wang et al., 2017; Jang & Chung., 2018). However, since the use of the oxidant or acid is essential for a desorption process, it might not be economical to recover lithium using adsorption in a large scale (He et al., 2018; Xu et al., 2020). Also, for the ion exchange method, fouling such as calcium sulfate can occur during a regeneration process due to the significant amount of calcium ions in the geothermal fluid (Patel. 2016; Scheiber et al., 2012).

The electrochemical method uses lithium-selective electrodes like λ-MnO_2 or $HFePO_4$ to capture the lithium ions from solutions (Kim et al., 2021; Wang et al., 2021). The electrochemical method showing the high lithium selectivity does not require the chemicals such as organic solvent or acid. However, high energy consumption is expected due to the application of high voltage during the operation (Kanoh et al., 1993; Battistel et al., 2020; Joo et al., 2020; Kim et al., 2021).

The solvent extraction method uses the transfer of a compound from one liquid phase to another based on the different solubility or distribution coefficients of the compound (Chen & Wang., 2016). This method requires a usage of a massive amount of organic solvent that can cause environmental pollution when is not controlled properly however in this dissertation, the solvent extraction method was tested due to the simplicity of the process and the relatively short operation time (Jang et al., 2017; Yang et al., 2003; Masmoudi et al., 2021). In many studies, it was shown that the contact time of less than an hour (few minutes at least) was enough for the process (Yang et al., 2003; Jin et al., 2014; Silva et al., 2005). Also, the recyclability of the solvent makes this method beneficial. For the usage of industrial application, a massive amount of organic solvent is needed and the extraction process can be formed as a continuous or countercurrent process (Zhang et al., 2018; Geow et al., 2021). The continuous process is operated in a continuous

mode of a single, batch equilibrium contact and allows a continuous flow of feed material and solvent throughout the extraction process and the countercurrent operation is operated by a repeating single-stage contacts, with the aqueous and organic streams moving in opposite directions (Bernardini, 1976; Kassing et al.,2010). Based on the advantages described above, the solvent extraction method is used extensively in industrial applications to recover valuable metal ions from solutions (Yen et al., 2016).

Chapter 3. Selective lithium recovery from geothermal water

3.1 Introduction

Geothermal water has a high TDS, including silicate ions, which usually is produced by geochemical reactions of silicate minerals (Lee & Chung, 2021). A high concentration of silicate ions (130 – 409 mg/L) was reported for the GPK-2 production well of the Soultz-sous-Forêts EGS on different sampling dates (Sanjuan et al., 2006). The existence of silicate ions existence can possibly inhibit the extraction efficiency of metal ions and furthermore can occur the precipitation of silicate minerals in the pipe or reservoir during the circulation of the fluid, so fracture closure can decrease the permeability of the EGS (Putera et al., 2018; Sanjuan et al., 2010; Lee & Chung, 2020a). The silicate ions show a great impact during the circulation of EGS or the relationship between the silicate ions and the specific metal extraction efficiency during solvent extraction. To observe the effect of silicate ions during solvent extraction, different concentrations of dissolved SiO_2 were added to the synthesizing geothermal water to observe the lithium extraction efficiency changes. In a study by Jang et el. (2017), two-step liquid extraction was used to selectively extract lithium ions from shale gas produced water. The first step was proposed to remove most of the divalent ions with a low lithium concentration extraction, while the second step was used to extract lithium ions selectively (Lee & Chung, 2020b). The experimental process in this study followed the two-step solvent extraction method, as in the study (Jang et al., 2017) by injecting organic compounds in the synthesized produced water to observe the effect of organic compounds. Due to a similar chemical composition especially for the cation concentration in geothermal water, the two-step solvent extraction

process was used to the synthesized geothermal water that includes silicate ions to recover lithium selectively.

During the hydraulic stimulation in the geothermal site, the chemical composition of the production fluid changes abruptly compared to that of the injection fluid. The composition changes usually take place due to the mixing of an indigenous fluid and an injected fluid or geochemical reactions between an injected water and the bedrock (Owen et al., 2020; Lee & Chung, 2020a). Through the hydraulic stimulation, the total dissolved solids (TDS) of the production fluid increase due to geochemical reactions, and lithium ions especially increase in water of the EGS sites (e.g., Soultz-sous-Forêts EGS).

According to the previous research Jang et al. (2017), the divalent ions from the shale gas produced water have been removed during the previous stage to recover lithium during the second stage. Most of the divalent ions were removed (>94.4%), but there was also lithium loss (25.1%) during the removal stage. For an effective method to decrease the lithium loss, a chemical precipitation method is applied. Chemical precipitation is usually used to treat heavy metal wastewater by increasing the pH, and thus soluble metal ions convert to insoluble hydroxide, carbonate, or sulfide forms (Zhang & Duan., 2020). This process is simple and inexpensive, and during the precipitation process, large amounts of solids are formed in the solution (Pohl, 2020; Zhang & Duan., 2020). According to the results of previous research, various types of metal ions can be precipitated using chemical precipitation from wastewater. For example, $Ca(OH)_2$ is used to remove most of the Cr ions from wastewater by chemical precipitation and remove other ions such as Ni, Zn, and Fe ions with an acceptable efficiency (Reyes-Serrano et al., 2020). In an experiment using Na_2CO_3 as a precipitation agent, Cu(II) and Ni(II) was

targeted to be removed from a solution, and the percentage of Cu(II) removal was higher at lower pH values compared to Ni(II) removal (Junuzović et al., 2019). It is known that $Ca(OH)_2$ and Na_2CO_3 are used to precipitate various metal ions from a solution. Thus, these two precipitation agents were used to remove metal ions, excluding lithium ions from the geothermal fluid in this research.

In this dissertation, a combined method of precipitation and solvent extraction was applied to extract lithium ions effectively from the geothermal fluid. The first part of the process is to remove most of the divalent cations and silicate ions from the geothermal fluid. The second part of the process is to extract lithium ions selectively by solvent extraction.

3.2 Materials and Methods

The Soultz-sous-Forêts geothermal water was synthesized to obtain a similar chemical composition as that reported in the literature (Scheiber et al., 2012). Table 3.2.1 shows the various chemical compounds that were added to the synthesized water based on the chemical composition of the geothermal water and major ions were usually targeted (> 100 ppm) compared with the real geothermal water. It is believed that the experimental results can show a difference due to the small amount of ions however this experiment focused on the major concentration that has a high amount inside the geothermal water.

Even in the same Soultz-sous-Forêts EGS, the geothermal water properties were different due to sampling time and borehole type. Due to Pauwels et al. (1992), a short duration injection test was applied in Soultz-sous-Forêts EGS and the concentration of lithium ions from the production fluid increased from 0 to 63

mg/L lithium ions after 42 h of backflow. In a long-term circulation from the GPK-2 production well in the Soultz-sous-Forêts EGS this showed a relatively high lithium content (approximately 150 mg/L) (Scheiber et al., 2012). The concentration of lithium ions due to the long-term circulation from the GPK-2 in the Soultz-sous-Forêts EGS is higher than the worldwide concentrations (i.e., 1–100 mg/L) reported by Flexer et al. (2018), so this data was selected in this research to recover Li from geothermal water.

Synthetic geothermal water was used as the solution for lithium extraction in this research (Table 3.2.2). The content of Si ions is measured and converted into SiO_2 content that can be converted to a soluble form of silica in the geothermal water. In this study, 0, 150, and 350 mg/L of dissolved SiO_2 solutions were put to the geothermal water, and they were classified as samples A, B, and C in this study. The experiment that is introduced in Jang et al. (2017) shows a high TDS concentration of a shale gas produced water that might inhibit the efficient lithium recovery during solvent extraction process. The concentrations of other cations can suppress lithium recovery thus various shale gas produced water dilution ratio was implemented to find the appropriate dilution ratio (Jang et al., 2017). The solvent extraction was applied in a 50 times diluted shale gas produced water of which the TDS concentration was up to 157,000 mg/L (Jang et al., 2017). The dilution was held by using deionized water. Soultz-sous-Forêts geothermal water has a high TDS value, i.e., approximately 100,000 mg/L (Scheiber et al., 2012), therefore, due to the similar TDS level of two waters, 50 times diluted synthesized geothermal water was chosen to be tested for the lithium recovery from geothermal water.

In all stages of the solvent extraction, D2EHPA (97 %, Sigma Aldrich, St.

Louis, MO, USA) was used as an extractant, and kerosene (Sigma-Aldrich, St. Louis, MO, USA) was used as a diluent to control the molarity of the organic phases. The produced water was used 200 mL in the initial stage of extraction and throughout the experiments, the organic phase and aqueous phase solutions were mixed with the same volumetric ratio (1:1) in an Erlenmeyer flask and stirred in a shaking incubator (SH-BSI16R, Samheung Instrument, Seoul, S. Korea) at 150 rpm and 25℃ for 30 minutes. After mixing, the solution settled in a separating funnel to reach equilibrium, with the aqueous phase withdrawn for ICP and IC analysis.

The aqueous solution was reused for multistage solvent extractions up to four times to improve the efficiency of the removal of the divalent cations and fresh organic solvents (1.0 M D2EHPA) were applied in every multistage solvent extraction. The process of the second stage was similar to the previous one but TBP was used for lithium recovery in the mixture of D2EHPA and kerosene as an additive. Fresh organic solvent (1.5 M D2EHPA + 0.3 M TBP) was used in every repetition and the aqueous solution was reused for multistage solvent extractions. The schematic of solvent extraction experiment was shown in Fig. 3.2.1.

The permeate was analyzed cations by inductively coupled plasma optical emission spectrometry (ICP-OES, Optima 8300, Perkin Elmer, USA) and the organic solution was analyzed by Fourier transform infrared spectroscopy (FT-IR spectra, Nicolet 6700, Thermo Fisher Scientific, Waltham, MA, USA) to analyze the changes in the absorbances of the major functional groups.

Table 3.2.1 Purity and suppliers of the reagents used to synthesize geothermal water

Product	Purity	Supplier
LiBr	54 wt% in H_2O	Sigma Aldrich
LiCl	95-100 %	Merck
$CaCl_2 \cdot 2H_2O$	99 %	Sigma Aldrich
$MgCl_2$	99 %	Yakuri Pure Chemicals
KCl	99.5 %	Waku Pure Chemicals
NaCl	99 %	Daejung
$NaHCO_3$	99.5 %	Sigma Aldrich
$FeCl_2 \cdot 4H_2O$	≥99.0 %	Kanto chemical
$BaCl_2 \cdot 2H_2O$	99 %	Kanto chemical
$SrCl_2 \cdot 6H_2O$	98 %	Duksan Pure Chemicals
HCl	37 %	Merck
H_2SO_4	60 %	Daejung
$Na_2O(SiO_2)x \cdot xH_2O$ (Sodium silicate solution)	Na_2O 10.6 % SiO_2 26.5 %	Sigma Aldrich

Table 3.2.2 The composition of real & synthetic geothermal water (mg/L)

	Geothermal Water	Synthesized Geothermal Fluid
pH	5.2-5.5	5.0-5.3
Ca	6850-7588	6344.9-7140.8
Li	150-152	155.9-183.1
Na	21340-26677	19341.7-23048.2
Sr	397-479	357.0-394.7
Mg	124-155	115.1-135.7
Ba	9.6-19.4	18.1-20.6
SiO_2	189-226	0, 150, and 350 mg/L
Fe	28.5-68.9	
B	34.5-37.6	
Mn	14.8-15.8	
As	8.1-8.7	
Rb	23.4-26.4	
Cs	14.6-14.8	

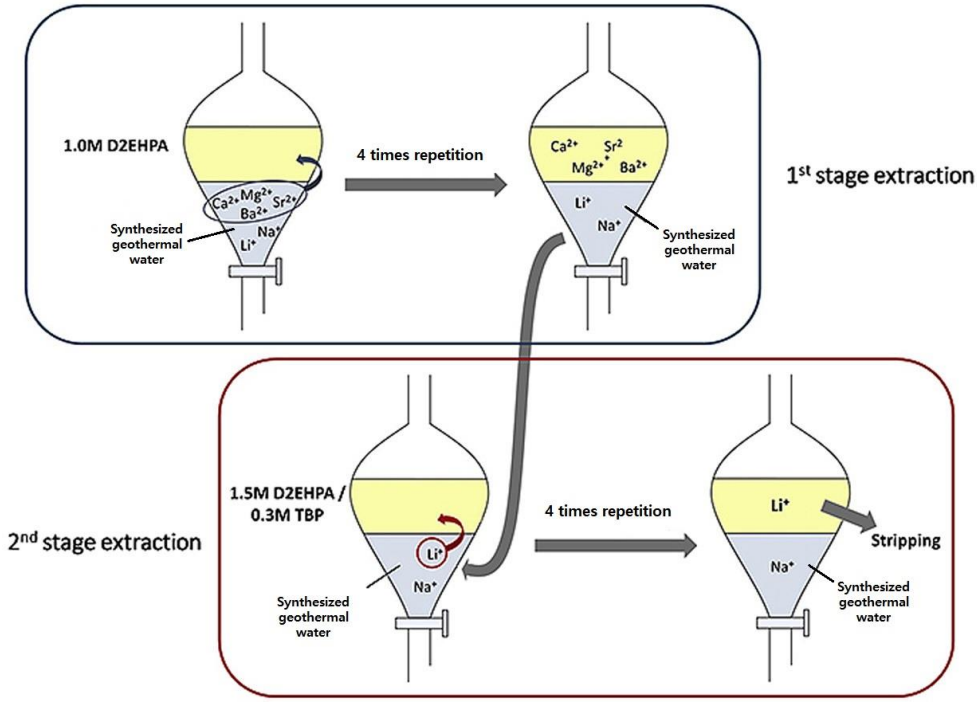

Fig. 3.2.1. Schematic of solvent extraction experiment.

After implementing the experiment to observe the Li extraction efficiency from geothermal water containing different SiO_2 concentrations, the next experimental procedure in this study followed a combined procedure of chemical precipitation and solvent extraction to selectively extract lithium ions. Selective precipitation of divalent ions was applied using $Ca(OH)_2$ and Na_2CO_3 for the minimum influence of lithium ions in the geothermal fluid. $Ca(OH)_2$ is used to precipitate Mg^{2+} and silicate ions from the solution (Karidakis et al., 2005; Castaño et al., 2021; Putera et al., 2018), and Na_2CO_3 targets Ca^{2+}, Sr^{2+}, and Ba^{2+} ions to precipitate from the solution (Jang & Chung., 2018). $Mg(OH)_2$ has a lower solubility product (Ksp) compared to $Ca(OH)_2$ which is less soluble in water however the other ions like Sr^{2+}, Ba^{2+}, Li^{+}, and K^{+} is generally much higher than that of $Mg(OH)_2$ (Shen et al., 2009; Ehsani et al., 2022). As a result, magnesium ions have a higher tendency to react and form the insoluble precipitate of $Mg(OH)_2$. Also by using Na_2CO_3, divalent ions show a low solubility of their carbonate compounds compared to monovalent ions (Battaglia et al., 2022).

$Ca(OH)_2$ was used for the first step, considering the exchange Ca^{2+} concentration in solution to remove in the second step. The required amount of $Ca(OH)_2$ was calculated based on the sum of the moles of the Mg^{2+} and silicate ions, and that of Na_2CO_3 was calculated based on the sum of the divalent ions (Ca^{2+}, Sr^{2+}, Ba^{2+}) in the synthesized geothermal fluid. The different molar ratio of the ion sum was compared by observing the removal rate of metal ions. The precipitation and fluid reaction time was 1 h, and the magnetic stirrer was set at 300 rpm for mixing. After the chemical reaction, the precipitate was separated using a centrifuge (LaboGene 1248, Gyrozen Inc., Daejeon, Korea) at approximately 5000 rpm for 10 min. The amount of $Ca(OH)_2$ (molar ratio of 1:1) was calculated based

on the sum of the moles of the Mg^{2+} and SiO_2, (sum 0.43 mmol). After applying $Ca(OH)_2$ to the synthesized geothermal fluid, Na_2CO_3 was applied to remove divalent metal ions (Ca^{2+}, $Sr^{2+}$and Ba^{2+}). In work by Jang and Chung (2018), Na_2CO_3 was calculated in various molar ratios considering Ca^{2+}, Sr^{2+}, Ba^{2+}, and Mg^{2+} and a molar ratio of 1.2:1 Na_2CO_3 was applied to the experiment due to a high removal rate (>99%). Due to applying $Ca(OH)_2$ to remove Mg^{2+} and SiO_2 in the previous stage, Ca ions increased in the synthesized geothermal fluid. The Ca ion concentration was newly analyzed to consider the sum of the molar ratio. For removing Ca^{2+}, Sr^{2+}, and Ba^{2+} (sum 7.34 mmol), the different molar ratios of the ion summary were considered (i.e., 1:1, 1.1:1, 1.2:1). The elemental composition of the precipitation was analyzed using the Scanning Electron Microscopy with Energy Dispersive X-ray analysis (SEM-EDX) (EM- 30AX, Coxem, Daejeon, Korea) and X-ray diffractometer (XRD) (SmartLab, Rigaku, Tokyo, Japan).

After the precipitation stage for divalent ions, 1.5 M D2EHPA and 0.3 M TBP was used in the research as an organic phase. As an aqueous phase, 100mL of the synthesized geothermal fluid is mixed with the organic phase in the same volumetric ratio (1:1) in a flask and stirred in a shaking incubator (SH–BSI16R, Samheung Instrument, Seoul, Korea). The mixing conditions are applied at 150 rpm, 25℃, and 30 min. After mixing the aqueous and organic phase, the solution is settled in a separating funnel to reach equilibrium, and the aqueous phases are sampled. Four repeated solvent extractions were performed at each stage, and the pH was measured by a multimeter (Orion Star A329, Thermo Fisher Scientific, Waltham, MA, USA). The collected aqueous phase samples were analyzed for inorganic cations after filtering using a 0.45-μm filter by inductively coupled plasma optical emission spectrometry (ICP-OES, Optima 8300, PerkinElmer,

USA). The scheme of the experiment method (previous and improved) for the overall chapter is shown in Fig 3.2.2.

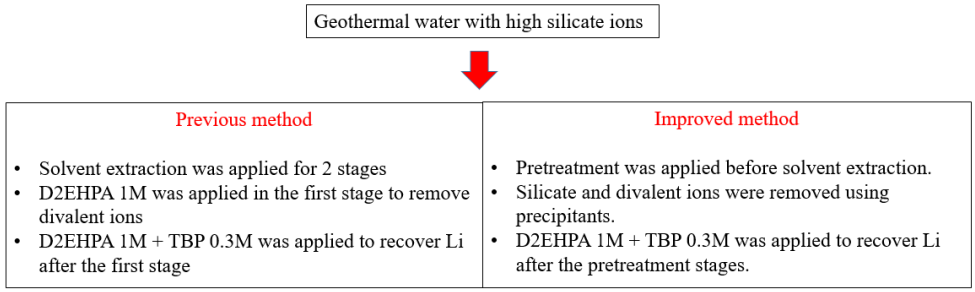

Fig. 3.2.2. The scheme of the experiment method

3.3 Effect of different concentrations of silicate ions during lithium recovery using solvent extraction

The influence of different dissolved SiO_2 concentrations (0, 150, 350 mg/L) in geothermal water was observed during the solvent extraction process of metal ions (Lee & Chung., 2022b). Fig. 3.3.1 shows the extraction efficiency of cations (Ca^{2+}, Sr^{2+}, Mg^{2+}, Li^{+}, Na^{+}) in geothermal water, with different dissolved SiO_2 concentrations for four extraction processes. Ba^{2+} was not drawn in the figure due to its lower concentration (< 0.4 mg/L) in the initial fluid after 50 times dilution. The dilution was held by using deionized water. The pH of the aqueous solution was measured after every repetition extraction process, and the range of the pH values was 1.8 - 2.1 due to the production of hydrogen ions, as described in equation (2.1.2). In other researches, the solution pH should be controlled after every stage in order to have acceptable extraction yields (Lupi and Pilone, 2020). The pH of the extraction system plays a crucial role in the distribution of metals and in Keller et al. (2022), saponification is recommended due to the strong influence on the equilibrium pH value and lowers the effective H^{+} emission of the extraction process (Equation 2.1.2). It is believed that the pH change can be fixed due to the saponification and the extraction efficiency can also be changed.

The removal efficiencies of Ca^{2+}, Mg^{2+}, and Sr^{2+} were greater than 90 % after four repetitions in all three samples. The removal rates of SiO_2 were also calculated after each step and the values were significantly low. For sample A and C, the removal rates of silicate ions from the aqueous side were 0 % and, for sample B, the removal rate was measured as about 7 % after 4 repetitions. D2EHPA affinity for cation extraction has been reported to be in the order of $Ca^{2+} > Sr^{2+} > Mg^{2+} >$

$Li^+ > Na^+$ (Hano et al., 1992; Jang et al., 2017), and all the cations tendency satisfied in three samples. For example, as D2EHPA shows the highest affinity for Ca^{2+} compared to other divalent ions (Hano et al., 1992; Jang et al., 2017), the removal efficiency showed the highest values in all conditions as shown in Fig. 3.3.1.

The removal efficiency of cations including lithium increased as the SiO_2 concentration increased. Especially, the lithium removal efficiency in solution A at the first extraction was 55.5 %, and the efficiency increased to 66.8 % and 77.9 % in solutions B and C, respectively. To observe the effect of dissolved SiO_2 in the solution, distribution ratio of the cations were calculated for the first (1-1) extraction (Table 3.3.1). The D_{Na} values in all samples indicate that the extraction of Na^+ was not significant during the first solvent extraction. The distribution ratio of Ca^{2+} showed a decrease while the SiO_2 concentration increases but the other divalent ions (Sr^{2+} and Mg^{2+}) and Li^+ showed higher distribution ratio in higher SiO_2 concentration solution.

After four stages of extraction, more cations were extracted from the aqueous phase and the distribution ratio of cations increased. The separation factors of three divalent ions over lithium after four stages were calculated as shown in Table 3.3.2. Ca^{2+} had the highest selectivity factors in the geothermal water without SiO_2, and the selectivity increased when the SiO_2 concentrations increased in the solution. However, Sr^{2+} and Mg^{2+} showed slight decreased separation factors with the increase of SiO_2 concentrations.

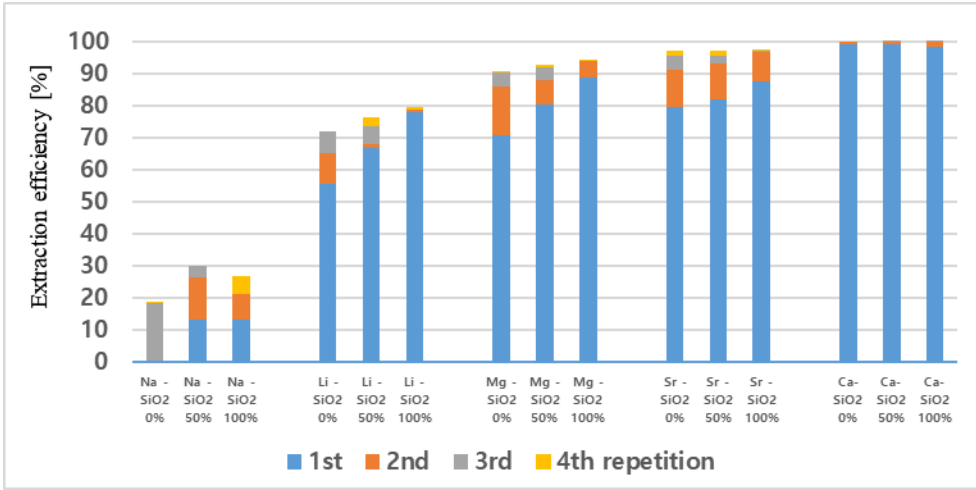

Fig. 3.3.1. 1st step removal efficiency of cations in different SiO_2 concentrations of geothermal water

(Sample A-SiO_2 0 mg/L; Sample B-SiO_2 150 mg/L; Sample C-SiO_2 350 mg/L)

Table 3.3.1 Distribution ratio of cations ions in the first extraction stage (1-1)

	D_{Ca}	D_{Sr}	D_{Mg}	D_{Li}	D_{Na}
Sample A	137.1	3.9	2.4	1.2	-
Sample B	99.7	4.5	4.1	2.0	0.2
Sample C	64.3	7.0	7.9	3.5	0.2

Table 3.3.2 Separation factor of divalent ions over lithium after the first extraction step

	$S\ \frac{Ca}{Li}$	$S\ \frac{Sr}{Li}$	$S\ \frac{Mg}{Li}$
Sample A	238.5	12.4	3.9
Sample B	268.0	9.9	4.0
Sample C	411.6	9.2	3.9

The absorbance of the metal-D2EHPA complex in the organic phase was analyzed using FT-IR to observe the change in the functional group during solvent extraction (Fig. 3.3.2). The result for D2EHPA before the extraction is shown in red line, and the sample A, B, and C results are shown in Fig. 3.3.2 (a), (b), and (c), respectively. Due to the formation of a metal-D2EHPA complex during the extraction with no SiO_2 ions (sample A), the absorbance of the P=O bond (1034 cm^{-1}) and the P-O-H bond (1230 cm^{-1}) decreased after extraction (Fig. 3.3.2 (a)). It seems that the metal ion and an electronegative P=O bond from D2EHPA form a bond, and a hydrogen from the P–O–H bond is replaced with a metal ion. Fig. 3.3.2 shows that the wavenumbers for the absorbance peaks increase as the SiO_2 concentrations increased, which indicates that the existence of the SiO_2 ions interferes with the loading of the metal ion during the solvent extraction.

Although the formation of metal-D2EHPA complex was slightly inhibited by the SiO_2 ions in the aqueous fluid (Fig. 3.3.2), more metal ions were extracted from the aqueous solution in the existence of the SiO_2. One of the explanation for that could be the silica polymerization. The silanol group (Si-O-H) originated from dissolved SiO_2 in geothermal water can form polymeric, colloidal, and particulate silica due to various conditions, such as pH or the presence of other ions (Park et al., 2020). The polymerization of silicic acid occurs rapidly in neutral or slightly alkaline pH values and is formed slowly below pH 6.5 (Putera et al., 2018; Park et al., 2020). Due to a low pH solution (1.8 - 2.1) after every repetition extraction process, the polymerization of silicic acid actually occurs probably at a slow rate. With other divalent cations, silica polymerization can be formed because silicic acid is classified as a weak acid in geothermal water (Park et al., 2020; Brown, 2013).

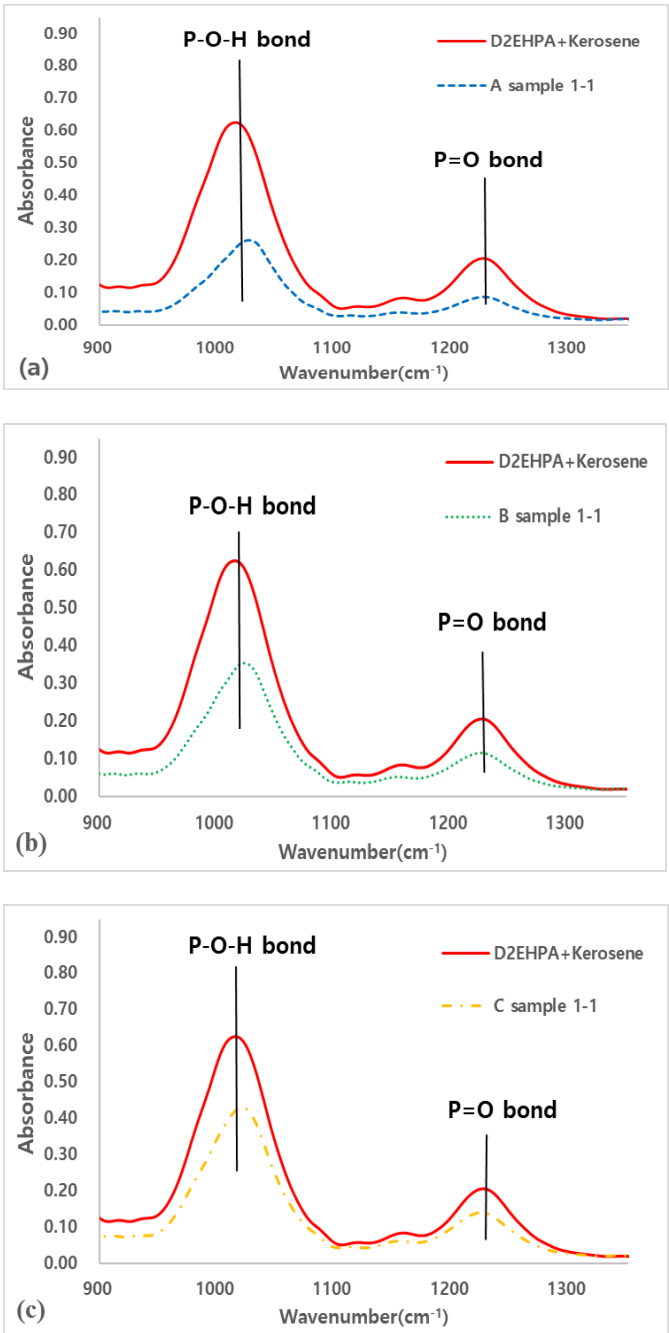

Fig. 3.3.2. FT-IR spectra of samples (a) D2EHPA + Kerosene & D2EHPA + Kerosene after the 1st stage solvent extraction of the geothermal water without SiO_2; (b) D2EHPA + Kerosene & D2EHPA + Kerosene after the 1st stage of solvent extraction of the geothermal water that contained 150 ppm of SiO_2; (c) D2EHPA + Kerosene & D2EHPA + Kerosene after the 1st stage of solvent extraction of the geothermal water that contained 350 ppm of SiO_2

Due to Krasucka et al. (2016), polymer-SiO2 composite from highly porous silica adsorbents were characterized by using scanning and transmission electron microscopy (SEM and TEM and X-ray diffraction (XRD). In this dissertation, the synthesized geothermal water before experiment contains a suspended solid. The suspended solid was separated with the solution using a centrifuge at approximately 5000 rpm for 10 min and dried at an oven for 24 hours. The suspended solid was analyzed using Scanning Electron Microscopy with Energy Dispersive X-ray analysis (SEM-EDX) (EM- 30AX, Coxem, Daejeon, Korea) and X-ray diffractometer (XRD) (SmartLab, Rigaku, Tokyo, Japan) (Fig. 3.3.3 & 3.3.4). The suspended solid is composed with Si (16.8 %), O (43.4 %), Ca (6.7 %), Na (6.3 %), K (3.1 %) and Cl (24.8 %) as elemental components. Due to the SEM-EDS results, the Si contains the highest composition compared to the other cations in the dried suspended solid.

The XRD diffractogram of the dried suspended solid are shown in Fig. 3.3.4. The dried suspended solid is composed with silicon chloride minerals [(200), (202), (220), (301), (400), (205), (420), and (116)], halite (NaCl) [(111), (200), (220), (311), (222), (420), and (422)] and Ca minerals [(110), (200), (211), (220), (310), and (222)]. Due to other researches, the amorphous silica is usually formed as a diffuse wide peak around 20° through XRD data and the crystalline silica observes distinct several peaks (Biswas et al., 2018; Rana et al., 2021). The SEM-EDS and XRD results shows the dried suspended solid is formed with crystalline silica structure that can influence the polymerization of silicic acid.

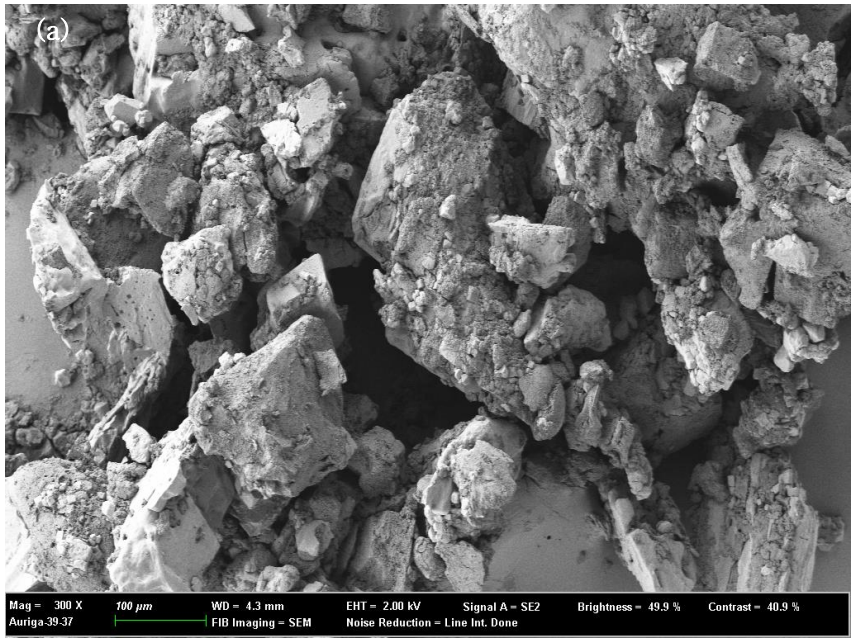

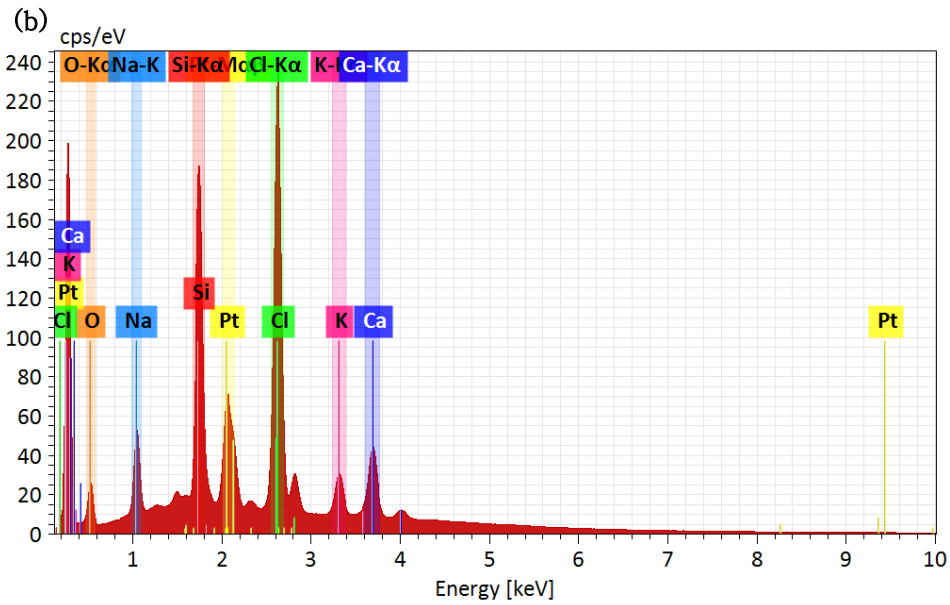

Fig. 3.3.3. SEM-EDX micrographs of suspended solid (a) Image of the sample (× 300), (b) EDX peak of suspended solid.

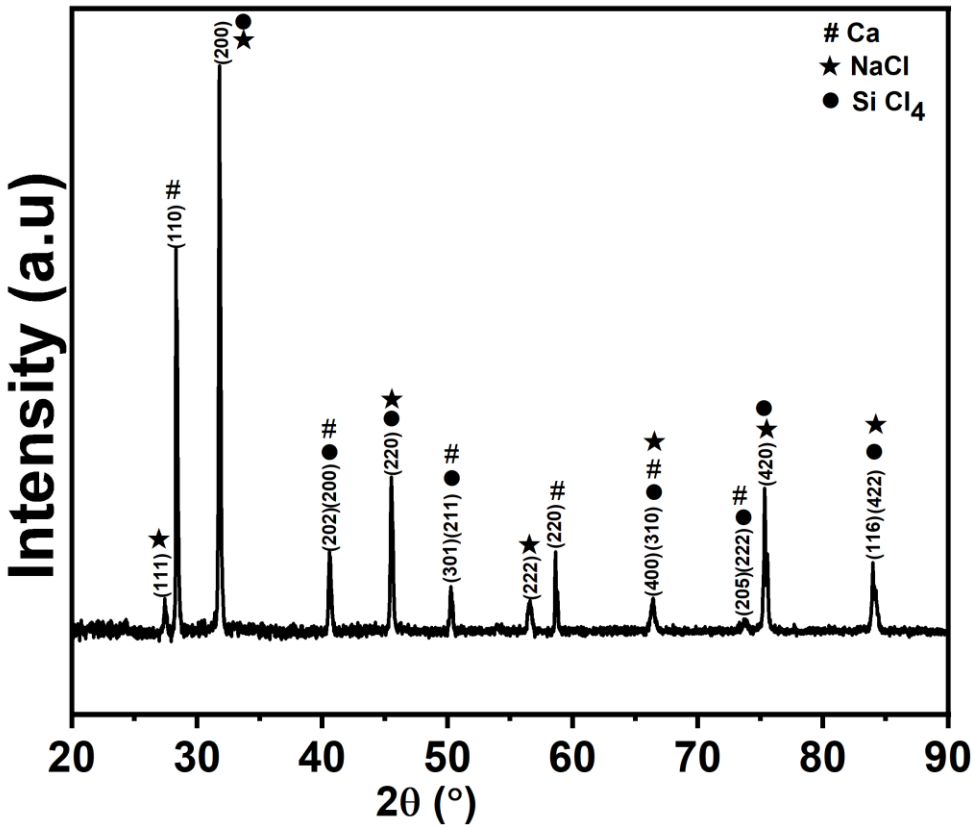

Fig 3.3.4. Diffractogram of the dried suspended solid.

After removing the divalent cations from the geothermal water in the first extraction step, lithium was extracted during four repetitive cycles in the second step (Fig. 3.3.5). The $[C]_{in,aq}$ value in equation (3) for all data points (2-1, 2-2, 2-3 and 2-4) is the concentration value measured after the stage 1-4 is completed, and the $[C]_{fin,aq}$ value implies the concentration measured after each stage. Li^+ had a higher extraction efficiency than the other monovalent cation, Na^+, for all three samples and the Li^+ extraction efficiency ranged from 21.9 to 24.8 %.

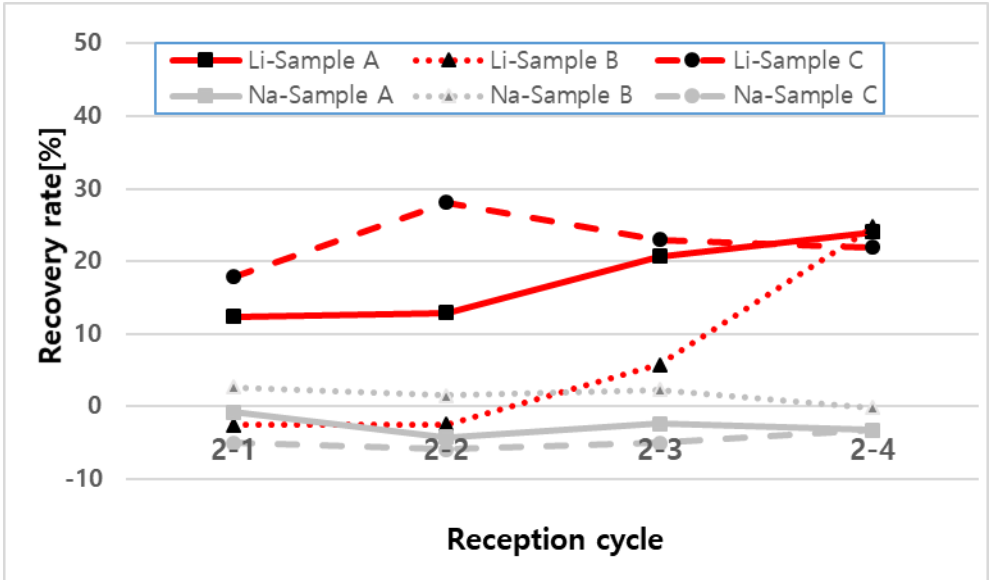

Fig. 3.3.5. 2nd step removal efficiency of Li and Na in different SiO_2 concentrations of geothermal water.

After removing most of the divalent ions in the first step, the overall extraction efficiency of Li was calculated as shown in Fig. 3.3.6. In the first stage extraction, 71.9-79.50 % of the original lithium was lost and 21.9-24.8 % of the remaining lithium was recovered during the second stage extraction. Therefore, the overall lithium recovery rate was calculated as 4.5-6.8 %. The overall recovery of Li^+ decreased from 6.8 % to 4.5 % as the SiO_2 concentration increased. The overall recovery didn't show a big difference however the difference between the Li^+ recovery rates depends mainly on the loss of Li^+ in the first step of the extraction process compared to the second step.

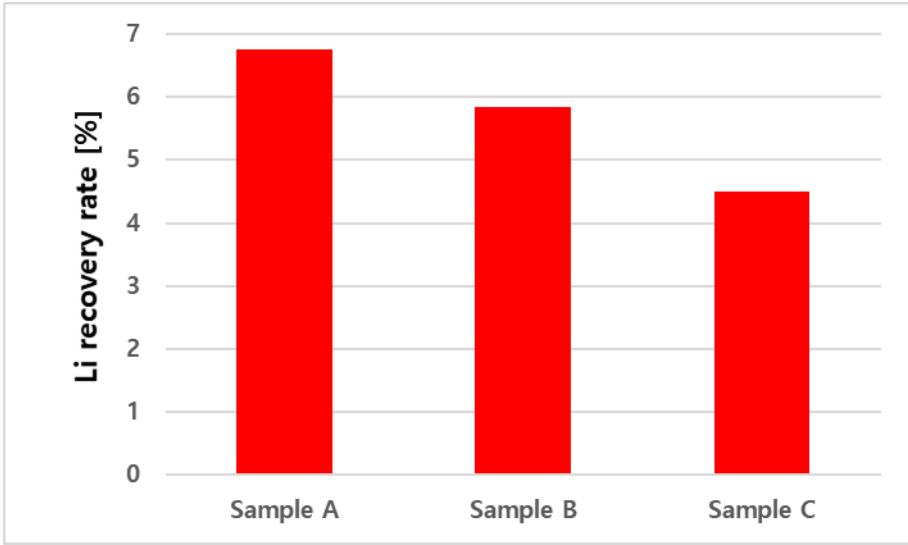

Fig. 3.3.6. Overall Li recovery efficiency in different SiO_2 concentrations of geothermal water.

3.4 Improvement of lithium recovery (pretreatment)

The amount of $Ca(OH)_2$ (molar ratio of 1:1) was calculated based on the sum of the moles of the Mg^{2+} and SiO_2, (sum 0.43 mmol) and approximately 0.62 g of $Ca(OH)_2$ were used to remove the Mg^{2+} and silicate ions from 1 L geothermal water. The ion composition before and after applying precipitant $Ca(OH)_2$ was shown in Table 3.4.1 and the removal ratio is shown in Figure 3.4.1.

The TDS can be measured using the conductivity and the ratio of TDS/EC (k) of brine water that has the TDS value more than 100,000 mg/L can be defined as 0.75 (Rusydi, 2018). The TDS of the solution before and after the application of precipitant was measured by using the conductivity value. The average TDS value of the geothermal water was measured 111,675 mg/L and decreased to 104,850 mg/L after applying $Ca(OH)_2$.

The removal of lithium ions was insignificant, and 98% and 97% of Mg^{2+} and SiO_2 were removed, respectively. Ba^{2+} ions also showed a removal rate of 74% during the chemical precipitation. Mg^{2+} ion reacts with the precipitant $Ca(OH)_2$ and forms a magnesium hydroxide as a solid form, and Equation (3.4.1) shows the chemical reaction (Bologo et al., 2009). SiO_2 is also removed by the precipitant $Ca(OH)_2$ and forms a calcium silicate (Putera et al., 2018). According to Johnston et al. (2008), H_3SiO4^-, which is produced by dissolved silica such as geothermal water, can react with $Ca(OH)_2$ and form a nanostructured calcium silicate precipitate shown in Equation (3.4.2) (Johnston et al., 2008). This chemical reaction takes place over a short time at a low temperature which didn't exceed 10 min and 70 ℃ respectively (Putera et al., 2018), so 60 min of chemical reaction was sufficient to remove the SiO_2. In Equation (5.2.2), a and b is approximately 2:

$$Mg^{2+} + Ca(OH)_2 \rightarrow Mg(OH)_2 + Ca^{2+} \quad (3.4.1)$$

$$Ca^{2+} + H_3SiO_4^- + OH^- \rightarrow CaSiO_a(OH)_b + H_2O \quad (3.4.2)$$

Table 3.4.1 The composition of before and after applying precipitant $Ca(OH)_2$ (mg/L)

Synthesized Geothermal Fluid	Before applying precipitant	After applying precipitant
pH	5.1-5.6	10.8-11.0
Conductivity (mS/cm)	148.1-149.7	139.5-140.1
Ca	6108.1-7517.0	1.6-1.9
Li	157.1-181.5	173.4-175.6
Na	24325.4-26853.4	24678.3-26362.1
Sr	397.5-424.4	3.1-5.2
Mg	103.6-131.1	0.9-1.0
Ba	2.3-17.2	2.6-4.4
SiO_2	200.3-244.5	0.7-4.7

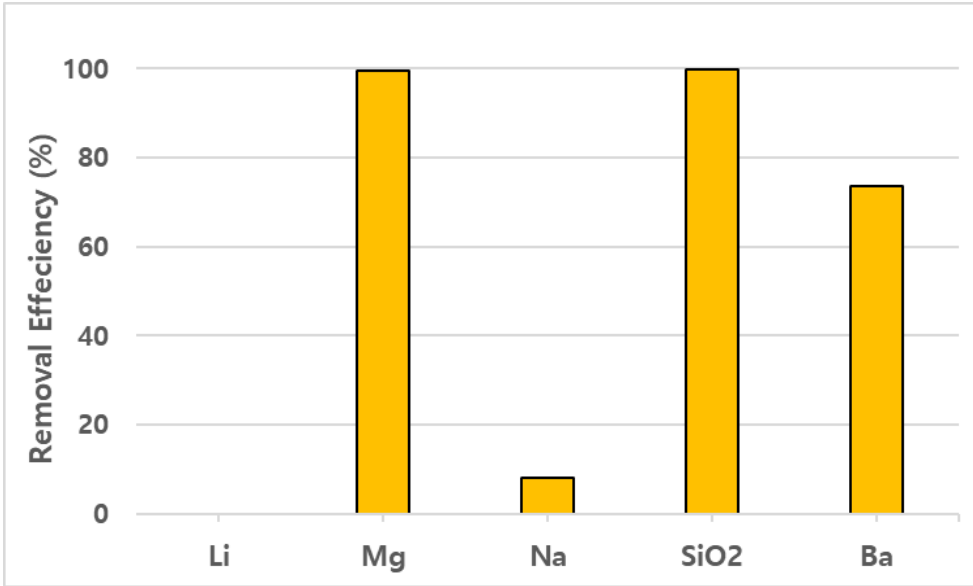

Fig. 3.4.1. The removal efficiency of cations after applying $Ca(OH)_2$ (molar ratio of 1:1 of Mg^{2+} and SiO_2).

The precipitation sample was prepared in powder form and coated with Au for SEM-EDX analysis. Fig. 3.4.2 (a) shows the image of the sample (× 300), and Fig. 3.4.2 (b) shows the EDX peak results. The precipitation sample contains O (30.6%), Cl (23.4%), Na (17.5%), Si (10.5%), Ca (9.8%), and Mg (8.3%) as elemental components.

The XRD diffractogram of the precipitation sample is shown in Fig. 3.4.3. The precipitation sample is composed with silicon chloride [(200), (202), (220), (400), (205), and (420)], halite (NaCl) [(111), (200), (222), (220), (400), (420), and (422)], Mg [(110) and (211)], Sylvine (KCl) [(200), (220), (222), (400), and (422)] and Na (110). Due to the SEM-EDS and XRD results, Mg and Si-containing minerals were precipitated due to chemical precipitation, and additional Na and Ca-containing minerals were observed.

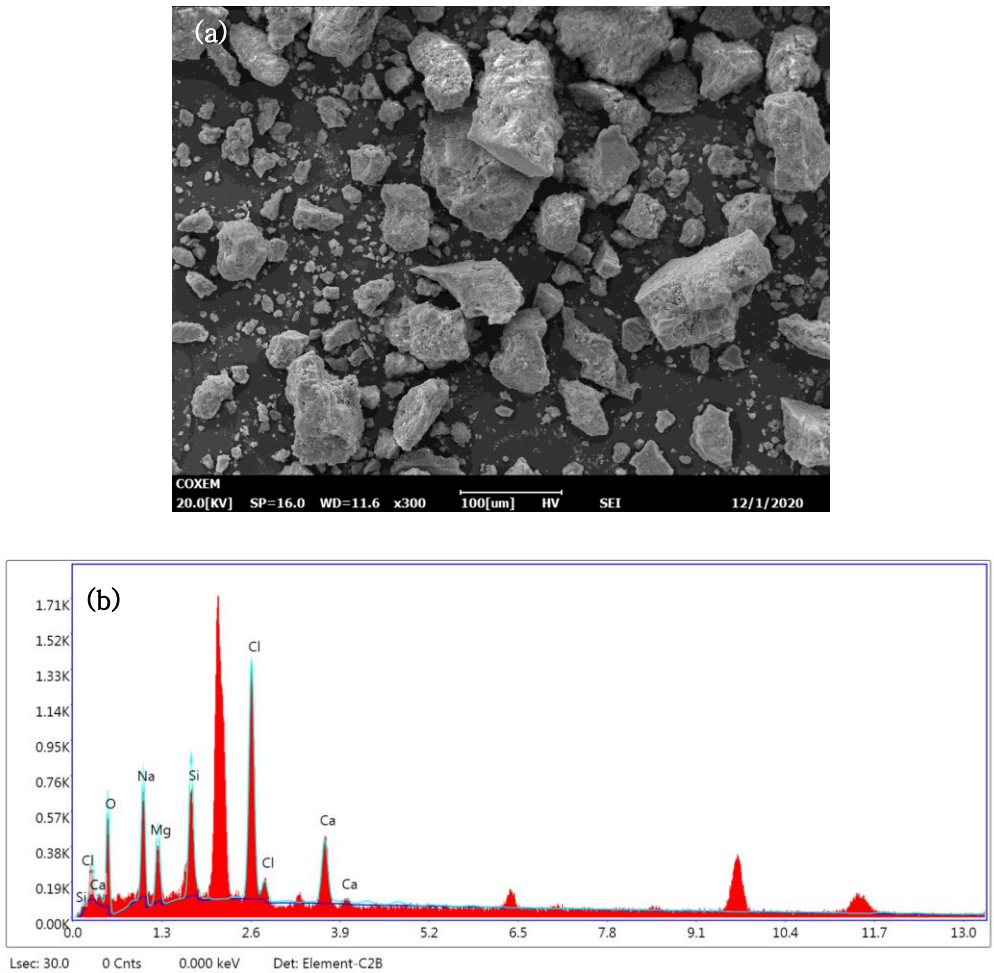

Fig. 3.4.2. SEM-EDX micrographs of precipitation after applying $Ca(OH)_2$ (a) Image of the sample, (b) EDX peak of precipitation.

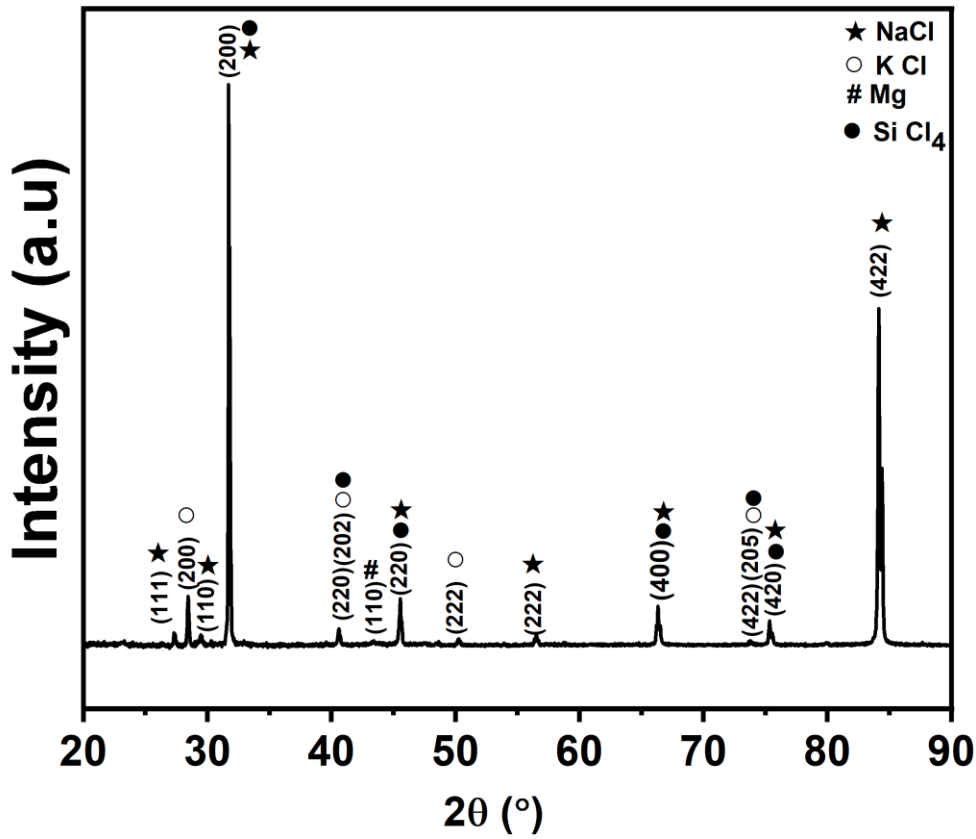

Fig. 3.4.3 XRD diffractogram of the precipitation after applying $Ca(OH)_2$.

Ca^{2+}, Sr^{2+}, and Ba^{2+} (sum 7.34 mmol) were removed after applying $Ca(OH)_2$ to the synthesized geothermal fluid, the different molar ratios of the ion summary were considered (i.e., 1:1, 1.1:1, 1.2:1), and Fig. 3.4.4 shows the removal rate of the total cations. The composition of before and after applying precipitant Na_2CO_3 (molar ratio 1.2:1) was shown in Table 3.4.2.

The TDS of the solution before and after the application of Na_2CO_3 was measured by using the conductivity value and the average TDS value before applying Na_2CO_3 was measured 104,850 mg/L and decreased to 99,825 mg/L after applying Na_2CO_3. Compared to the initial solution, the TDS decreased 10.6 % after applying the 2 steps of precipitant.

Lithium ions showed a negligible effect of precipitation, and $Ca^{2+}$and Sr^{2+} showed a removal rate higher than 95% in all three different Na_2CO_3 dosage molar ratios of reaction. Ba^{2+} showed a removal efficiency of 84% in Na_2CO_3 dosage molar ratio 1:1 and 1.1:1, and 98% was removed by the dosage molar ratio of 1.2:1. For a higher removal rate of divalent ions, Na_2CO_3 dosage molar ratio 1.2:1 was chosen to remove the Ca^{2+}, $Sr^{2+}$and Ba^{2+} ions as shown in Equation (3.4.3). Approximately 18.6 g of Na_2CO_3 were used to remove Ca^{2+}, Ba^{2+}, and Sr^{2+} ions from 1 L geothermal fluid and M is abbreviated as a divalent metal ion.

$$M^{2+} + Na_2CO_3 \rightarrow MCO_3 + 2Na^{+} \qquad (3.4.3)$$

The precipitation formed after applying Na_2CO_3 was prepared in a powder form and coated with Au. Fig. 3.4.5 (a) shows the image of the sample (× 300), and Figure 3.4.5 (b) shows the EDX peak results. Due to the EDX peak, the precipitation sample contains Ca(59.1%) and O(40.9%) as an elemental component.

Fig 3.4.6 shows the XRD diffractogram results of the sample. The precipitation sample is composed with calcium carbonate minerals like aragonite ($CaCO_3$) [(110), (111), (021), (121), (102), (022), (211), (220), (221), (041), (013), (132), (310), (311), (321), (330), (242), (124), (161), (350), (115), and (042)], vaterite ($CaCO_3$) [(101), (002), (100), (102), (103), (004), (110), (112), (104), (202), (203), (114), (006), (204), (106), (212), (302), and (206)] and calcite ($CaCO_3$) [(104), (110), (113), (024), (116), (122), (214), (125), (217), (128), (134), (226), and (211)] plane. The SEM-EDS and XRD results shows a high amount of Ca bearing minerals. Due to a high amount of Ca^{2+} (61081.1–7517.0 ppm) compared to $Sr^{2+}$and Ba^{2+} (399.8–441.6 ppm) in the synthesized geothermal fluid, the SEM-EDX and XRD only showed the Ca^{2+} metal ions for the precipitation.

Table 3.4.2 The composition of before and after applying precipitant Na_2CO_3 (molar ratio 1.2:1) (mg/L)

Synthesized Geothermal Fluid	Before applying precipitant	After applying precipitant
pH	10.8-11.0	10.7-12.7
Conductivity (mS/cm)	139.5-140.1	132.5-133.7
Ca	1.6-1.9	1.0-1.8
Li	173.4-175.6	173.4-180.9
Na	24678.3-26362.1	28362.1-29007.7
Sr	3.1-5.2	1.6-3.0
Mg	0.9-1.0	0.6-0.8
Ba	2.6-4.4	0.3-2.3
SiO_2	0.7-4.7	4.9-6.0

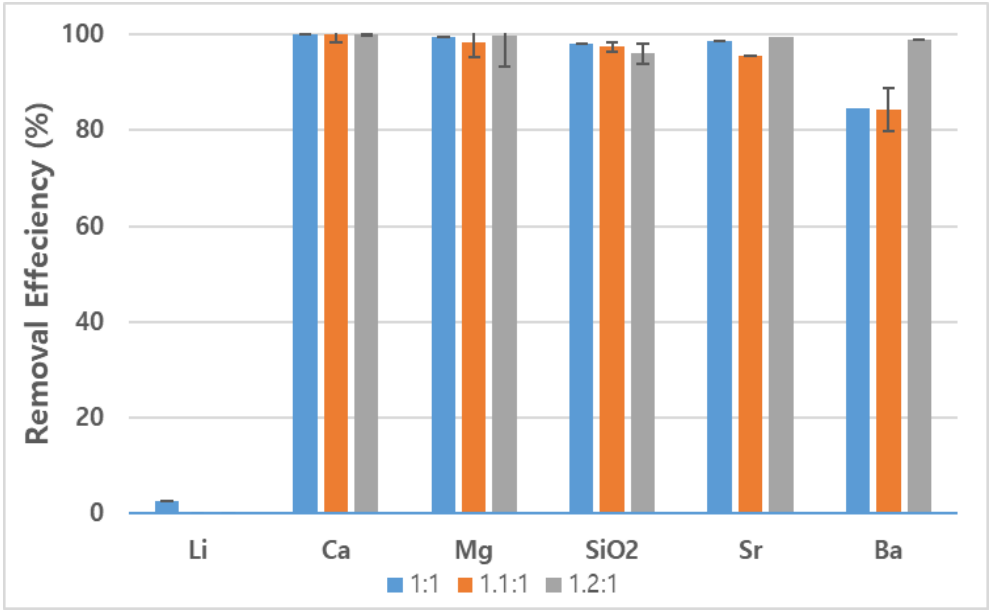

Fig. 3.4.4. Removal efficiency of cations after applying Na_2CO_3 (molar ratios of 1:1, 1.1:1, 1.2:1 of Ca^{2+}, Sr^{2+}, and Ba^{2+}).

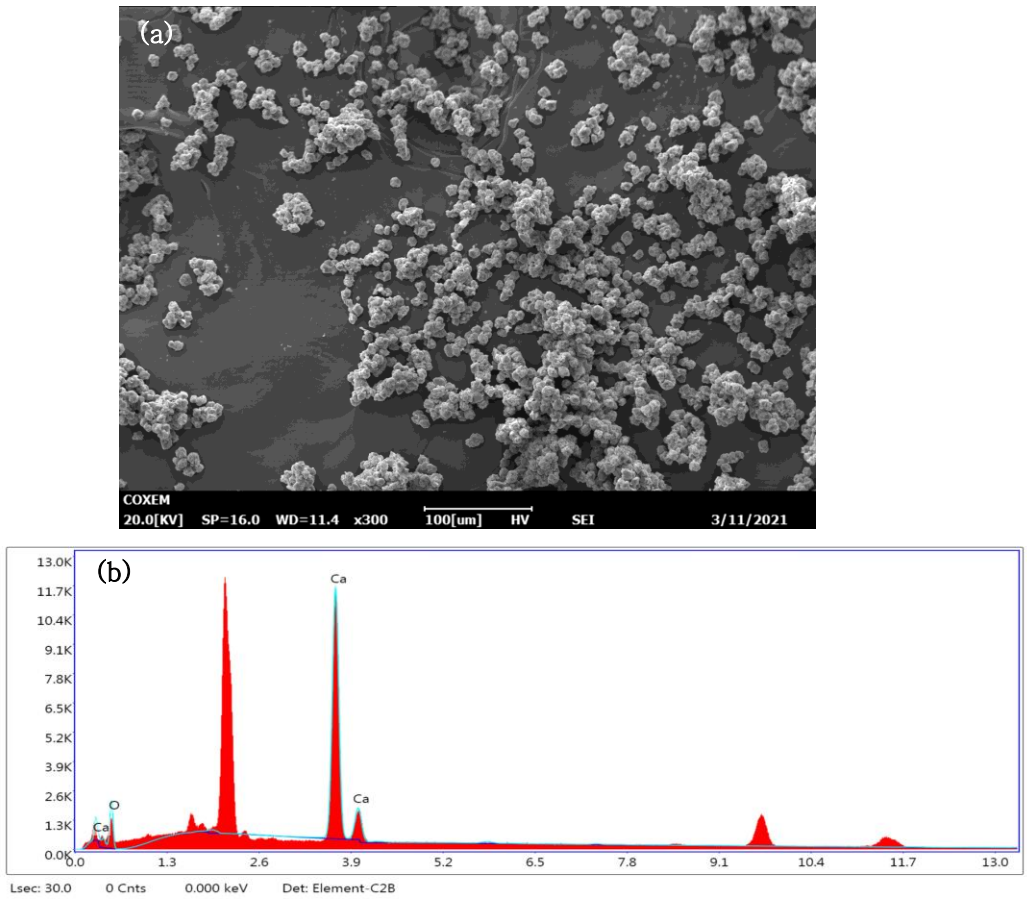

Fig. 3.4.5. SEM-EDX micrographs of precipitation after applying Na_2CO_3 (a) Image of the sample, (b) EDX peak of precipitation.

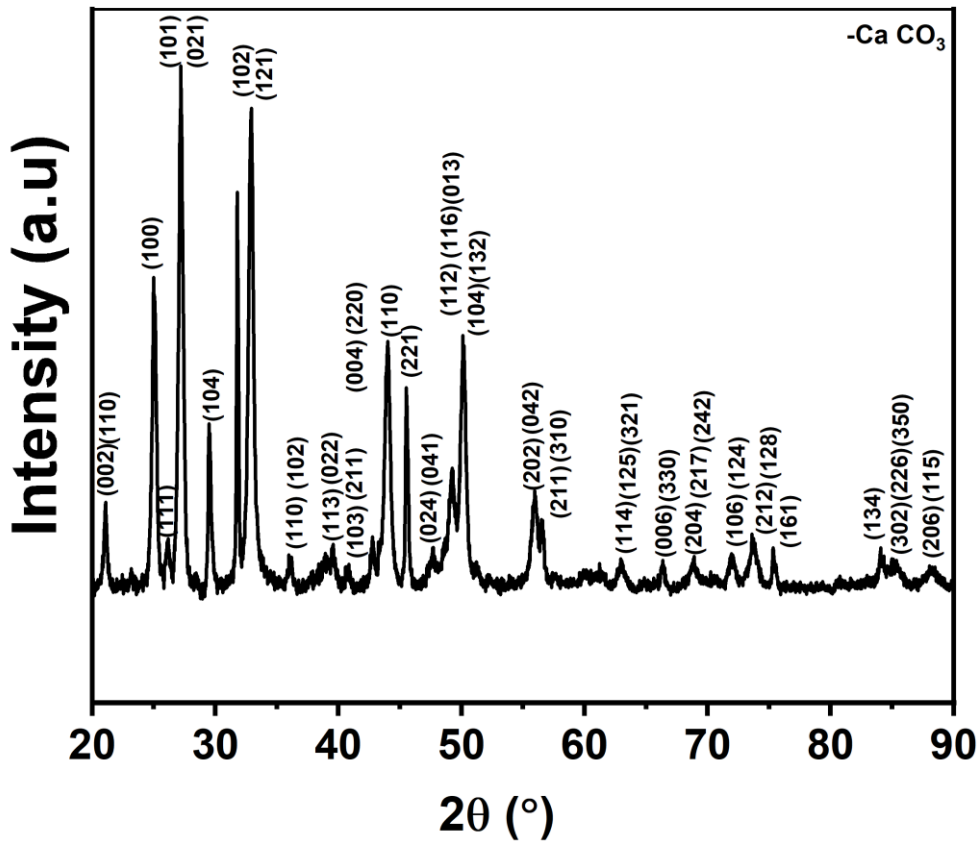

Fig. 3.4.6. XRD diffractogram of the precipitation after applying Na_2CO_3.

Two stages of chemical precipitation using $Ca(OH)_2$ and Na_2CO_3 were applied to remove metal ions from the synthesized geothermal fluid. By applying $Ca(OH)_2$, more than 97% of Mg^{2+} and SiO_2 were removed, and Na_2CO_3 removed more than 98% of Ca^{2+}, Sr^{2+}, and Ba^{2+} from the synthesized geothermal fluid. Lithium ions showed an insignificant change due to 2 stages of chemical precipitation. The usage of $Ca(OH)_2$ and Na_2CO_3 for removal stage cannot be economical for the industry application however the usage of waste like limestone ($Ca(OH)_2$) and salt rock (Na_2CO_3) can be a substitute for the removal process of silicate or divalent ions (Kasikowski et al., 2008; Galván-Ruiz et al., 2009).

3.5 Improvement of lithium recovery (solvent extraction)

A solvent extraction experiment was implemented after removing divalent ions and SiO_2 from the synthesized geothermal fluid. By applying Na_2CO_3 in the 2nd chemical precipitation stage, the Na ion concentration increased in the fluid. Despite the increase in Na concentration, the D2EHPA has an affinity for divalent ions > Li^+ > Na^+ (Jang et al., 2017), so the experiment for lithium-ion extraction is considered appropriate.

In the work of Hano et al. (1992), the solvent extraction to extract lithium was applied in a TDS of 2,255 mg/L water. The previous study also observed different diluted (1×, 25×, and 50×) produced water with a TDS value of 200,000 mg/L to recover Li selectively (Jang et al., 2017). The extraction efficiency of cations including Li decreases with high TDS levels so the produced water was diluted in this research. The Soultz-sous-Forêts geothermal fluid is reported to contain a TDS of 95,000 g/L (Sceiber et al., 2012), which is approximately 50 times higher than the work of Hano et al. (1992). Three types of different diluted (1×, 25×, and 50×) synthesized geothermal fluids were applied to observe the most favorable dilution ratio for solvent extraction. Fig. 3.5.1 shows the four stage solvent extraction of three types of different diluted synthesized geothermal fluid.

In the case of four repeated extractions at no dilution of geothermal fluid, 38.5% and 17.3% of Li^+ and Na^+ were extracted, respectively. In the 25 and 50 times dilution of geothermal fluid, more than two times higher extraction efficiency of lithium ions was shown (78.1% and 87.7%, respectively). However, the extraction efficiency of Na^+ also increased in the 25 and 50 times dilution test (37.9% and 40.1%, respectively). To observe the separation factor of L^+ and Na^+

after the solvent extraction, the separation factor was calculated. Separation factor (S), a cation separated to each other from one cation to another cation, is determined through the distribution ratio (D_m) that can be described by Equation (3.5.1) (Jang et al., 2017).

$$S_{M2}^{M1} = \frac{D_{M1}}{D_{M2}}$$

$$= \frac{Ratio\ of\ (M_1\ ion\ in\ the\ organic\ phase\ /\ M_1\ ion\ in\ the\ aqueous\ phase)}{Ratio\ of\ (M_2\ ion\ in\ the\ organic\ phase\ /\ M_2\ ion\ in\ the\ aqueous\ phase)} \quad (3.5.1)$$

By using Equation (5.3.1), three types of different diluted synthesized geothermal fluid S $\frac{Li}{Na}$ were calculated (Table 3.5.1).

As the dilution ratio increases from 0 to 50 times, the Li/Na S increased to 71.7%. As the highest lithium extraction rate and selectivity, 50 times of diluted synthesized geothermal fluid was favorable to extract lithium ions.

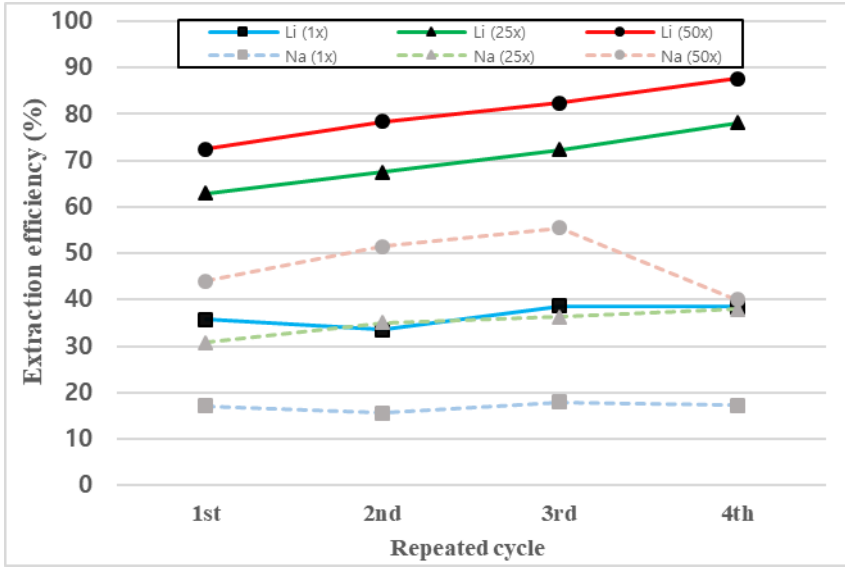

Fig. 3.5.1. Lithium and sodium extraction efficiency at different dilution rates of synthesized geothermal fluid (1×, 25×, and 50×)

Table 3.5.1 Separation factor of lithium over sodium in solvent extraction

	$S\ \frac{Li}{Na}$
No dilution	3.0
25×	5.8
50×	10.6

To find the chemical reaction of Li-D2EHPA, the logarithmic distribution ratio (D_m) of Li^+ from the 50 times diluted synthesized geothermal fluid was calculated in different D2EHPA concentrations (0.3 M to 1.5 M) (Fig. 3.5.2). In Equation (3.5.5), $\frac{(n + x)}{2}$ is denoted as the slope (approximately 0.6) and n = 1 for the valent number of Li^+; thus, the solvation number (x) was calculated as 0.1. The reaction between D2EHPA(HR) and lithium ions can be described by Equation (5.3.2) in the synthesized geothermal fluid during solvent extraction.

$$Li^+ + 0.6\,(HR)_2 \leftrightarrow LiR_1(HR)_{0.1} + H^+ \qquad (3.5.2)$$

As seen in the reaction (3.5.2), the D2EHPA-Li complex loads from the aqueous phase to the organic phase with a solvation number of 0.1. After two methods of the experiment using precipitation and solvent extraction, Li^+ was loaded at a rate of 87.7% in a 50 times diluted geothermal fluid.

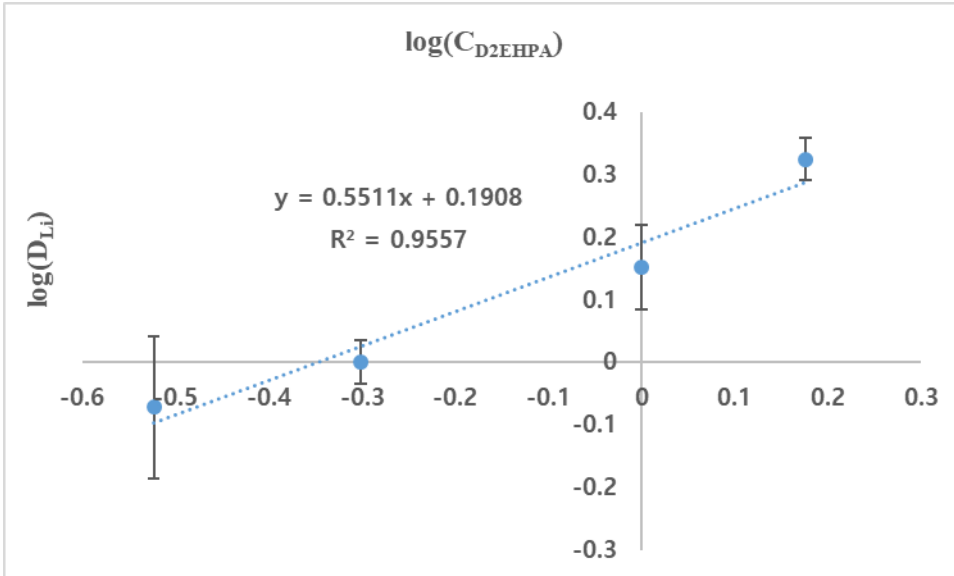

Fig. 3.5.2. The distribution ratio of lithium (D_{Li}) in different D2EHPA concentrations.

In Fig. 3.5.1 a high extraction efficiency of Na ions (40 %) coexists with the Li ions (87.7 %) in the organic phase when the solvent extraction was implemented in a 50 times diluted geothermal water. Due to a low selectivity of Li in this condition, the pH isotherm experiment was held to know the appropriate pH condition of extraction (Fig. 3.5.3). Usually Na can be selectively removed by using an ion exchange resin to exchange with other cations however this requires an additional process to remove the exchanged cations that increases in the solution (Zuo et al., 2013). Thus finding the appropriate condition for extracting Li without extracting Na is needed. The pH of the geothermal water after the 2 stages of removal step was controlled 1 to 10 by HCl. Each solution with different pH was sampled after a steady pH value and was maintained for 10 min. After the equilibrium of organic and aqueous phase, the raffinate was separated using a separation funnel. As the pH of solution gets higher, the Li and Na extraction efficiency increased and a similar equilibrium behavior was also observed in other studies for Li and Na (Meshram et al., 2022; Lee et al., 2022). At the condition of pH 7, approximately 60 % of Li was extracted to the organic phase whereas the extraction of Na was extracted less than 10 %. Therefore, a pH range of 6–7 was assumed as suitable for loading Li with loading relatively less Na to the organic phase using extractant condition 1.5 M D2EHPA and 0.3 M TBP. To earn the appropriate pH condition and extractant concentration a further study is needed by studying the pH isotherm with various condition of extractants.

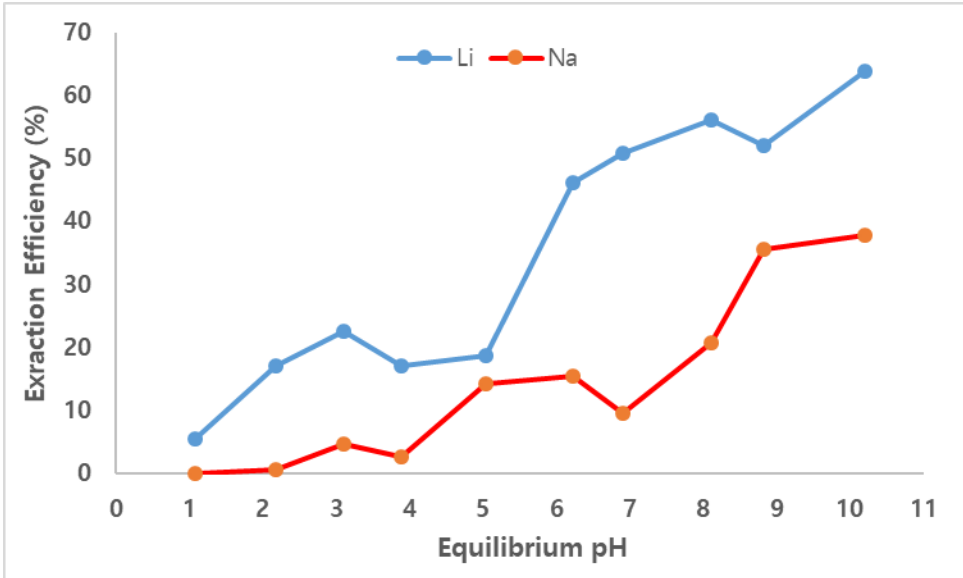

Fig. 3.5.3. Lithium and sodium extraction efficiency at different dilution rates of synthesized geothermal fluid (1×, 25×, and 50×).

3.6 Summary

Two experiments were implemented by using geothermal water. Solvent extraction was implemented in two repetitive stages for the recovery of Li^+ from geothermal fluid in the first experiment to observe the SiO_2 ion effect. The second experiment was to improve the method to recover lithium by using a combined method of chemical precipitation and solvent extraction on synthesized geothermal fluid.

In the first experiment, the first stage of solvent extraction was used to remove divalent cations, and the second stage was to recover Li^+ selectively from the geothermal water. During the two step solvent extraction process, the total lithium recovery efficiency decreased from 6.8 % to 4.5 % as the SiO_2 ion concentrations increased. As the concentration of SiO_2 ions increased from 0 mg/L to 350 mg/L in the geothermal water, the loss of Li ions from the aqueous phase in the first step increased from 55.5% to 77.9 % and the Li recovery rates in the second step did not show significant difference (21.9-24.8 %) in different SiO_2 concentrations.

Accordingly, the overall Li^+ recovery efficiency has been decreased and it indicates that the influence of SiO_2 on the Li^+ recovery occurs mainly in the first step of the extraction process. The separation factor of divalent ions such as Sr^{2+} and Mg^{2+} over Li^+ decreased as increased SiO_2 concentration because greater amounts of Sr^{2+} and Mg^{2+} have been extracted with the existence of SiO_2 ions in the geothermal fluid. It is well known that SiO_2 ions in the geothermal fluid can cause the scaling problem in geothermal systems and it was found, in this study, that SiO_2 ions also inhibits the selective recovery of lithium from the geothermal water. Therefore, controlling the concentrations of SiO_2 ions in geothermal

reservoirs is suggested for the efficient operation of geothermal systems and successful recovery of lithium from the geothermal fluid.

In the second experiment, the first stage using $Ca(OH)_2$ and Na_2CO_3 for chemical precipitation targeted only the divalent ions and silica ions to influence the lithium ions insignificantly. More than 97% of the Mg^{2+} and SiO_2 were removed by using $Ca(OH)_2$, and more than 98% of Ca^{2+}, Sr^{2+}, and Ba^{2+} were removed by using Na_2CO_3 from the synthesized geothermal fluid. The silicate ions or divalent ions shows a different concentration due to the bedrock composition or EGS process. Impurities amount, especially the silicate ions that causes the scale formation inside the borehole should be checked properly due to sampling or monitoring to remove the exact amount before the process of Li recovery.

After applying chemical precipitation, solvent extraction using an extractant D2EHPA with the addition of TBP (1.5 M D2EHPA & 0.3 M TBP) to improve ion extractability was used for the second stage. Due to the high TDS of the geothermal water, the extraction efficiency of lithium was low. Thus, the 1, 25 and 50 times dilutions of synthesized geothermal water were compared. The highest lithium extraction efficiency of 87.7% was observed from the dilution ratio of 50 times. Since the geothermal fluid loss takes place due the EGS operation, injecting or supplementing an additional fluid would be required. Since the lithium extraction in this study is favorable in a dilute solution, an increased amount of the solution after the extraction can complement the circulating geothermal fluid in EGS only if the solution pH condition does not impede the stable operation.

Chapter 4. Selective lithium recovery from produced water

4.1 Introduction

Shale gas produced water includes many organic compounds, such as aliphatics, cycloaliphatics, aromatics, and polycyclic aromatics and especially the aliphatic hydrocarbons shows the major component in Marcellus shale gas produced water (Strong et al., 2014). Among various types of aliphatic hydrocarbons, the shale gas produced water of the Marcellus area predominantly contains alkanes, especially C_6-C_{16} of linear hydrocarbons (Maguire-Boyle and Barron, 2014). While increasing the carbon number of alkanes from 6 to 16, the solubility of the compound in aqueous solutions decreases (Maguire-Boyle and Barron, 2014). In this dissertation, the representative organic compounds, n-hexane (C_6H_{14}), n-undecane ($C_{11}H_{24}$), and n-hexadecane ($C_{16}H_{34}$) were selected to represent the organic compound in the shale gas produced water to investigate their influence on lithium recovery. A total amount of total organic carbon (TOC) in the Marcellus produced water is 2,348 mg/L on average (Maguire-Boyle and Barron, 2014). Assuming 2,348 mg/L of the TOC concentration as 100%, the alkane concentrations were controlled from 0% to 100%. To observe lithium extraction efficiency in different concentrations and types of alkanes in the produced water, n-hexane was added with a concentration of 0%, 50%, and 100%. In addition, three alkanes with different chain lengths, with n-hexane, n-undecane, and n-hexadecane, were introduced in the solution with a concentration of 100%.

Shale gas produced water is wastewater that is generated during the production of oil and gas and contains a variety of contaminants, including hydrocarbons, heavy metals, and naturally occurring radioactive materials

(NORMs) (Gregory et al., 2011; Haluszczak et al., 2012). The composition of produced water can vary depending on the type of formation from which it is extracted and the specific methods used to extract the oil and gas. The organic compounds present in shale gas produced water can have a variety of environmental impacts and some of these compounds can be toxic to organisms (Maguire-Boyle and Barron, 2014). The organic compounds that exist in the shale gas produced water needs a treatment like biological degradation, chemical oxidation, and activated carbon adsorption (Pawar et al., 2022). Especially Zaman et al. (2021) explains activated carbon is feasible to remove TOC and BTEX that exists in the shale gas produced water without removing TDS and salt concentrations. As explained in Lee and Chung, (2020b), the existence of organic compounds can hinder the lithium recovery during the solvent extraction hence the organic compounds were removed using an activated carbon without affecting the lithium ions.

The divalent ions that exist together with the lithium ions in the shale gas produced water have been removed during the previous stage to recover lithium during the second stage in the previous study (Jang et al., 2017). Due to the affinity of D2EHPA, the divalent ions were removed (>94.4%) mostly however the lithium showed a high loss (25.1%) during the removal stage. For an effective method to decrease the lithium loss, a same chemical precipitation method using $Ca(OH)_2$ and Na_2CO_3 are applied to remove divalent ions as written in Chapter 3.

Ionic liquid was used as an extractant for solvent extraction process after removing organic compounds and divalent ions from the synthesized produced water. Ionic liquid is known for the favorable properties such as negligible vapor pressure, low flammability, and high thermal stability to be useful for the design of

relevant solvent extraction systems (Zante et al., 2020; Shi et al., 2017). There are many ionic liquids that are used to extract specific ions however ionic liquid that is designed by using Cyphos IL 101 and D2EHPA was not researched yet. IL extracting agent [Cyphos IL 101][D2EHPA] (1 M) was used as an extractant in this study and for comparison, several different concentration conditions of extractants including D2EHPA, D2EHPA + TBP, IL extracting agent [Cyphos IL 101][D2EHPA] was used as an extractant to observe the Li extraction efficiency. TBP is used as a synergistic additive to improve the targeting metal ion extractability (Hano et al., 1992). As described in chapter 3, Li was extracted from the synthesized produced water using 1.5 M D2EHPA + 0.3 M TBP as an extractant (Lee and Chung, 2020b). However, Zante et al. (2020) shows that ionic liquid can increases the extraction ability of D2EHPA higher than using the TBP as an additive. Solvent extraction was applied for three different dilution levels (No dilution, 25×, and 50×) for produced water using D2EHPA 1M after removing organic compounds and divalent ions.

In this research using the produced water, two experiments were held. The first is to observe lithium extraction efficiency in different concentrations and types of alkanes in the produced water and to improve the Li recovery method, a combined method of adsorption, precipitation and solvent extraction was applied to extract lithium ions effectively from the produced water. The first part of the process is to remove organic compounds that exists in the produced water. The second part of the process is to remove the divalent ions that can inhibit the lithium recovery during solvent extraction.

4.2 Materials and Methods

The produced water sample properties like ion concentrations or pH can be different due to sampling time and borehole types. The produced water that was used in this dissertation is the median concentrations after 14 days of flowback from seven horizontal wells (C, E, F, G, K, M and O) located in the Marcellus region (Haluszczak et al., 2013). The median concentrations of TDS was measured 157,000 mg/L and lithium was measured 95 mg/L (Haluszczak et al., 2013).

As described in Jang et al. (2017), the produced water was synthesized for a similar chemical composition reported in the literature (Haluszczak et al., 2013). The produced water was assumed to be a mixture of fracturing fluid and formation water, with the same volume ratio. First, the fracturing fluid was prepared with isopropanol, polyacrylamide, ethylene glycol, guar gum, hydrochloric acid, and 40/70 mesh sand (212 - 420 μm). Then, various chemical compounds were added based on the chemical properties of the formation water (Table 4.2.1) and major ions were usually targeted (> 100 ppm) compared with the real produced water. The small amount of ions should also be considered however this experiment focused only on the major concentration that has a high amount inside the produced water. The synthesized fluid allowed 24 hours of settlement time, so that the supernatant could be obtained. Table 4.2.2 shows the chemical properties of the synthetic produced water and the real produced water (median value after 14 day flowback) ion concentration data.

Table 4.2.1 Purity and suppliers of the reagents used to synthesize produced water

Product	Purity	Supplier
LiBr	54 wt% in H_2O	Sigma Aldrich
$CaCl_2 \cdot 2H_2O$	99 %	Sigma Aldrich
$MgCl_2$	99 %	Yakuri Pure Chemicals
NaCl	99 %	Daejung
$NaHCO_3$	99.5 %	Sigma Aldrich
$FeCl_2 \cdot 4H_2O$	≥99.0 %	Kanto chemical
$BaCl_2 \cdot 2H_2O$	99 %	Kanto chemical
$SrCl_2 \cdot 6H_2O$	98 %	Duksan Pure Chemicals
HCl	37 %	Merck
Glutaraldehyde	25 %	Junsei
Ammonium persulfate	98.0 %	Wako
N,N-dimethyl formamide	99.5 %	Wako
Guar gum		Sigma Aldrich
Citric acid	99.5 %	Sigma Aldrich
KCl	99.5 %	Waku Pure Chemicals
Ethylene glycol	99 %	Sigma Aldrich
Isopropanol	70 %	Merck
Polyacrylamide		Sigma Aldrich

Table 4.2.2 Properties of synthetic produced water (mg/L)

	Produced Water	Synthesized Produced Water
pH	6.2	5.6-6.3
Ca	11200	10,985 – 11,796
Li	95	90.7 - 98.1
Na	36400	25,868 – 27,950
Sr	2330	2,277 – 2,412
Mg	875	869 - 919
Ba	1990	1,825 – 1,973
Mn	5.6	
Zn	0.09	
Al	0.5	

The experimental process in this study followed the two step solvent extraction method, as explained on the previous study (Jang et al., 2017). In Jang et al. (2017) solvent extraction experiment, the first-stage solvent extraction was designed for the removal of divalent cations which can inhibit the Li recovery. More than 94.4 % of divalent ions (Ca^{2+}, Mg^{2+}, Sr^{2+}, and Ba^{2+}) were removed and the lithium loss showed 25.1 % by using 1.0 M D2EHPA. After removing the divalent ions, the second stage solvent extraction was applied to recover lithium and 41.2 % was extracted by using 1.5 M D2EHPA and 0.3 M TBP. Thus the total amount of lithium recovered in Jang et al. (2017) was measured as 30.8 % for the two step solvent extraction.

In this dissertation, D2EHPA was added to kerosene in an organic phase, while alkanes were added in the shale gas produced water in an aqueous phase. There are many diluents commercially used in several industries, but kerosene was chosen, as it has negligible chemical interaction with D2EHPA (Azizitorghabeh, 2016). 1 L of produced water was synthesized and the same amount of extractant was prepared. 100mL of the solution was used for the first of solvent extraction stage and throughout the experiments, the organic phase and aqueous phase solutions were mixed with the same volumetric ratio (1:1) in an Erlenmeyer flask and stirred in a shaking incubator (SH-BSI16R, Samheung Instrument, Seoul, S. Korea) at 150 rpm and 25℃ for 30 minutes. After mixing, the solution settled in a separating funnel to reach equilibrium, with the aqueous phase withdrawn. After the first step for divalent cation removal, the second step in the extraction of lithium recovery was performed. TBP was used with D2EHPA in the second stage, with the same process. The optimal conditions reported in the previous study (i.e.,

1.0 M D2EHPA and 1.5 M D2EHPA + 0.3 M TBP in the first and the second stages, respectively) were applied in the experiments. Eight stage solvent extractions were performed at two steps. The solution was reused after each eight stages and the initial organic phases were replaced for each eight stage solvent extractions. The schematic of solvent extraction experiment was shown in Fig. 4.2.1.

The pH and conductivity of the aqueous solution were measured by a multimeter (Orion Star A329, Thermo Fisher Scientific, Waltham, MA, USA) and 0.45 μm polytetrafluoroethylene filtered solution was analyzed for major cation concentration, with inductively-coupled plasma optical emission spectrometry (ICP-OES, Optima 8300, PerkinElmer, Waltham, MA, USA) for each eight stage solvent extractions. The organic phase was analyzed by a fourier transform infrared spectroscopy (FT-IR spectra, Nicolet 6700, Thermo Fisher Scientific, Waltham, MA, USA).

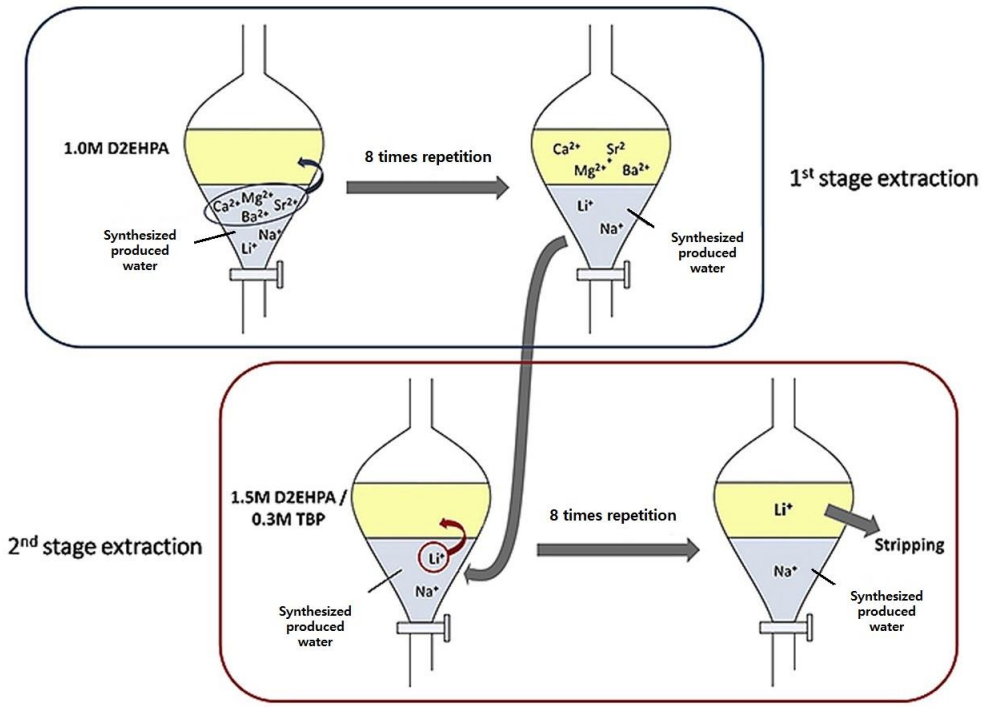

Fig. 4.2.1. Schematic of solvent extraction experiment.

After observing the effect of organic compounds during Li recovery in the produced water, chemical adsorption was applied to remove organic compounds from the synthesized produced water. In the Riegel et al. (2023), a short time was requested to remove a short chain alkane sufficiently by using an activated carbon, and targeting a long chain alkane consumed a longer time. A fundamental experiment was held to remove the organic compound in the produced water so due to the common organic compound used in the first experiment by comparing different concentrations and chain length, the shortest alkane hexane among other organic compounds was injected to the synthesized produced water to match the Marcellus produced water TOC amount.

The amount of organic compounds was measured by using a TOC analyzer (Total Organic Carbon Analyzer, Sievers 5310 C, GE, USA). The measured TOC was considered 100% of TOC in the shale gas produced water and activated carbon as an adsorbent was injected with a molar ratio of 1:1 of TOC in an erlenmeyer flask and mixed in a shaking incubator (SH-BSI16R, Samheung Instrument, Seoul, S. Korea) at 150 rpm and 25℃ for 24 hours. After mixing, the organic compounds were removed in a constant pressure mode using a vacuum filtered (vacuum pump, DOA-P704-AC, GAST, USA).

After chemical adsorption process, the selective precipitation of divalent ions divalent ions like Ca^{2+}, Sr^{2+}, Mg^{2+}, and Ba^{2+} was applied using $Ca(OH)_2$ and Na_2CO_3 for the low influence of lithium ions in the produced water. The experimental process for removing divalent ions in this study followed the two consecutive steps of applying different precipitants as written in Chap 5. The first step of the experiment is to apply 0.04 g $Ca(OH)_2$ to remove Mg^{2+} by considering the same molar ratio in the 1 L of produced water. The second step of the

experiment is to apply 0.55 g Na_2CO_3 to remove Ca^{2+}, Sr^{2+}, and Ba^{2+} from the produced water (molar ratio of 1:1.2). Mg^{2+} can react with $Ca(OH)_2$ to form $Mg(OH)_2$ and Ca^{2+}, Sr^{2+}, and Ba^{2+} can react with Na_2CO_3 to form MCO_3 (M is abbreviated as divalent metal ions) with a short chemical reaction time (1 hour) (Bologo et al., 2009; Lee and Chung. 2022a). The elemental composition of the precipitation powder for two steps were analyzed using the Scanning Electron Microscopy with Energy Dispersive X-ray analysis (SEM-EDX) (EM- 30AX, Coxem, Daejeon, Korea).

Solvent extraction was applied for three different dilution levels (No dilution, 25×, and 50×) for produced water using D2EHPA 1M after removing organic compounds and divalent ions. The dilution was held by using deionized water. For a comparison, D2EHPA, D2EHPA + TBP, and Ionic liquid was also used as an extractant for solvent extraction process after removing organic compounds and divalent ions from the synthesized produced water. All the solvent extractions steps were held for 4 stages like Chap 3, for the purpose to measure the cumulative extraction efficiency after removing the purities.

IL extracting agent [Cyphos IL 101][D2EHPA] (1 M) was used as an extractant in this study and for comparison, different concentration conditions(0.3, 0.5, 1.0 M) of D2EHPA and D2EHPA + TBP was used to observe the Li extraction efficiency. The scheme of the experiment method (previous and improved) for the overall chapter is shown in Fig. 4.2.2.

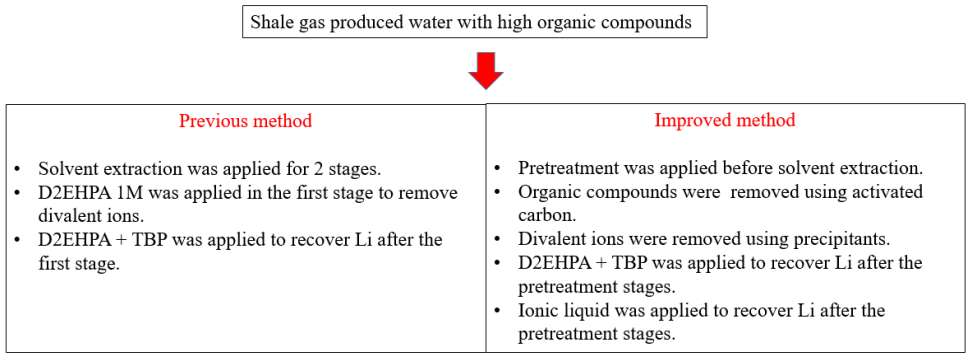

Fig. 4.2.2. The scheme of the experiment method

4.3 Effect of different chain lengths of alkanes during lithium recovery using solvent extraction

Experiments were implemented in order to observe the influence of different lengths of organics. Fig. 4.3.1 shows the extraction efficiency of major cations in the produced water, with different types of alkanes after eight stages of the extraction. The pH value was measured in a range of 1.5-1.8 after every repetition in both stages due to the production of hydrogen ions as described in Equation 2.1.2. The measured temperature in the aqueous solution ranged from 24.0 to 24.5 ℃.

The extraction efficiency showed the highest in the first stage out of eight stages of solvent extraction. Usually the solution pH should be controlled after every stage in order to have acceptable extraction yields (Lupi and Pilone, 2020). The pH of the extraction system plays a crucial role in the distribution of metals between the aqueous and organic phases during solvent extraction process. By adjusting and controlling the pH through saponification, the selectivity and efficiency of metal extraction can be optimized (Keller et al., 2022; Liu et al., 2017). In Keller et al. (2022), saponification is recommended due to the strong influence on the equilibrium pH value and lowers the effective H^+ emission of the extraction process (Equation 2.1.2). This can be explained that a higher pH solution enhances the ion extraction compared to untreated D2EHPA.

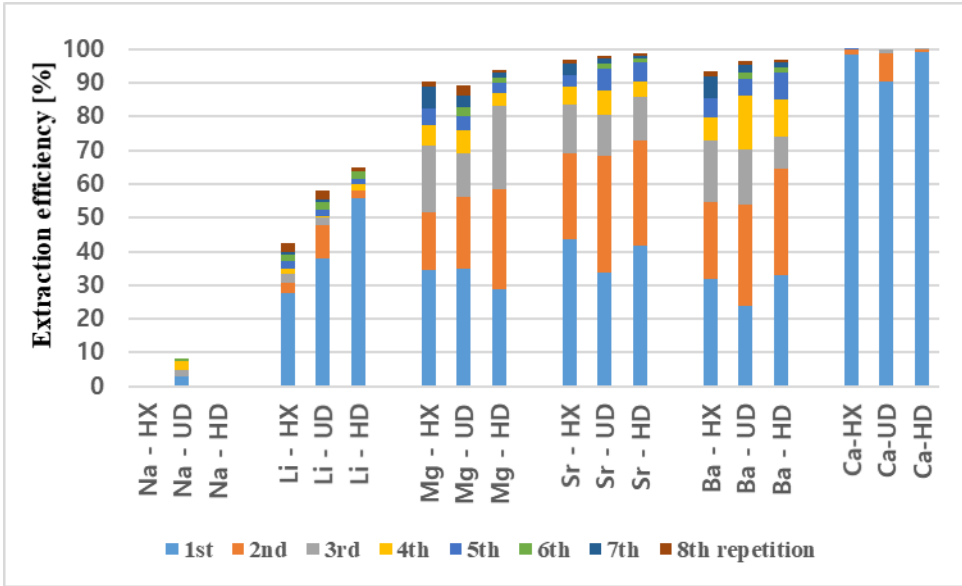

Fig. 4.3.1. Multistage solvent extraction efficiency of major cations in the synthetic produced water containing (a) hexane(HX), undecane(UD), and (c) hexadecane (HD).

It is known that D2EHPA has an affinity for Ca^{2+} > Sr^{2+} > Ba^{2+} > Mg^{2+} > Li^{+} > Na^{+} (Jang et al., 2017) and this is well-reflected in the resulting extraction efficiency in Fig. 4.3.1.

The influence of alkanes on the removal efficiency for Ca and Na was not observed. More than 99% of calcium was removed and sodium showed significantly low removal efficiency regardless of the alkanes type. More than 97.0 % of Mg, Sr, and Ba was removed, with extraction efficiency in n-hexadecane-containing solution higher than those in n-hexane containing fluid. However, it is difficult to claim that the changes in removal efficiency originated from the alkanes type. In the case of lithium, it is clearly observed that the extraction efficiency increases as the chain length of alkanes increase. In addition, the effect of alkanes type on the removal efficiency is predominant at the first cycle of the repetition and decreased during the multistage solvent extraction.

Fig. 4.3.2 shows the extraction efficiency for each different D2EHPA concentrations (0.3, 0.5, 1.0, and 1.5 M) and Fig. 4.3.3 shows the logarithmic distribution ratio of lithium ($D_{Li} = \frac{\text{Li concentraion in organic phase}}{\text{Li concentraion in aqueous phase}}$) in different D2EHPA concentrations (C_{D2EHPA}). As previous published, the relationship between the distribution ratio and the extractant concentration is linear and the number of solvation can be inferred using the slope in the graph. The solvation number is one of the main factors affecting the loading of the ion. It is known that the loading of ion increases with decreasing the solvation number (Biswas and Singha, 2007).

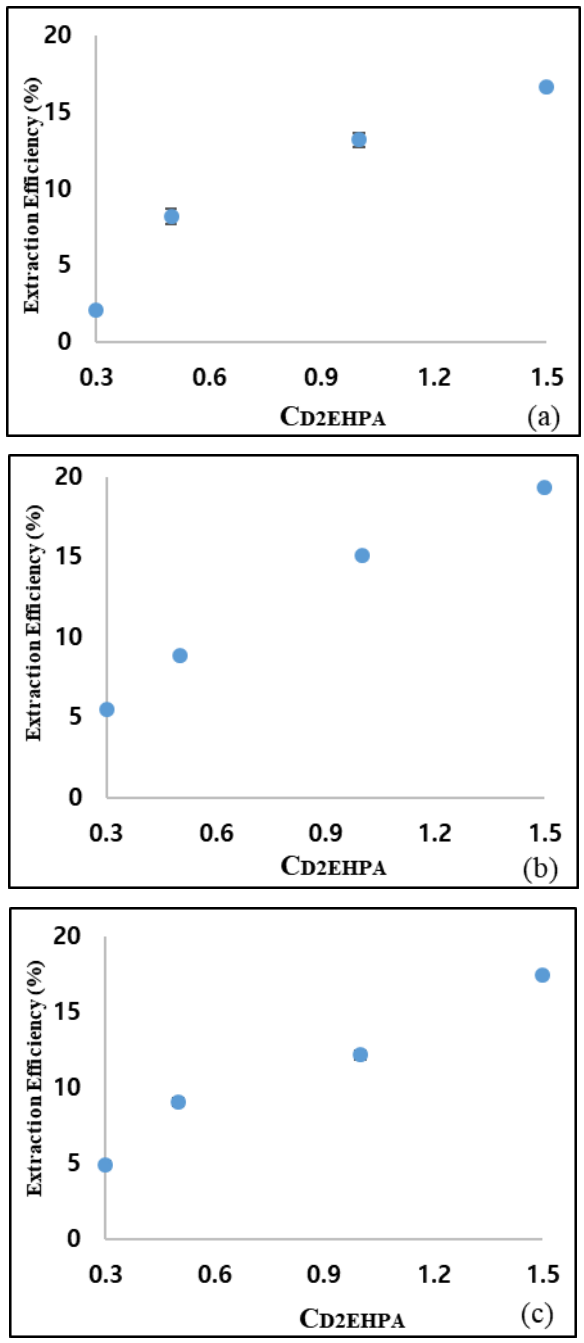

Fig. 4.3.2. Extraction of lithium(%) in different D2EHPA concentrations (C_{D2EHPA}) with the shale gas produced water containing (a) n-hexane (b) n-undecane, and (c) n-hexadecane.

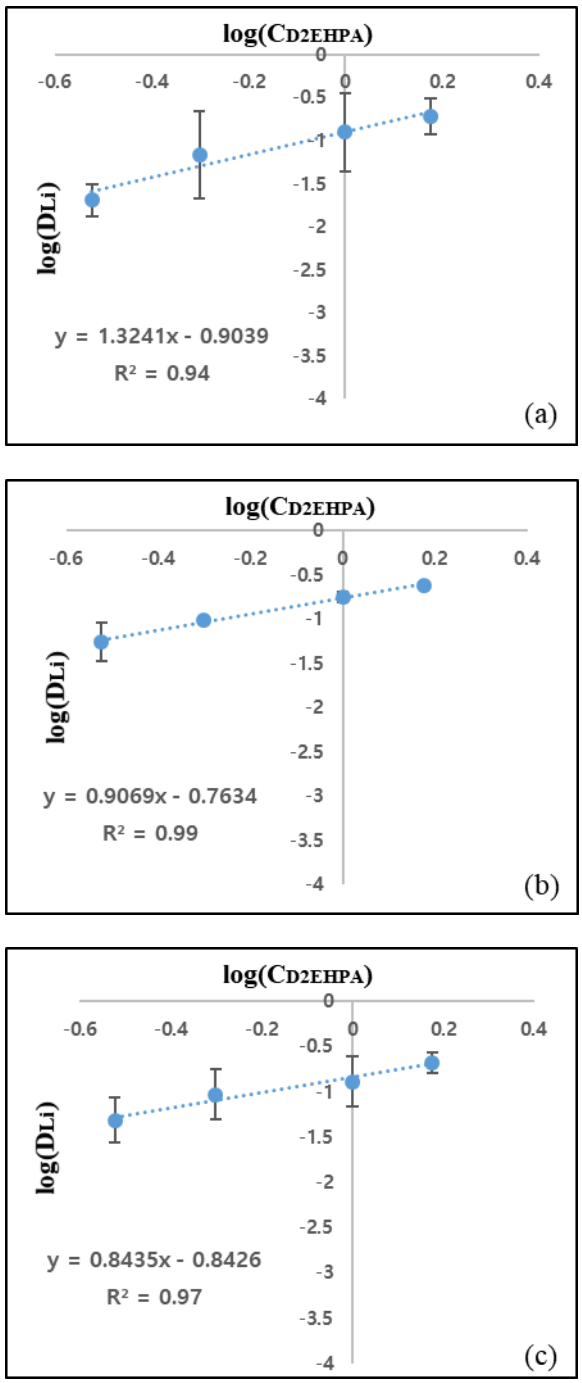

Fig. 4.3.3. Distribution ratio of lithium (D_{Li}) in different D2EHPA concentrations (C_{D2EHPA}) with the shale gas produced water containing (a) n-hexane (b) n-undecane, and (c) n-hexadecane.

The graphs in Fig. 4.3.3 (a), (b), and (c) show a slope of 1.32, 0.91, and 0.83, respectively. Therefore, the reactions occurred in the produced water with no organic compound, hexane, undecane, and hexadecane can be expressed as in Equation 4.3.1, 4.3.2, 4.3.3 and 4.3.4, respectively (Equation 4.3.1 was referred by the previous study Jang et al., 2017).

$$Li^+ + 1.56\ (HR)_2 \leftrightarrow LiR(HR)_{2.12} + H^+ \qquad (4.3.1)$$

$$Li^+ + 1.32\ (HR)_2 \leftrightarrow LiR(HR)_{1.65} + H^+ \qquad (4.3.2)$$

$$Li^+ + 0.91\ (HR)_2 \leftrightarrow LiR(HR)_{0.81} + H^+ \qquad (4.3.3)$$

$$Li^+ + 0.83\ (HR)_2 \leftrightarrow LiR(HR)_{0.66} + H^+ \qquad (4.3.4)$$

Accordingly, the solvation numbers of Li-D2EHPA complex were calculated as 2.12, 1.65, 0.81, and 0.66 for none organic, n-hexane, n-undecane, and n-hexadecane containing produced water. Therefore, the existence of alkanes decreased the solvation number of the lithium-D2EHPA complex. Also, the solvation numbers decreased with an increasing chain length of alkanes, which might cause the increased extraction efficiency of lithium. The solvation numbers of divalent ion-D2EHPA complex were slightly increased as the alkane chain length increased. It implies that alkanes with relatively long chain which has greater hydrophobicity and lower water solubility tend to interfere the formation of divalent cation-D2EHPA complex, and thus more lithium-D2EHPA complex could be formed.

In addition, selectivity of divalent cations over lithium ($S = \frac{D_{divalent\ cations}}{D_{lithium}}$) was determined as shown in Fig. 4.3.4. Except for calcium, in which removal

efficiency was over 99.9% in all conditions, divalent cations such as Sr, Ba, and Mg in n-hexane solution showed the highest selectivity values in n-hexane-containing solutions, among others. As expected from the solvation number changes of cation-D2EHPA complexes, the selectivity values decreased as the chain length of alkanes increases, which means that relatively large amount of lithium has been moved to organic phase.

After removing most of the divalent ions in the produced water, eight stage solvent extractions for selective lithium recovery were conducted as shown in Fig. 4.3.5. In Fig. 4.3.5, sodium, whose chemical affinity with D2EHPA is the weakest among several others, showed negligible extraction efficiency throughout the repetition. The lithium recovery efficiency reached over 20% after eight cycles of the extraction, but the efficiency did not show a significant difference in various alkane types. Although the recovery efficiency does not show a significant change in Fig. 4.3.5, Table 4.3.1 shows the selectivity of lithium over a competitive cation (i.e., sodium)., which decreased with increasing chain length of alkanes. Selectivity was especially decreased in n-hexadecane solution by about 40%, compared to that in n-hexane solution.

Without alkanes in the produced water, the lithium selectivity over sodium at second stage was infinite because no sodium was extracted into the organic phase (Jang et al., 2017). Therefore, it was found that the existence of alkanes caused significant decrease in the selectivity during the solvent extraction.

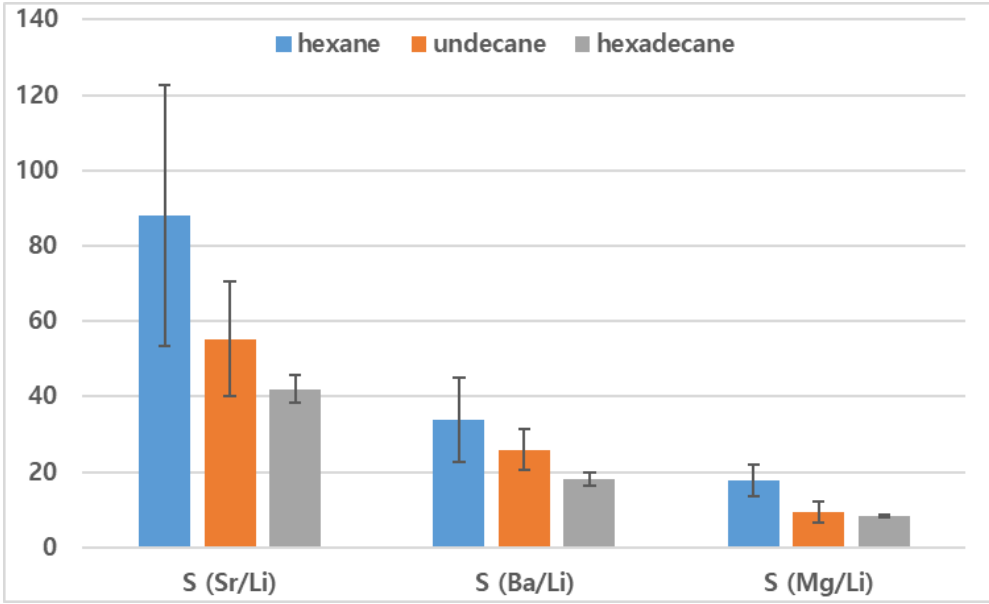

Fig. 4.3.4. Selectivity of divalent cations over lithium after first-step extraction.

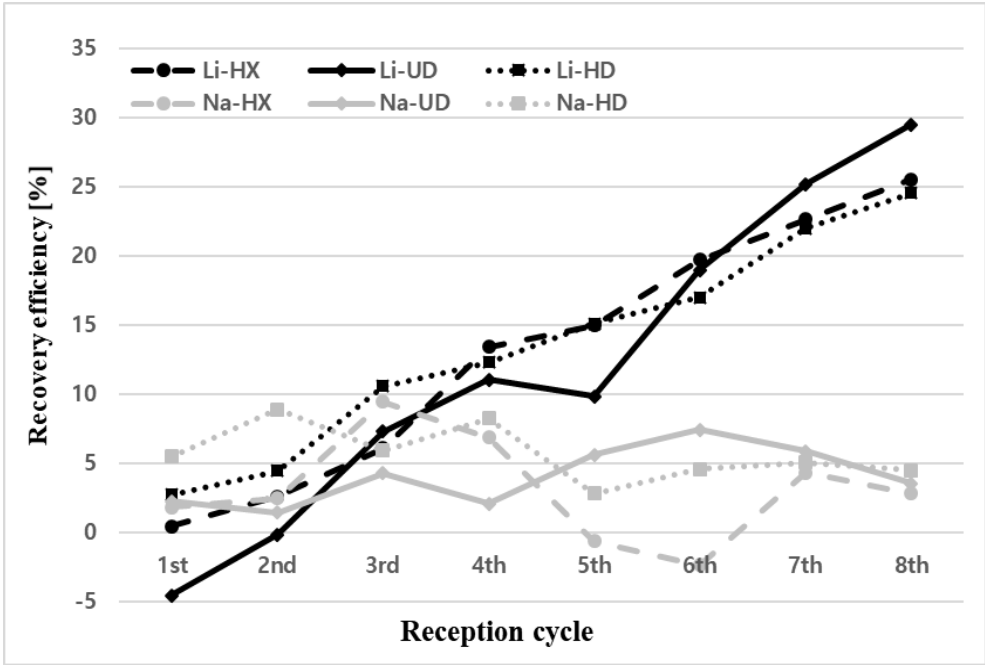

Fig. 4.3.5. Multistage solvent extraction results of monovalent cations in the produced water, containing n-hexane (HX), n-undecane (UD), and n-hexadecane (HD).

Table 4.3.1 Selectivity of lithium over sodium in second-stage extraction

	$S_{Li/Na}$
n-Hexane	11.7
n-Undecane	11.4
n-Hexadecane	6.9

4.4 Effect of different concentrations of hexane during lithium recovery using solvent extraction

To investigate the influence of the organics concentration, the extraction processes of major cations were conducted in the produced water with 1,174 mg/L and 2,348 mg/L of n-hexane (assuming 2,348mg/L as a 100% TOC concentration). The results from the produced water without alkanes (0%) were taken from previous research by Jang et al. (2017).

Figure 4.4.1 depicts the extraction efficiency of cations in the fluids during eight stage solvent extractions. After the first step of solvent extraction, over 90% of divalent ions were removed in the order of $Ca^{2+} > Sr^{2+} > Ba^{2+} > Mg^{2+}$. The calcium ions were removed by 98% during the first extraction in every condition, and 99.9% was extracted after eight extraction cycles. The other divalent cations such as Mg, Sr, and Ba showed relatively high removal efficiency. In particular, the extraction efficiency of those ions after the first cycle decreased by about 25% with the addition of hexane 1,174 mg/L (50%). Decreases in the 1st cycle extraction efficiency were not noticeably different with different hexane concentrations. The effect of alkanes starts to diminish after the 3rd cycle of repetitions, which became insignificant when the 8th cycle of extraction was completed. The final removal efficiency differences between 0% and 50% hexane conditions for Mg, Sr, and Ba were 3.3%, 1.7%, and 1.0%, respectively.

Only the lithium ion showed increased extraction efficiency as the hexane concentration increased. The lithium removal efficiency in the solution after eight stages of extraction with no organics with no organics was 33.3%, and the efficiency increased up to 44.9% and 42.3% when 1,174mg/L and 2,348mg/L of

hexane were added.

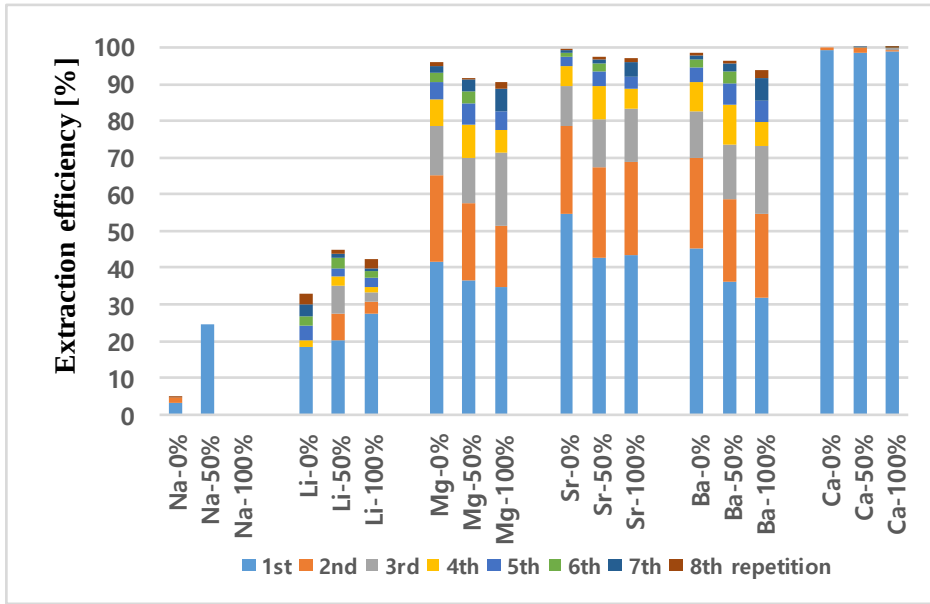

Fig. 4.4.1 Multistage solvent extraction efficiency of major cations in the synthetic produced water containing no organics (0%), hexane with 50% of TOC concentration, and hexane with 100% of TOC concentration.

The FT-IR spectra of metal-D2EHPA complex with and without hexane are shown in Figure 4.4.2. After the first stage of solvent extraction with no organics in the produced water, the absorbance of P=O bond and P-O-H bond decreased (line ③), which indicates that the metal-D2EHPA complex was formed. The absorbance decrease on 1230 cm^{-1} is due to the metal ions bond formation in P=O bond, and the absorbance decrease on 1034 cm^{-1} is due to the replacement of hydrogen to metal atom on the P-O-H bond. This IR spectrum result of D2EHPA-metal extraction is similar with many other research (Jin et al., 2013; Guozhi et al., 2016). To investigate the influence of hexane, the FT-IR spectra of metal-D2EHPA complex in the produced water including hexane (line ②) was obtained. The result showed that the formation of the complex but the absorbance peaks were higher than those without hexane. It means that hexane might cause interference on loading metal ions during the solvent extraction. The D2EHPA is a well known hydrophobic extractant (Warshawsky et al., 2002) and also n-alkanes are hydrophobic (Naether et al., 2013). The effect of a segment of alkyl chain of D2EHPA can be entangled with another hydrophobic association and the alkane which has a long alkyl chain has greater hydrophobicity than short alkanes (Gao et al., 2017). Therefore, the metal-D2EHPA forming mechanism can be interfered by the hydrophobic interaction of alkane and D2EHPA.

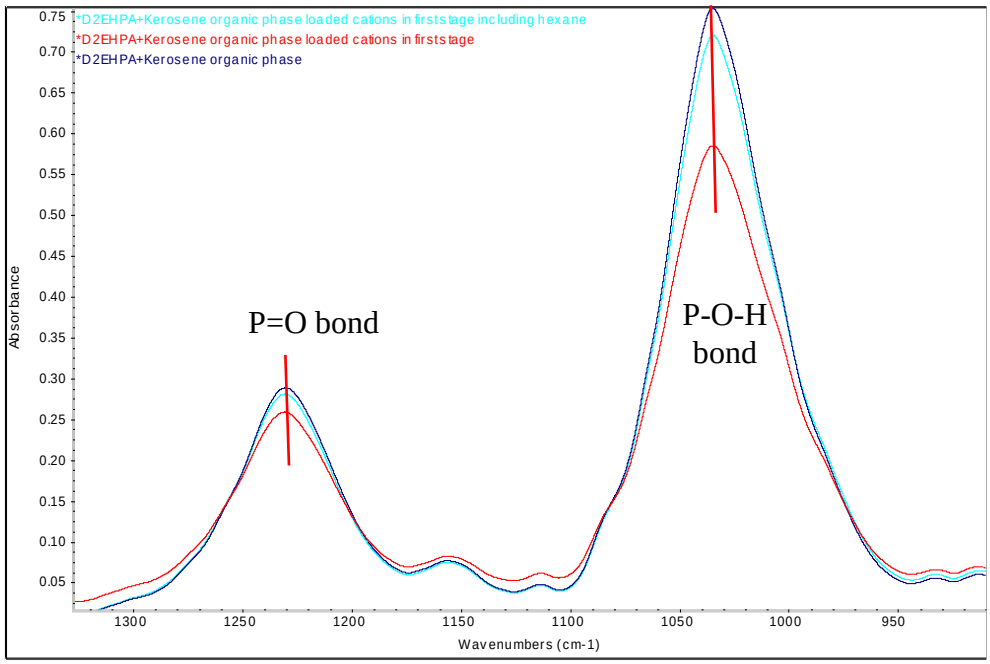

Fig. 4.4.2. FT-IR spectra. ①-D2EHPA+Kerosene, ②-D2EHPA+Kerosene after 1st stage solvent extraction of the produced water containing hexane (100 % TOC), ③-D2EHPA+Kerosene after 1st stage solvent extraction of the produced water without hexane.

According to Silva et al. (2005), the removal efficiency of organic pollutants in soil through solvent extraction would change with the different concentrations of organics. In their study, sand (in which carbon content was higher), showed greater pollutant removal efficiency than soil.

As expected from the extraction efficiency of lithium and divalent cations, such as Sr, Ba, and Mg, the selectivity of divalent cations over lithium significantly decreased when n-hexane was added to the solution (Figure 4.4.3). Regardless of its concentration, the selectivity in the solution with hexane was less than half of that in the solution without hexane.

As shown in Figure 4.4.4, lithium showed higher recovery efficiency than sodium throughout the eight extraction cycles, due to their different affinity to the extractant. In addition, no obvious increase or decrease was observed in the lithium recovery efficiency with n-hexane concentrations in the solution. Thus, the selectivity of lithium over sodium varied. The selectivity value was infinite when there was no addition of hexane, as a negligible amount of sodium was extracted (Table 4.4.1). However, relatively low selectivity was observed in 50% hexane solution, with selectivity of lithium over sodium increasing as the alkane concentration increased to 100%.

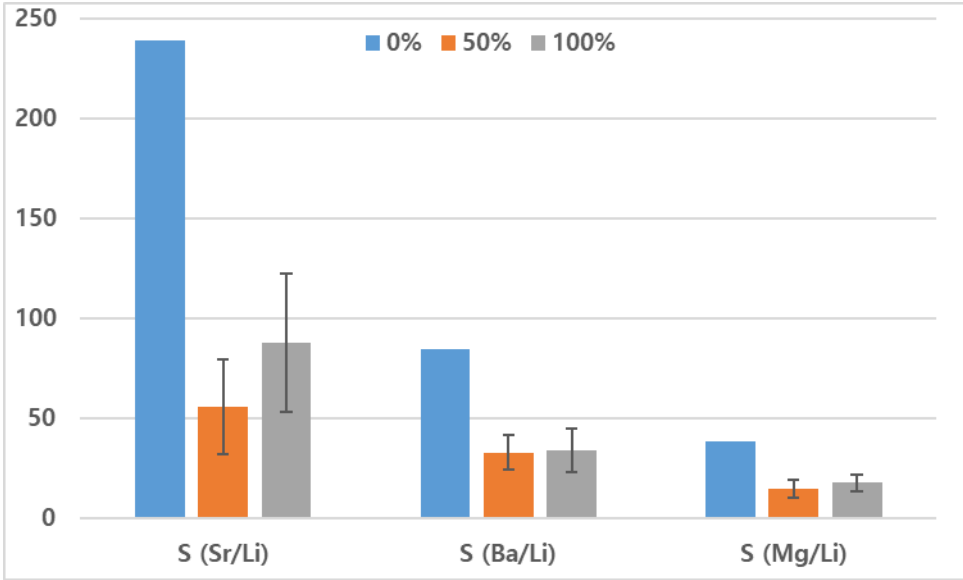

Fig. 4.4.3. Selectivity of divalent cations over lithium after first-step reaction.

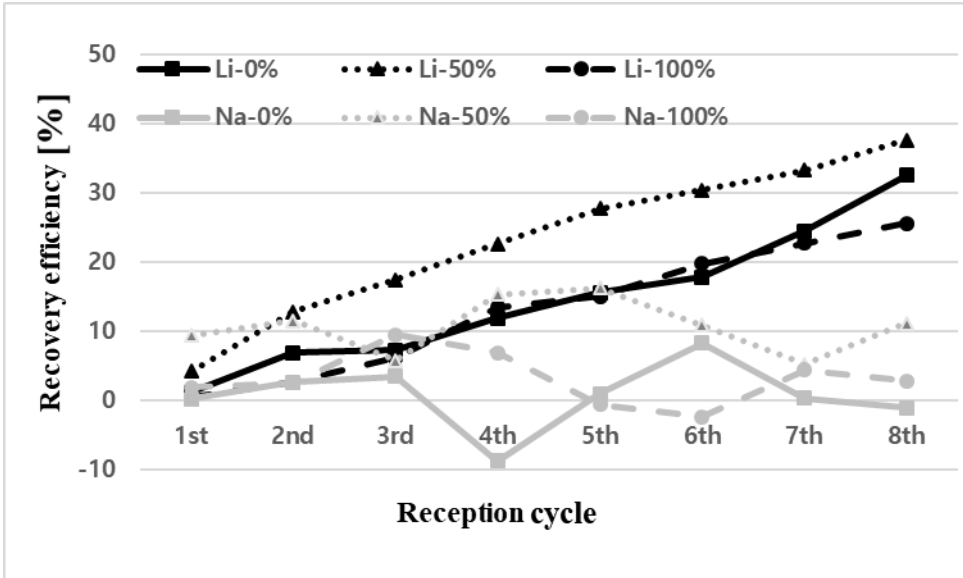

Fig. 4.4.4. Multistage solvent extraction results of monovalent cations in the produced water, containing no organics (0%), 1,174 mg/L (50%), and 2,348 mg/L (100%) of n-hexane

Table 4.4.1 Selectivity of lithium over sodium in the second-stage extraction

	$S_{Li/Na}$
Hexane 0%	-
Hexane 50%	4.8
Hexane 100%	11.7

4.5 Overall recovery efficiency of lithium

After the two-step extraction process, overall extraction efficiency for lithium were calculated and shown in Figure 4.5.1. Although the results of second-step extraction for lithium recovery did not show a significant difference for various types of alkanes, the final recovery efficiency for lithium decreased with an increased alkane chain length - mainly due to the loss of lithium in the first stage of the process. With different concentrations of n-hexane, the overall recovery efficiency declined as the concentration increased to 100% (2,348 mg/L), also caused by the first step for divalent removal, as recovery efficiency generally depend on extraction efficiency in the first stage.

After using the extraction processes, the loaded ions can be easily stripped using acidic solutions (Harvianto et al., 2016; Zhou et al., 2019). Many studies have compared various types of inorganic and organic acids for leaching (Harvianto et al., 2016). The usage of strong acids allows high leaching efficiency to be achieved thus HCl solution was used in this dissertation (Urbańska, 2020). The Li loaded organic phase after the second stage was stripped using equal volume of 0.2 M HCl solution. Stripping efficiency of the produced water with no alkanes, hexane in 100% of TOC concentration, and hexadecane in 100% of TOC concentration was shown in Figure 4.5.2 and the total lithium recovery considering the two-step extraction and stripping process were calculated and shown in Figure 4.5.3. As shown in Figure 4.3.1 and 4.4.1, the existence of alkanes influences dominantly on the first cycle and the effect is diminished as the extraction cycle repeats and it was expected the stripping efficiency did not show significant change with the existence of alkanes or their type. However, the result implies that some

portion of alkanes could move to the organic phase and affect the stripping of lithium.

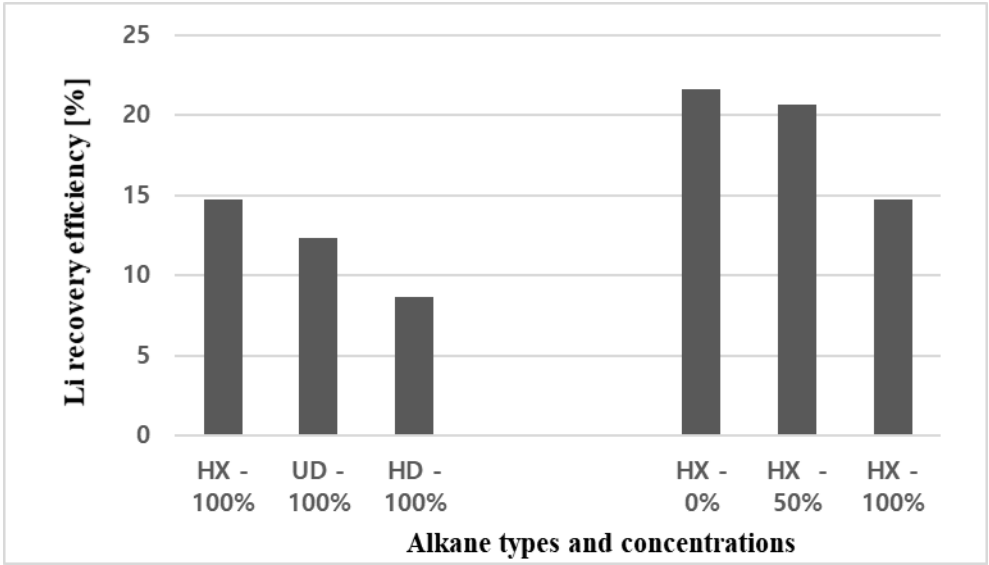

Fig. 4.5.1. Li recovery efficiency after 2 steps of solvent extraction in the shale gas produced water, containing different types and concentrations of alkanes.

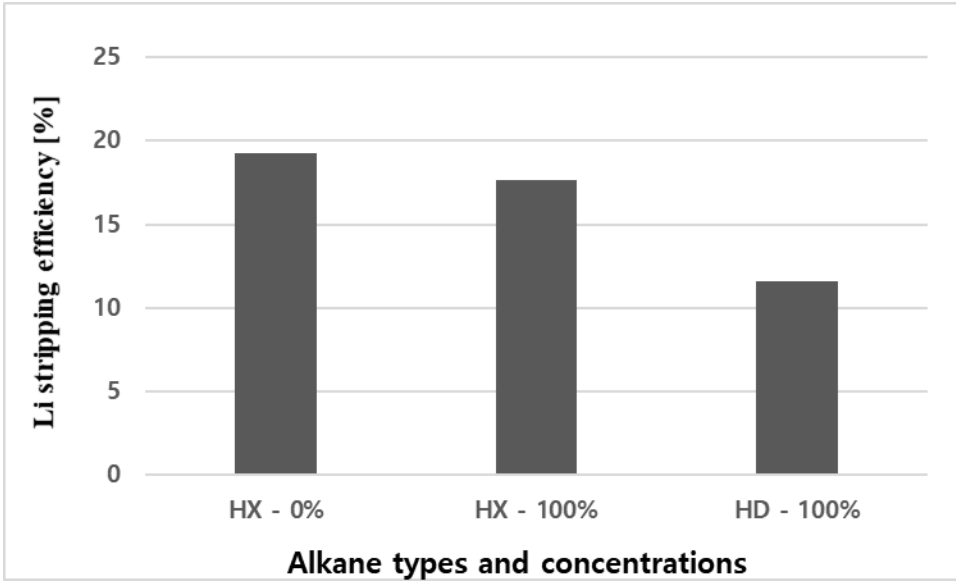

Fig. 4.5.2. Li Stripping efficiency after 2 stages of extraction process using 0.25M HCl containing no organics, hexane and hexadecane with 100% TOC concentration.

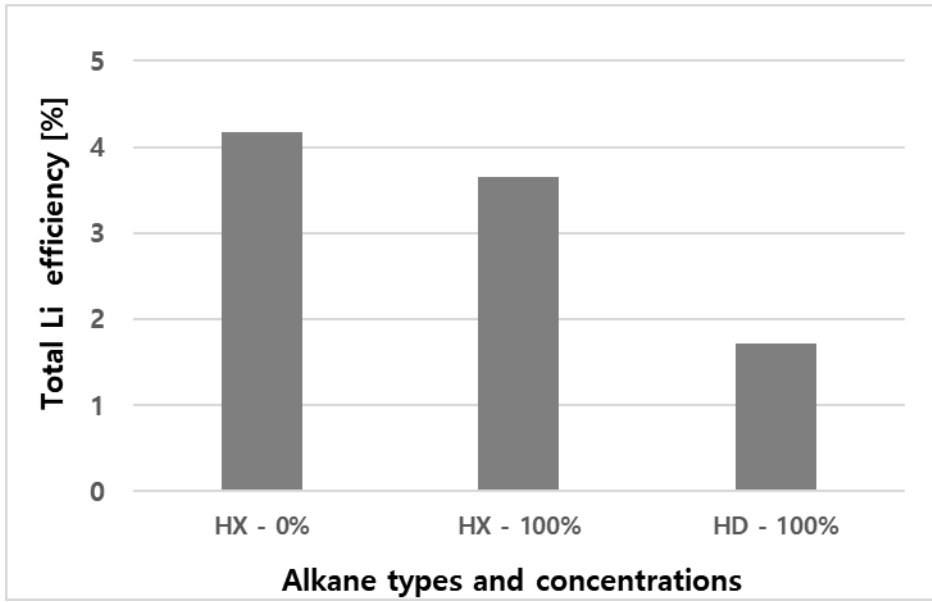

Fig. 4.5.3. Total Li recovery containing no organics, hexane and hexadecane with 100% TOC concentration.

4.6 Improvement of lithium recovery (pretreatment)

Marcellus produced water TOC was measured 2,348 mg/l as an average value (Maguire-Boyle and Barron, 2014), hence the previous article describes that the different types of organic compounds were injected 2,348 mg/l each in the synthetic produced water (Lee and Chung., 2020b). However due to the same volume of mixture of fracturing fluid and shale formation water, organic compounds like isopropanol and polyacrylamide are also included in the fracturing fluid (Jang et al., 2017).

Table 4.6.1 shows the TOC of synthetic produced water before and after applying the activated carbon. The TOC of the synthetic produced water considering the hexane 2,348 mg/l and the organic compounds that coexist in the original fracturing fluid composition shows the value of 3,561-3,795 mg/l. This value of TOC was considered 100% of TOC in the shale gas produced water and activated carbon as an adsorbent was injected 1.63 mmol (molar ratio of 1:1 of TOC) for mixing, and after applying the activated carbon, the TOC of the synthetic produced water was measured 3.3-4.4 mg/l that shows a removal efficiency higher than 99.9 %.

Table 4.6.1 TOC measurements of produced water

TOC measurements of produced water (mg/l)	
Before applying AC	3561-3795
After applying AC	3.3-4.4

Selective precipitation of divalent ions was applied using $Ca(OH)_2$ and Na_2CO_3 for the low influence of lithium ions in the produced water. The ion concentration changes and removal ratio of each cations for the first and second experiment and including the total removal ratio including applying activated carbon is shown in Table 4.6.2 and Figure 4.6.1 respectively.

The TDS of the solution before and after the pretreatment was measured by using the conductivity value. As assuming the TDS/EC (k) value of brine water as 0.75 (Rusydi. 2018), the average TDS of the solution before pretreatment, after applying AC, $Ca(OH)_2$ and Na_2CO_3 were measured 144,638, 144,375, 139,913, and 135,113 mg/L respectively. The solution TDS decreased 6.6 % after all the pretreatments compared to the initial solution.

In the first precipitation stage, Mg^{2+} ions showed a 87.3% removal and Li^{+}, Sr^{2+}, and Ba^{2+} showed a removal efficiency lower than 10.3%. The Ca^{2+} showed an 3.4% increase due to the usage of $Ca(OH)_2$ precipitant. After removing most of the Mg^{2+} ions, Ca^{2+}, Sr^{2+}, and Ba^{2+} showed a removal rate higher than 91% during the chemical precipitation by applying Na_2CO_3. The total removal rate considering adsorption-2 steps of precipitation was also measured and Ca^{2+}, Sr^{2+}, and Ba^{2+} showed a removal rate higher than 91% and Li showed an 7.2% removal rate. Compared with the previous study Jang et al. (2017), lithium recovery is unfavorable due to a high loss (25.1%) during the removal stage by only using D2EHPA. For an effective method to remove the divalent ions with decreasing the lithium loss, applying activation carbon adsorption and precipitation method using $Ca(OH)_2$ and Na_2CO_3 are preferred.

Table 4.6.2 The composition changed of the produced water by the pretreatment using AC, $Ca(OH)_2$, and Na_2CO_3 (mg/L)

Synthesized Produced water	Before applying pretreatment	After applying AC	After applying $Ca(OH)_2$	After applying Na_2CO_3
pH	5.8-6.3	6.8-7.1	10.7-10.9	10.5-11.5
Conductivity (mS/cm)	192.2-193.5	192.1-192.9	185.5-187.6	179.6-180.7
Ca	1331.5-1573.9	1020.2-1230.5	1312.1-1334.3	223.8-390.6
Li	72.1-74.6	71.0-73.1	68.6-70.5	66.5-72.0
Na	21273.6-21536.4	20056.1-20841.3	19828.9-20056.1	26929.3-27125.3
Sr	2089.7-2126.6	2013.9-2029.5	1029.5-1129.7	92.1-103.1
Mg	617.4-630.5	608.2-622.5	34.7-46.5	16.3-18.3
Ba	1697.8-1748.0	1576.2-1661.9	1418.2-1494.8	15.7-29.7

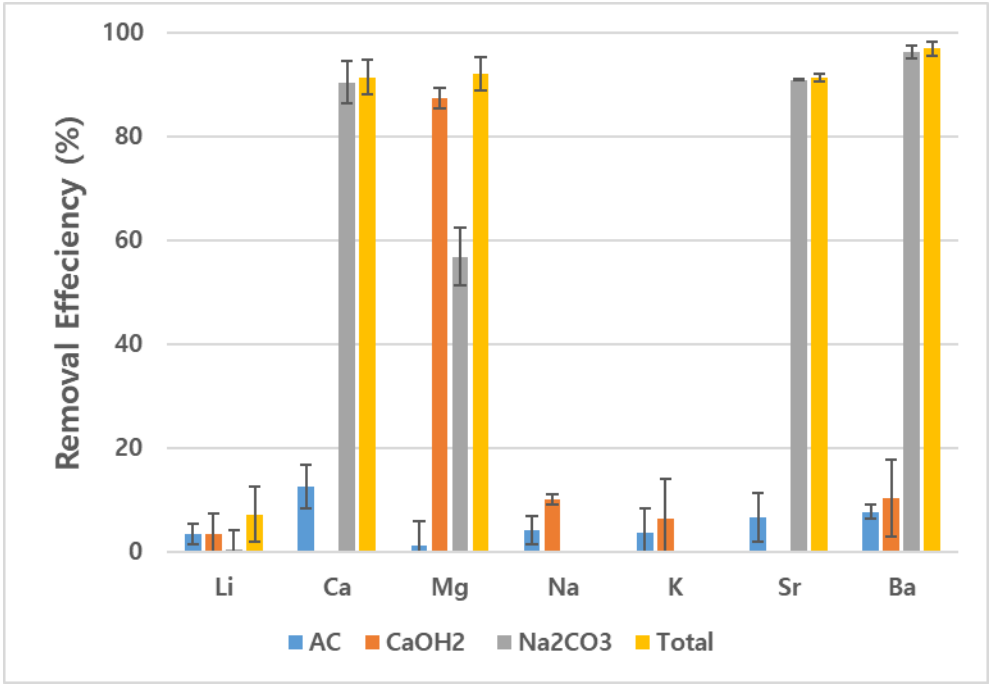

Fig. 4.6.1. The removal efficiency of cations after applying (1) Activated carbon, (2) $Ca(OH)_2$ (molar ratio of 1:1 of Mg^{2+}), (3) Na_2CO_3 (molar ratio of 1:1.2 of Ca^{2+}, Sr^{2+}, and Ba^{2+}), (4) Total removal rate.

Figure 4.6.2 shows the image (a) of the sample (× 300) and EDX peak results (b) after the first precipitation step applying $Ca(OH)_2$ and Figure 6.4.4 shows the image (a) of the sample (× 400) and EDX peak results (b) after the second precipitation step applying Na_2CO_3. Figure 4.6.3 and 4.6.5 shows the XRD diffractogram of the precipitation sample after the first and second precipitation step respectively.

The SEM images of the sediment by using $Ca(OH)_2$ and Na_2CO_3 showed a similar morphology as shown in Chap 3. The precipitation sample from the first removal step contains Na (7.11%), Mg (0.65%), Cl (5.89%), Ca (27.34%), Sr (3.89%), Ba (5.22%), and O (49.91 %) as elemental components. Due to the SEM-EDS results, the Mg minerals were precipitated due to chemical precipitation and due to the large amount of Ca^{2+} and Na^{+} included in the produced water, additional Na and Ca-containing minerals were also observed (Fig 4.6.2). Fig 4.6.3 shows the XRD diffractogram results of the sample after the first removal step. The precipitation sample is composed with calcium carbonate related minerals ($CaCO_3$) like vaterite and calcite which corresponds to [(002), (100), (101), (102), (004), (110), (112), (104), (202), (114), (006), (204), (106), (212), (300), (302), and (206)] and [(012), (104), (110), (113), (202), (024), (116), (211), (122), (214), (125), (300), (217), (128), (036), (0,1,14), (134), (318)]. Also halite (NaCl) which corresponds to [(111), (200), (220), (222), (400), (331), (420), and (422)] planes were observed. The SEM-EDS and XRD results shows a high amount of Ca bearing minerals. Due to a high amount of Ca^{2+} (10,985-11,796 ppm) compared to Mg^{2+} (869-919 ppm) in the synthesized produced water, the SEM-EDX showed a small amount of Mg composition and XRD mostly showed the Ca-related metal ions for the precipitation.

The precipitation sample from the second removal step contains Na (1.64%), Mg (0.92%), Cl (6.13%), Ca (32.90%), Sr (3.17%), Ba (3.55%), and O (51.68 %) as elemental components. Due to the SEM-EDS results, the Ca^{2+}, Sr^{2+}, and Ba^{2+} minerals were precipitated due to chemical precipitation and due to the large amount of Na^{+} included in the produced water, additional Na containing minerals were also observed (Fig 4.6.4). Fig 4.6.5 shows the XRD diffractogram results of the sample after the second removal step. The precipitation sample is composed with vaterite ($CaCO_3$) that corresponds to [(002), (100), (101), (102), (110), (104), (202), (006), (106), and (212)] and sodium chloride which corresponds to [(111), (200), (220), (222), (400), (331), (420), and (422)] planes. The XRD results shows a high amount of Ca and Na bearing minerals. Due to the SEM-EDS and XRD results, Ca containing minerals were mostly precipitated due to chemical precipitation and Sr^{2+} and Ba^{2+} showed a small composition out of the precipitated sample due to the SEM-EDS data.

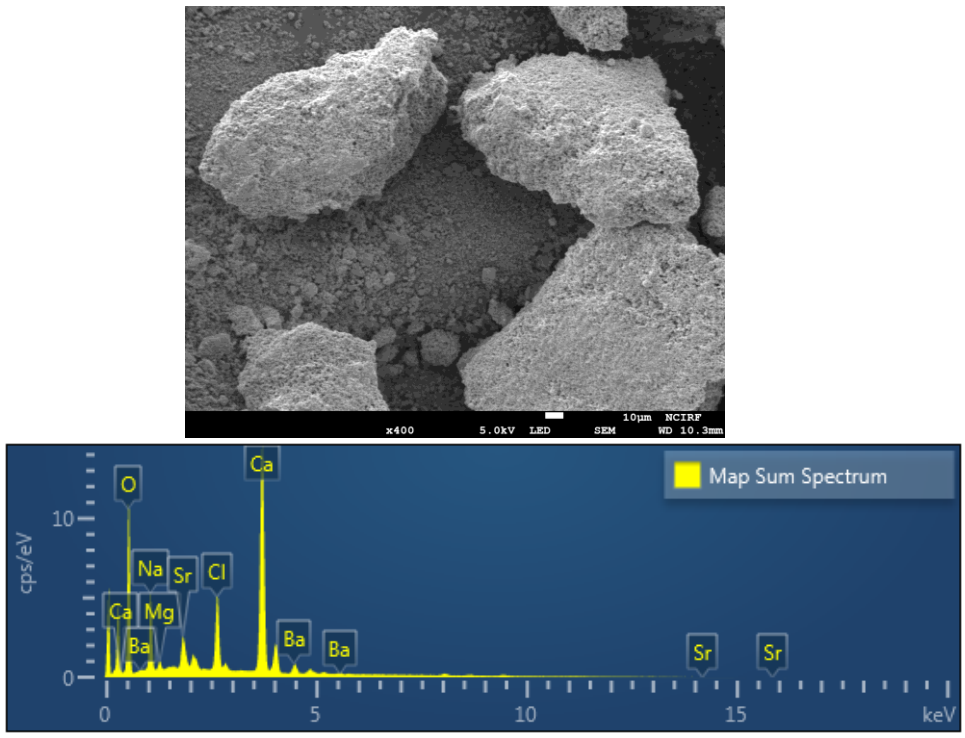

Fig. 4.6.2. SEM-EDX micrographs of precipitation after applying $Ca(OH)_2$ (a) Image of the sample, (b) EDX peak of precipitation.

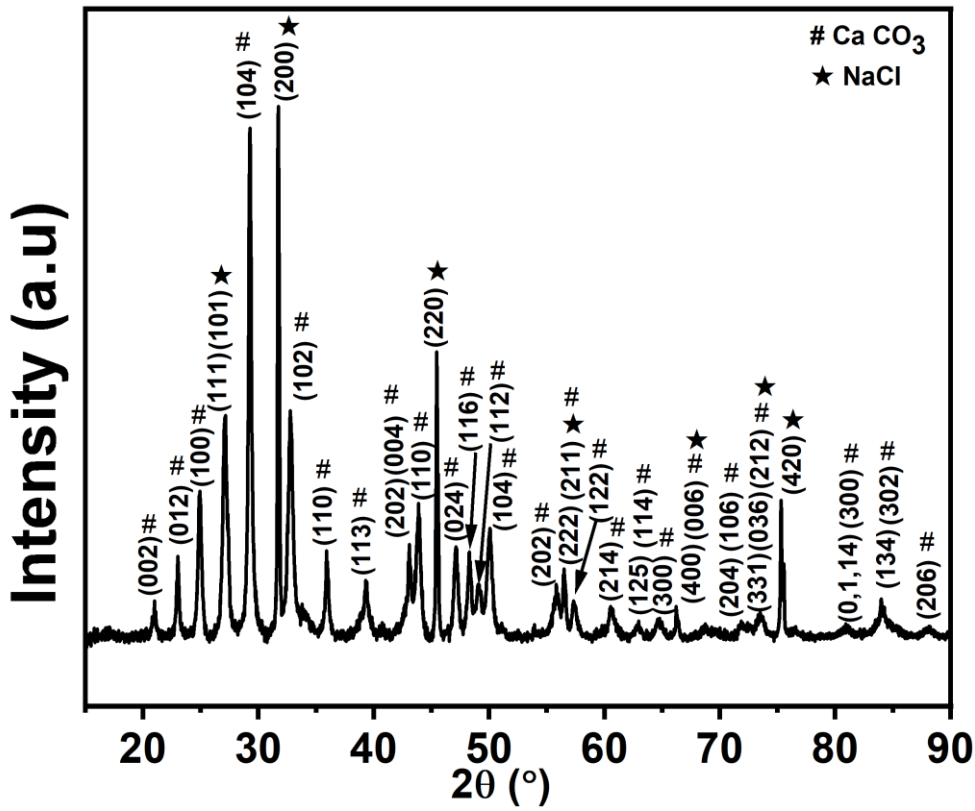

Fig. 4.6.3. XRD diffractogram of the precipitation after applying $Ca(OH)_2$.

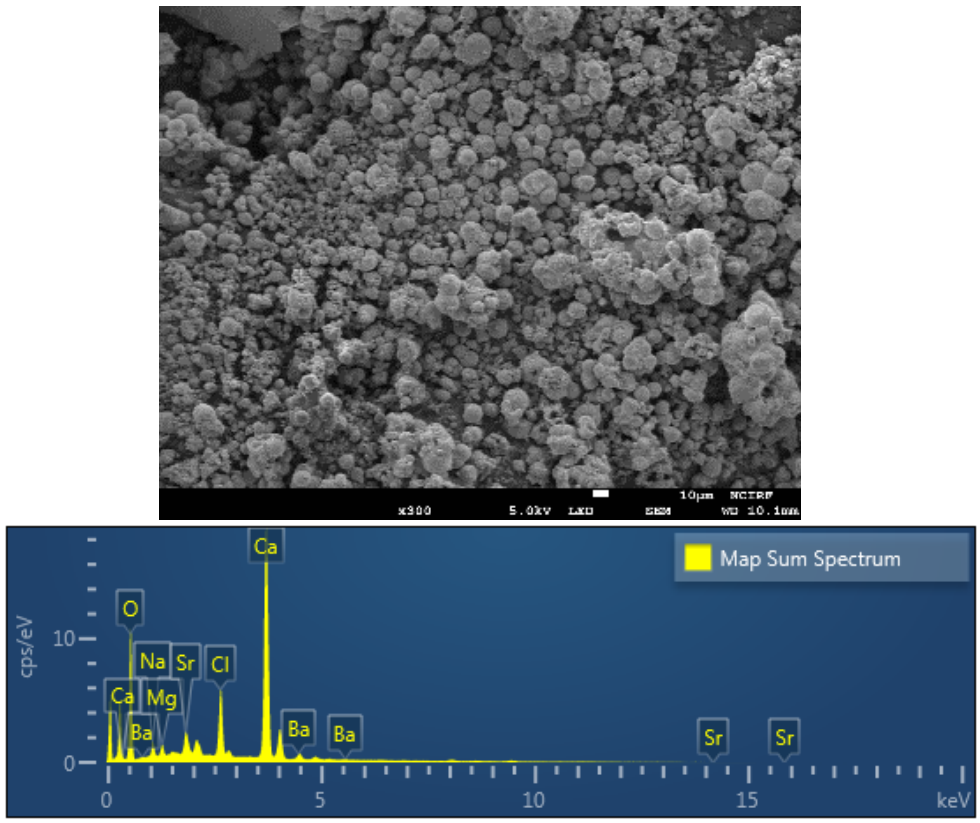

Fig. 4.6.4. SEM-EDX micrographs of precipitation after applying Na_2CO_3. (a) Image of the sample, (b) EDX peak of precipitation.

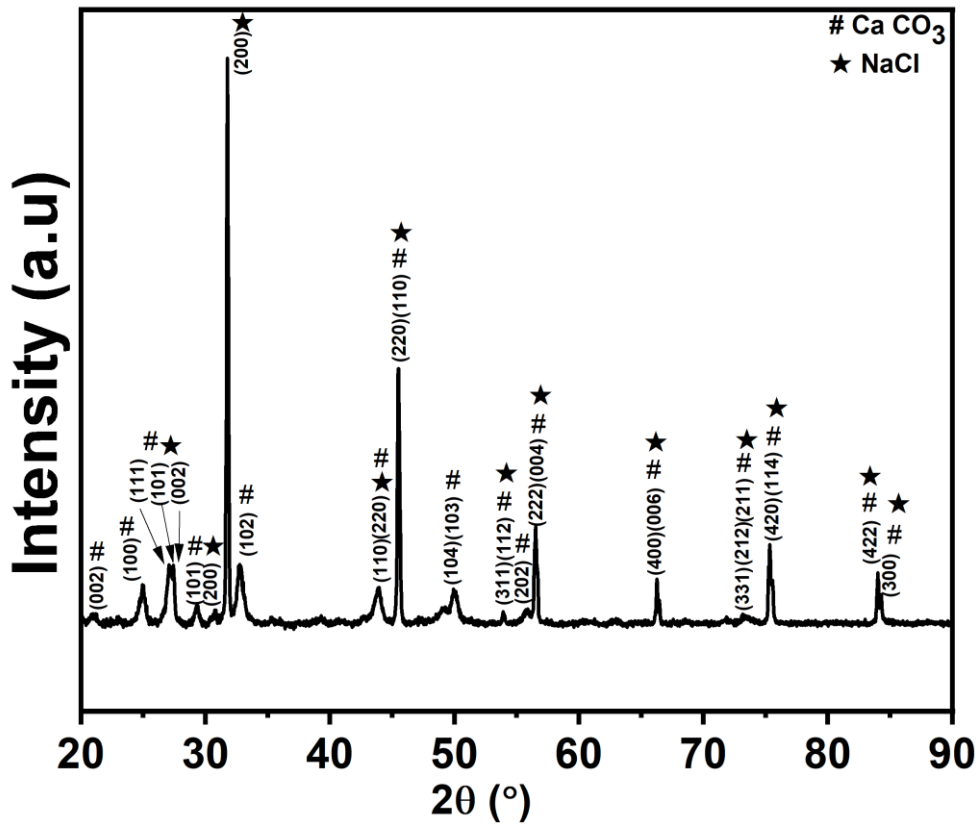

Fig. 4.6.5. XRD diffractogram of the precipitation after applying Na_2CO_3.

Two stages of chemical precipitation using $Ca(OH)_2$ and Na_2CO_3 were applied to remove metal ions from the synthesized produced water. By applying $Ca(OH)_2$, more than 87% of Mg^{2+} were removed, and Na_2CO_3 removed more than 91% of Ca^{2+}, Sr^{2+}, and Ba^{2+} from the synthesized geothermal fluid. The total removal rate considering adsorption and 2 steps of precipitation showed a removal rate higher than 91% for Ca^{2+}, Mg^{2+}, Sr^{2+}, and Ba^{2+}. Lithium ions showed an insignificant change (7.2 %) due to adsorption and 2 stages of chemical precipitation. As explained in Chap 3, the usage of $Ca(OH)_2$ and Na_2CO_3 for removal stage cannot be economical for the industry application. Thus the usage of waste like limestone ($Ca(OH)_2$) and salt rock (Na_2CO_3) can be a substitution for the removal process that can be used in this experiment to remove silicate or divalent ions (Kasikowski et al., 2008; Galván-Ruiz et al., 2009).

4.7 Synthesis of ionic liquid

Ionic liquid was used as an extractant after removing organic compounds and divalent ions from the synthesized produced water. and the IL extracting agent [Cyphos IL 101][D2EHPA] (1 M) was synthesized in two steps. The first step was to prepare equimolar concentrations of Cyphos IL 101 and D2EHPA in kerosene and was mixed in a separatory funnel. In order to remove the H^+ from D2EHPA and the Cl^- from Cyphos IL 101, $NaHCO_3$ was added into the separatory funnel to make a production of [Cyphos IL 101][D2EHPA]. The proposed chemical reaction of the ionic liquid involved in the process is shown on equation 4.7.1 and 4.7.2 as in two steps.

$$PR_4Cl + HD2EAPA \rightarrow PR_4Cl\text{-}HD2EAPA \quad (4.7.1)$$

$$PR_4Cl\text{-}HD2EAPA + NaHCO_3 \rightarrow PR_4\text{-}D2EAPA + NaCl\,(s) + CO_2\,(g) + H_2O\,(l) \quad (4.7.2)$$

To understand the detailed reaction mechanism for the ionic liquid, D2EHPA, Cyphos IL 101, and PR_4-D2EAPA was analyzed through FT-IR and ^1H NMR spectroscopy. IR and NMR data of all compounds were shown in Figures 4.7.1 and 4.7.2. The FT-IR spectra of D2EHPA, Cyphos IL 101 and 2 reactions of synthesis of ionic liquid are shown in Figure 6.4.1. IR data of D2EHPA shows an absorbance of P=O bond(1230 cm^{-1}) and P-O-H bond(1034 cm^{-1} and 1700 cm^{-1}). After the first step of the reaction, a slightly lower intensity of the P-O-H was observed. A lower P-OH peak was observed compared to the first reaction when the base ($NaHCO_3$) was added to the PR_4Cl-HD2EAPA (second step), indicating the possibility of

dissociation of D2EHPA dimer and formation of ionic liquid PR_4-D2EAPA. Moreover, the P=O absorbance peak of ionic liquid PR_4-D2EAPA was observed at a higher value than that of D2EHPA (Fig 4.7.1, 2^{nd} reaction), which may be due to the absence of intra-molecular hydrogen bonding in the ionic liquid PR_4-D2EAPA and the strong bond (O=P-O-) is formed with the more electronegative element (Nitrogen). These IR results shows the possibility for the synthesis of the ionic liquid and dissociation of the P-OH bond from the dimer D2EHPA. For an additional support for the P-OH bond dissociation NMR was also used to analyze the functional structure change.

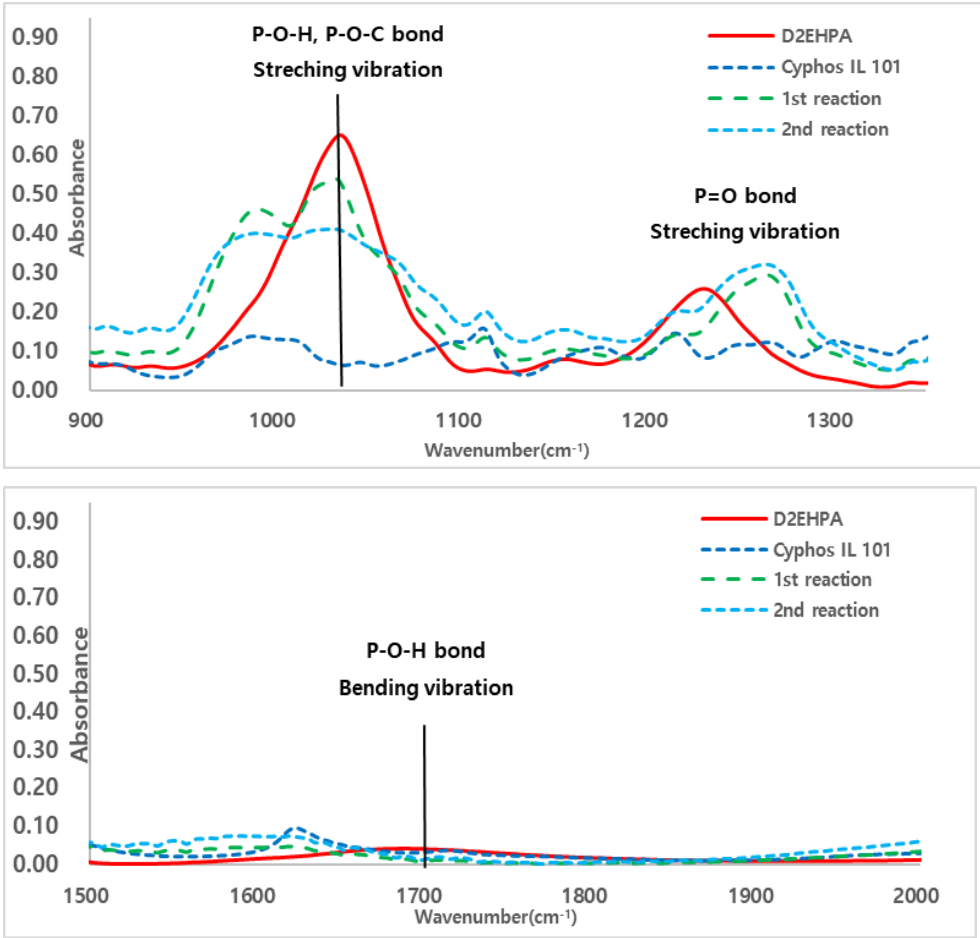

Fig. 4.7.1. FT-IR spectra of samples for each reaction (a) P-O-C, P-O-H, and P=O bond stretching vibration, (b) P-O-H bond bending vibration.

For the and ^{1}H NMR spectroscopy, all the samples were dissolved in a $CDCl_3$ solvent and the two reactants D2EHPA and Cyphos IL 101 showed the similar ^{1}H NMR results with other research (B. Dalai et al., 2015; Anderson et al., 2009). The peaks that is located between 0.8 and 1.6 ppm is interpreted to be the protons of alkyl chains. The equimolar amount of D2EHPA and Cyphos IL 101 was first reacted and the mixture shows the chemical shifts of $–PCH_2$ (2.4 ppm) and $–OCH_2$ (3.9 ppm) group originated from D2EHPA and Cyphos IL 101 respectively (Fig 4.7.1a and 4.7.1b). $NaHCO_3$ was added to wash the sodium chloride formed during the first reaction and the ^{1}H NMR results (4.7.1c) show that the functional group -OH from D2EHPA was deprotonated as the peak at 8.6 ppm disappears to form an ionic form with PR_4^+. D2EHPA exists predominantly as a dimer form in nonpolar organic solvents (Jang et al., 2017). As the D2EHPA forms to an ionic liquid, the hydrogen bond ability decreases and enhances its complexation ability towards the targeting metal ions (Zante et al., 2020).

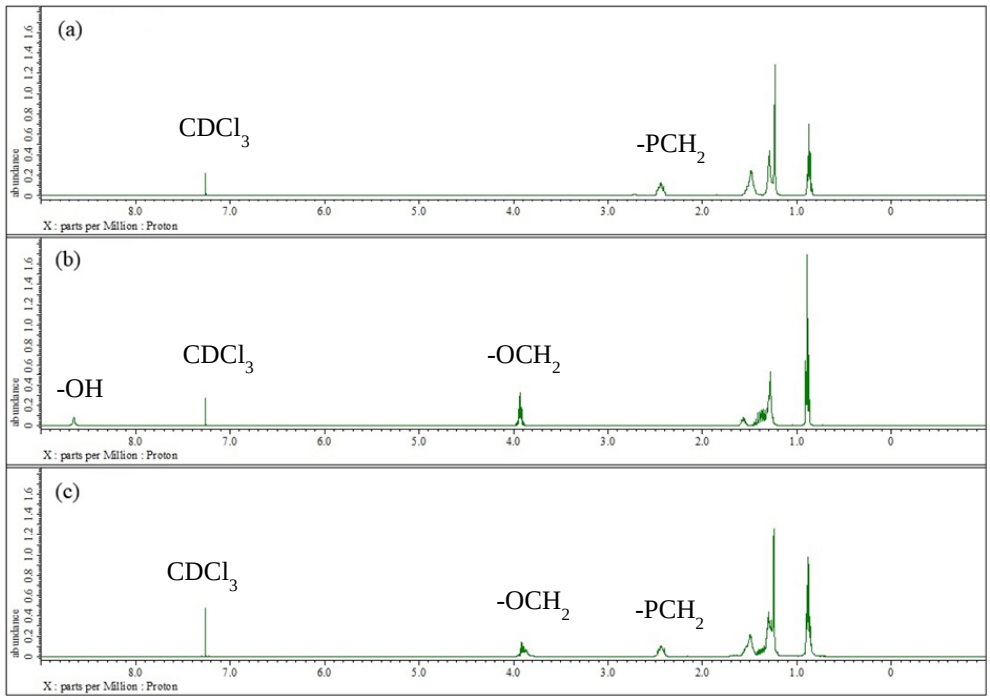

Fig. 4.7.2. ^{1}H NMR (400 MHz) spectra of (a) Cyphos IL 101, (b) D2EHPA, and (c) Ionic liquid [Cyphos IL 101][D2EHPA] form of the extractant in $CDCl_3$.

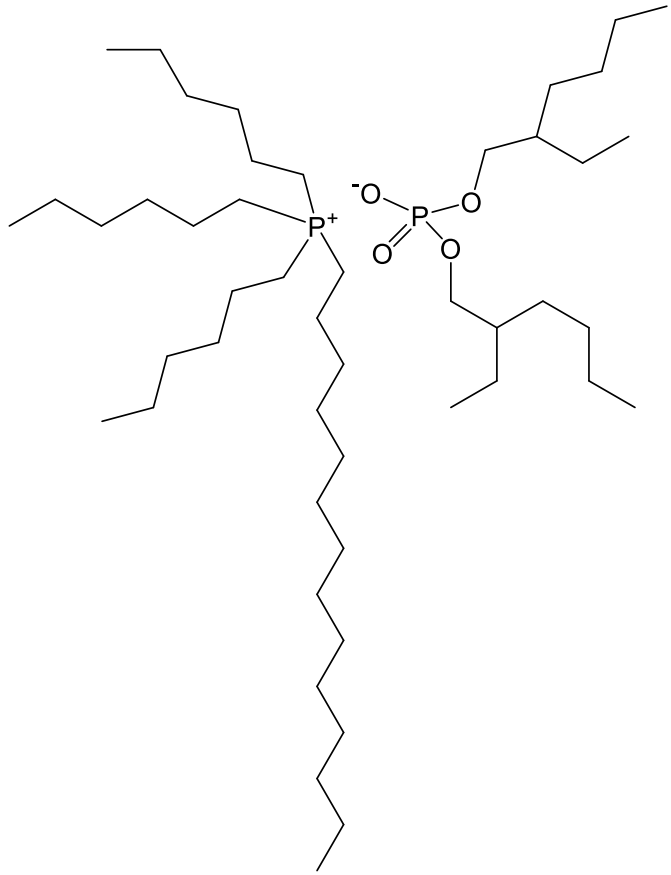

Fig. 4.7.3. Structure of the ionic liquid [Cyphos IL 101][D2EHPA]

4.8 Improvement of lithium recovery (solvent extraction)

Solvent extraction was applied for three different dilution levels (No dilution, 25×, and 50×) for produced water using D2EHPA 1M after removing organic compounds and divalent ions (Fig 4.8.1). The dilution was held by using deionized water. When no dilutions were implemented, lithium showed a lower removal efficiency than 30 %. In the 25 and 50 times diluted synthesized produced water, lithium was extracted 58.5 % and 45.9 % respectively. The lithium selectivity over sodium for the different dilution levels (No dilution, 25×, and 50×) showed 27.3, 58.5, and 45.9 respectively. The optimal condition was selected as 25 times produced water considering the highest lithium extraction efficiency and selectivity.

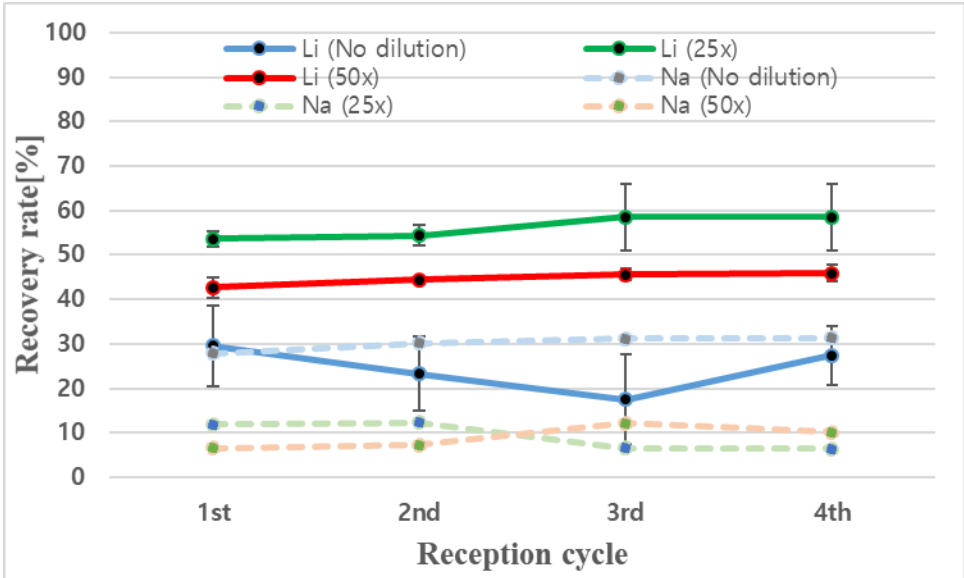

Fig. 4.8.1. Multistage solvent extraction efficiency of Li and Na in the three different dilution levels (No dilution, 25×, and 50×) of produced water using D2EHPA 1M.

The 25 times diluted produced water was chosen for the solvent extraction tests hence different concentrations of D2EHPA (0.3, 0.5, and 1.0M) were applied to select the most optimal extractant concentration (Fig. 4.8.2). All the different concentrations of D2EHPA (0.3, 0.5, and 1.0M) showed a similar lithium extraction efficiency from 54.1 to 60.6 however the lithium selectivity over sodium for the different dilution levels showed 9.4, 9.8, and 20.7 respectively. The optimal condition of D2EHPA concentration was selected as 1.0 M and 25 times of dilution for produced water considering the highest lithium extraction efficiency and selectivity.

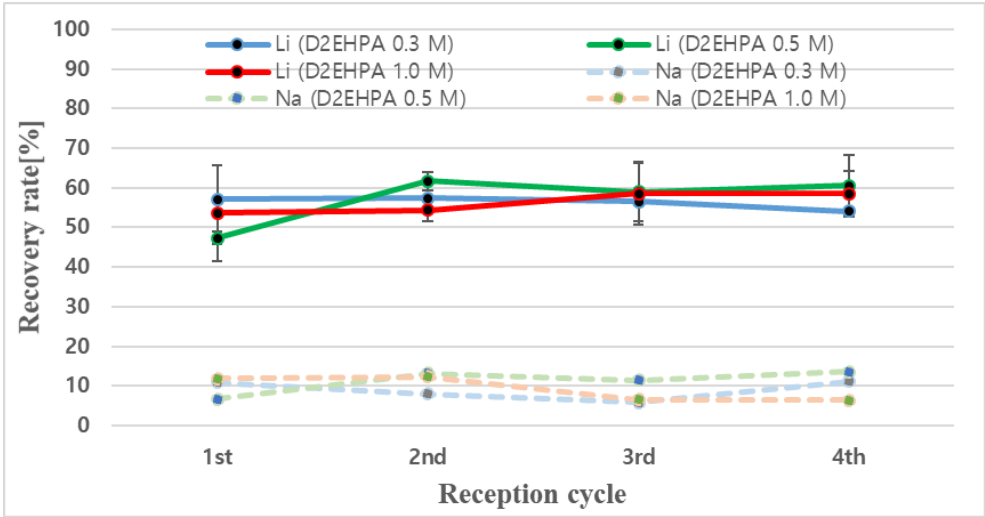

Fig. 4.8.2. Multistage solvent extraction efficiency of Li and Na in the three different D2EHPA concentrations (0.3, 0.5, and 1.0 M) of produced water.

Using D2EHPA 1M in the produced water was chosen as the optimal condition to recover lithium ions. Different concentrations of TBP used as a synergistic additive was also added to the extractant in the 25 times diluted produced water to observe the optimal condition to extract lithium ions. An appropriate amount of TBP is important to improve the lithium extraction efficiency. To determine the proper TBP concentration, four stage solvent extraction tests were designed with three TBP concentrations (0.3, 0.5, and 1.0M) using 1.0 M D2EHPA (Fig. 4.8.3).

In 25 times diluted produced water, the different concentrations of TBP (0.3, 0.5, and 1.0M) showed an extraction efficiency from 65.4, 67.7, and 28.3 respectively. The lithium selectivity over sodium for the different TBP concentration levels (0.3, 0.5, and 1.0M) showed 13.7, 14.5, and 3.9 respectively. TBP acts as a synergistic additive and displaces one molecule of D2EHPA in the Li-D2EHPA complex form and the displaced one molecule of D2EHPA can react with another Li that exists in the solution (Jang et al., 207). When excess TBP is present, D2EHPA-TBP can be polymerized through hydrogen bond (Haghshenas Fatmehsari et al., 2009). The formation of D2EHPA-TBP reduces the opportunity for the target components to interact and transfer into the organic phase. The usage of proper amount of TBP significantly improves the extraction efficiency of cations (Jang et al., 207). Due to equation (2.1.8), excess amount of TBP can directly react with D2EHPA and decrease the lithium extraction efficiency thus the condition was selected as D2EHPA 1M + TBP 0.5M by considering the lithium extraction efficiency and selectivity.

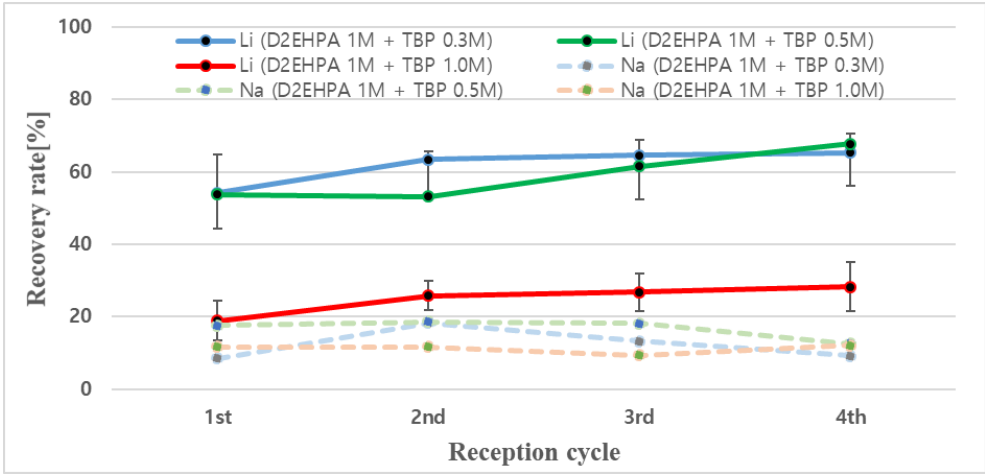

Fig. 4.8.3. Multistage solvent extraction efficiency of Li and Na in the three different TBP concentrations (0.3, 0.5, and 1.0 M) of 25 × of diluted produced water + D2EHPA 1M.

Solvent extraction was applied for two different dilution levels (25× and 50×) and the IL extracting agent [Cyphos IL 101][D2EHPA] (1M) was used as an extractant to observe the Li extraction efficiency (Fig. 4.8.4). In the 25 and 50 times diluted synthesized produced water, lithium was extracted 85.9 % and 57.2 % respectively. By only using a D2EHPA, the solution pH decreases quickly due to the release of H ions by equation (2.1.1). The aqueous raffinate pH should be controlled after every stage in order to have acceptable extraction yields (Lupi and Pilone, 2020). Usually saponified D2EHPA can be applied to overcome the pH change by exchanging the H^+ to other ions like Na^+ Ca^{2+}, and Mg^{2+}. (Lupi and Pilone, 2020; Liu et al., 2017). This exchange causes the raffinate pH not to decrease however, the usage of using the saponified D2EHPA can produce more amount of ions to the solution which needs an additional process for the recycled saponification procedure (Liu et al., 2017). The combination of bulky organic cations and the organic/inorganic anions of IL shows the same properties for not releasing H^+ ions into the solution so the process of the neutralization of solution or saponification of extractant can be avoided (Kumari et al., 2016). Also the usage of IL, is unaffected by changing the ion concentration of the solution due to saponification.

The lithium selectivity over sodium for the different dilution levels (25×, and 50×) both showed a negative value due to no sodium being extracted into the organic phase. The optimal condition was selected as 25 times diluted produced water considering the highest lithium extraction efficiency.

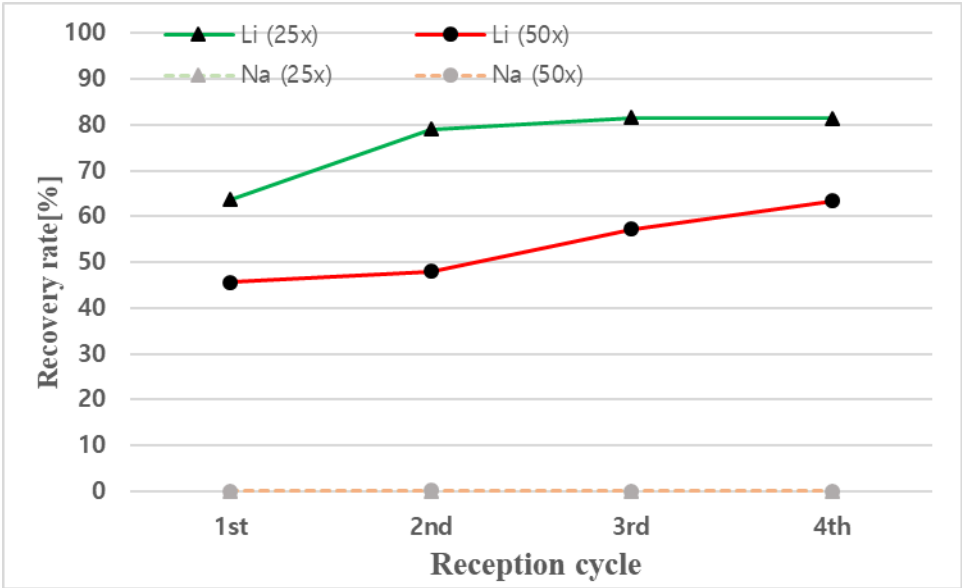

Fig. 4.8.4. Multistage solvent extraction efficiency of Li and Na in the two different diluted produced water (25 × and 50 ×) by using IL extracting agent [Cyphos IL 101][D2EHPA] (1M).

4.9 Overall recovery efficiency of lithium

After using the extraction processes, the loaded ions can be easily stripped using acidic solutions (Harvianto et al., 2016; Zhou et al., 2019). The Li loaded organic phase after the solvent extraction stage was stripped using equal volume of 1.0 M HCl solution. Stripping efficiency of the produced water by using D2EHPA 1M, D2EHPA 1M + TBP (0.3M, 0.5M, and 1.0M), IL extracting agent [Cyphos IL 101][D2EHPA] (1.0M) was shown in Fig 4.9.1. The IL extracting agent [Cyphos IL 101][D2EHPA] (1.0M) showed the highest stripping efficiency of 89.6% while the other extractants showed a smaller value of stripping efficiency of 60.2-70.2%. By using IL extracting agent [Cyphos IL 101][D2EHPA] (1.0M), no sodium was being extracted so only lithium can be stripped from the organic phase thus a high stripping efficiency was observed. However the other extractants (D2EHPA 1M, D2EHPA 1M + TBP (0.3M, 0.5M, and 1.0M)) coexist Li with Na in the organic phase showing a relatively low stripping efficiency of lithium.

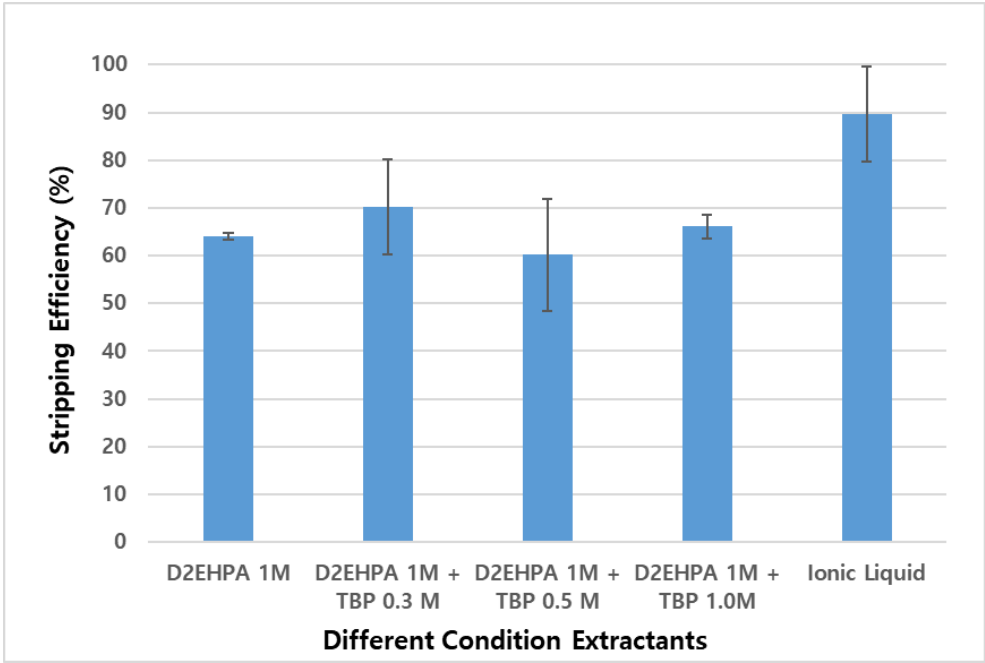

Fig. 4.9.1. Stripping efficiency in the shale gas produced water by using different condition of extractants.

The overall extraction efficiency for lithium considering adsorption, precipitation, solvent extraction, and stripping were calculated and shown in Figure 4.9.2. Using D2EHPA 1M + TBP 1.0M showed the lowest overall extraction efficiency of 17.4%. This can be explained due to the excess of TBP which lowers the extraction efficiency of lithium in the solvent extraction stage. The highest overall extraction efficiency was measured 71.5 % by using the IL extracting agent [Cyphos IL 101][D2EHPA] (1.0M).

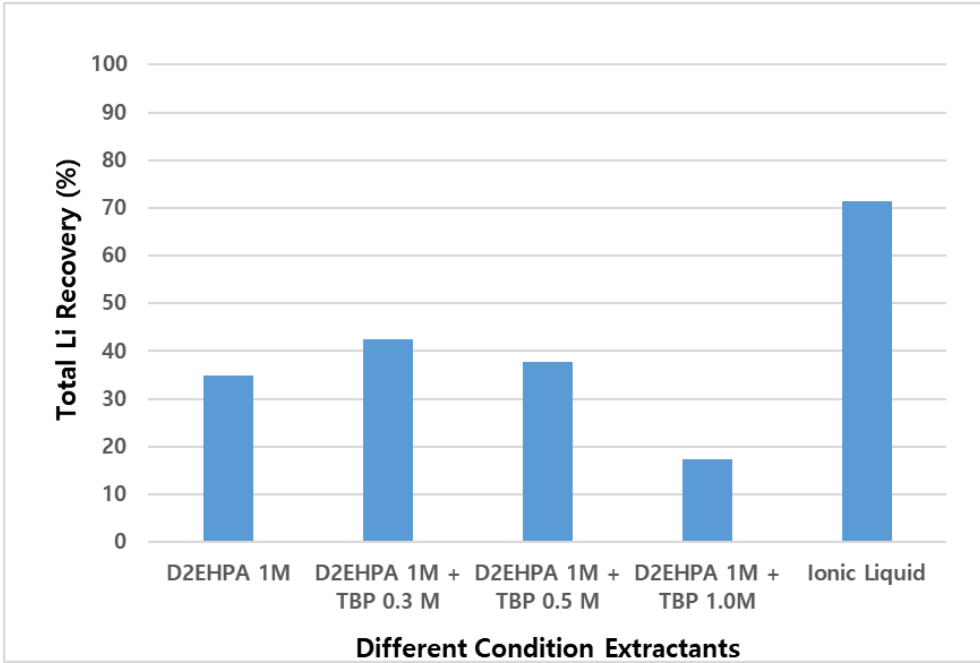

Fig. 4.9.2. Overall lithium recovery efficiency in the 25 times diluted shale gas produced water by using different condition of extractants.

4.10 Summary

Two experiments were implemented to the produced water. The first experiment was to observe the effect of different concentration and length of organic compounds. The second experiment was to improve the method to recover Li from produced water.

In the first experiment, the solvent extraction method was applied in two consecutive stages to recover lithium from shale gas produced water, containing a high concentration of organic compounds. The influence of different types and concentrations of alkane in the solvent extraction process was studied. It was found that the chain length of alkanes affected lithium recovery efficiency.

The total Li recovery efficiency after two stages of extraction decreased with increasing alkane chain length, probably due to the hydrophobicity of D2EHPA and alkanes through the solvation number change of Li-D2EHPA complex in the first stage. As the solvation number decreased with increasing alkane chain length, lithium ion-loading to the organic solvent phase increased. The presence of n-hexane in the solution affected the extraction efficiency of lithium. When hexane was added to the solution, more lithium and less divalent cations were removed in the first stage, with significantly lower selectivity. The FT-IR results showed that the existence of hexane affect the formation of metal-D2EDPA complex. It was found that selectivity in the second stage significantly decreased with hexane regardless of its concentration. For the application of solvent extraction to recover lithium from a solution, the removal of organic compounds, especially long chain alkanes, is suggested before implementing the extraction process.

For the second experiment, the lithium recovery was implemented using a

combined method of adsorption, precipitation and solvent extraction on synthesized shale gas produced water. The adsorption and precipitation stage using activated carbon, $Ca(OH)_2$ and Na_2CO_3 targeted the organic compounds and the divalent ions without influencing the lithium ions from the synthesized shale gas produced water. The organic compounds show a different concentration due to the bedrock composition or hydraulic fracturing process. Before Li recovery, the impurities amount should be measured properly to remove the exact amount of organic compounds.

For the solvent extraction method, a new Ionic liquid was designed by using Cyphos IL 101 and D2EHPA. After removing the organic compounds and divalent ions, solvent extraction using an ionic liquid was applied to improve ion extractability for Li extraction. The highest lithium extraction efficiency from synthesized shale gas produced water was measured 85.9% by using IL extracting agent [Cyphos IL 101][D2EHPA] (1.0M) and the overall lithium recovery considering stripping process by using 1.0 M HCl solution was measured 71.5 % from the dilution ratio of 25 times.

Chapter 5. Conclusion

Shale gas produced water/geothermal flowback water contains high concentrations of total dissolved solids that originated from various geochemical reactions between the fluid in the reservoir and the minerals in the rock and some region can be a potential source of lithium ions to recover. Marcellus shale gas produced and Soultz-sous-Forêts geothermal flowback contains a relatively high concentration of lithium however, these water also includes impurities like organic compounds or silicate ions that can show a probable inhibitory effect on the recovery of lithium. Lithium was recovered by using a solvent extraction method and the effect of the purities existence for each produced/flowback water was observed. Two consecutive stages of solvent extraction were used to separate the lithium from the produced/flowback water that contains different alkane chain or concentrations of organic compounds or different silicate ions respectively. Both the organic compounds and the SiO_2 inhibits the selective recovery of lithium in the first stage to a greater extent than it does in the second stage. The FT-IR results showed that the existence of organic compounds or silicate ions affect the formation of metal-D2EHPA complex for loading from the aqueous phase to the organic phase for separation. In addition, selective removal of organic compounds or silicate ions that can inhibit the selective recovery of lithium was implemented to increase the lithium extraction efficiency. A combined method of precipitation and solvent extraction was implemented to separate lithium from the geothermal water that contains various cations and silicate ions. Two precipitation steps were applied to remove the divalent and silicate ions and then lithium was successfully recovered using 1.5 M D2EHPA and 0.3 M TBP from the diluted geothermal water.

By comparing the results without using precipitant, the Li was removed 55-78 % in the 4 steps of solvent extraction and the 22-25 % of Li was extracted after the removal step of divalent ions from the 50 times diluted geothermal water. The overall recovery efficiency was measured 4.5-6.8 %, considering the Li loss from the first step and Li extraction from the second step of solvent extraction. After applying $Ca(OH)_2$ and Na_2CO_3 as a pretreatment, most of the divalent and silicate ions (98.0%) were removed with none of the Li loss. After removing the divalent and silicate ions the Li recovery was measured 87.7 %. A combined method of adsorption, precipitation and solvent extraction was implemented to separate lithium from the produced water that contains organic compounds and divalent cations. By comparing the results without using the adsorption and preciptant, the different dilution ratio of produced water was implemented and 25 times diluted water showed the highest extraction efficiency and selectivity of Li. Due to the pretreatment, most of the impurities were removed thus the sum of several ions concentrations (Ca^{2+}, Mg^{2+}, Ba^{2+}, and Sr^{2+}) is approximately 16,400 mg/L. Using the geothermal water also showed most of the impurities being removed and the sum of several ions concentrations (Ca^{2+}, Mg^{2+}, Ba^{2+}, Sr^{2+}, and SiO_2) is approximately 7,000-8,000 mg/L and 50 times dilution was the optimal condition. The produced water showed a higher amount of impurities to be removed compared to the geothermal water thus the dilution ratio can be lower than 50 times. The Li was removed 42 % in the 8 stages of solvent extraction and the 26 % of Li was extracted after the removal step from the 50 times diluted produced water. The overall recovery efficiency was measured 15 % considering the Li loss from the first stage and Li recovery from the second stage of solvent extraction. The direct comparison is impossible due to the different diluted water of the experiment using

adsorption and precipitant. The organic compounds were removed more than 99% and the divalent ions were removed more than 91 %. Many extractants were used to extract lithium from the produced water including D2EHPA 1M, D2EHPA 1M + TBP (0.3M, 0.5M, and 1.0M), IL extracting agent [Cyphos IL 101][D2EHPA] (1.0M). The highest lithium extraction efficiency from synthesized shale gas produced water was measured 85.9% from the dilution ratio of 25 times by using a synthesized ionic liquid. For the further study, other sources like waste water from battery recycling plant or brine water that contains a lot of amount of Li can also be considered with the method that was introduced in this dissertation. Also Li extraction from a massive amount of solution should be considered for industrial application.

References

1. A. Rusydi. (2018). Correlation between conductivity and total dissolved solid in various type of water: A review. *IOP Conf. Ser.: Earth Environ. Sci.* 118 012019.

2. Akob, D. M., Cozzarelli, I. M., Dunlap, D. S., Rowan, E. L., Lorah, M. M., (2015). Organic and inorganic composition and microbiology of produced waters from Pennsylvania shale gas wells. *Appl. Geochem*. 60, 116-125.

3. Alamdar Milani, S., Hafizi, M., Abolghasemi, H., and Zahakifar, F. (2021). Solvent extraction of strontium from leach liquor of central iran metasomatic ores using macrocyclic crown ether ligands. *J. water wastewater*. 32(2), 68-79.

4. Alonso, L., Arce, A., Francisco, M., Soto, A. (2008). Solvent extraction of thiophene from n-alkanes (C7, C12, and C16) using the ionic liquid [C8mim][BF4]. *J. Chem. Thermodyn*. 40(6), 966-972.

5. Amakiri, K. T., Canon, A. R., Molinari, M., Angelis-Dimakis, A. (2022). Review of oilfield produced water treatment technologies, *Chemosphere*, Volume 298, 134064.

6. Amani, P., Asadi, J., Mohammadi, E., Akhgar, S., and Esmaili, M. (2017).

Cooperative influence of D2EHPA and TBP on the reactive extraction of cobalt from sulfuric acid leach solution in a horizontal semi-industrial column. *J. Environ. Chem. Eng*. 5(5). 4716-4727.

7. An, J. W., Kang, D. J., Tran, K. T., Kim, M. J., Lim, T., Tran, T. (2012). Recovery of lithium from Uyuni salar brine. *Hydrometallurgy*. 117, 64-70.

8. Anderson, K., Rodríguez, H., and Seddon, K.R. (2009). Phase behaviour of trihexyl(tetradecyl)phosphonium chloride, nonane and water. *Green Chem*. 11, 780-784.

9. Axelsson, G. (2012). Role and management of geothermal reinjection. United Nations University Geothermal Training Program, 1-21.

10. Azizitorghabeh, A., Rashchi, F., Babakhani, A. (2016). Stoichiometry and structural studies of Fe(III) and Zn(II) solvent extraction using D2EHPA/TBP. *Sep. Purif. Technol*. 171, 197-205.

11. Bam, E.K.P., Bansah. S. (2020). Groundwater chemistry and isotopes reveal vulnerability of granitic aquifer in the White Volta River watershed, West Africa. *Appl. Geochem.* 119, 104662.

12. Battaglia, G., Berkemeyer, L., Cipollina, A., Cortina, J., Labastida, M., Rodriguez, J., Winter, D. (2022). Recovery of Lithium Carbonate from Dilute Li-Rich Brine via Homogenous and Heterogeneous Precipitation. *Ind. Eng.*

Chem. Res. 61(36), 13589-13602.

13. Battistel, A., Palagonia, M.S., Brogioli, D., Mantia, F.L., and Trócoli, R. (2020). Electrochemical Methods for Lithium Recovery: A Comprehensive and Critical Review. *J. Adv. Mater*. 32(23). 1905440.

14. Battistelli, A., Calore, C., Pruess, K. (1995). Analysis of salt effects on the depletion of fractured reservoir blocks. Conference: World Geothermal Congress 1995. Firenze, Italy, 1613-1618.

15. Bernardini, E. (1976). Batch and continuous solvent extraction. *J. Am. Oil Chem. Soc*. 53, 275–278.

16. Biswas, R., Khan, P., Mukherjee, S., Mukhopadhyay, A., Ghosh, J., Muraleedharan, K. (2018). Study of short range structure of amorphous Silica from PDF using Ag radiation in laboratory XRD system, RAMAN and NEXAFS, *J. Non-Cryst. Solids*, 488, 1-9.

17. Biswas, R.K., Singha, H.P., (2007). Solvent extraction of Cu(II) by purified cyanex 272. *Indian J. Chem. Technol*. 14 (3), 269–275.

18. Bologo, V., Maree, J.P. Zvinowasnda, C.M. (2009). Treatment of Acid Mine Drainage using Magnesium Hydroxide. International Mine Water Conference. Pretoria, South Africa, 19-23.

19. Bozau, E., & Berk, W. V. (2013). Hydro geochemical modelling of deep formation water applied to geothermal energy production. *Procedia Earth and Planetary Science*, 7, 97-100.

20. Braun, A., Evans, D., Gandhi, P. M., Garamszeghy, M., Geiser, H., Hooper, E. W.,et al. (2002). Application of Ion Exchange Processes for the Treatment of Radioactive Waste and Management of Spent Ion Exchangers. Technical Reports Series. Vienna: International Atomic Energy Agency.

21. Brown, K. (2013). Mineral scaling in geothermal power production, United Nations University Geothermal training program, Reports 2013-39, Reykjavik, Iceland, 1-25.

22. Castaño, S. V., Plante, E. C. L., Shimoda, S., Wang, B., Neithalath, N., Sant, G., Pilon, L. (2021). Calcination-free production of calcium hydroxide at sub-boiling temperatures. *RSC Adv*. 11, 1762–1772.

23. Caulk, R.A., Ghazanfari, E., Perdrial, J.N., Perdrial, N. (2016). Experimental investigation of fracture aperture and permeability change within Enhanced Geothermal Systems. *Geothermics*. 62. 12-21.

24. Charlton, S. R. & Parkhurst, D. L. (2011). Modules based on the geochemical model PHREEQC for use in scripting and Programming languages. *Comput. Geosci*, 37, 1653-1663.

25. Chen, H., Wang, L. (2016). Technologies for Biochemical Conversion of Biomass. Academic Press. 1st edition. 200-202.

26. Chon, H., Lee, J., Oh, S. (1999). Groundwater Chemistry and Water-Rock Interactions at Hydrocarbon Storage Cavern Sites in Korea. *Geosystem Engineering*, 2(1), 13-25.

27. Clark, C. E., Horner, R.M., Harto, C.B. (2013). Life cycle water consumption and water resource assessment for utility-scale geothermal systems: an in-depth analysis of historical and forthcoming EGS projects. United States: U.S. Department of Energy.

28. Clark, C.E., Horner, R.M., Harto, C.B. (2013). Life Cycle Water Consumption And Water Resource Assessment For Utility-Scale Geothermal Systems: An In-Depth Analysis Of Historical And Forthcoming EGS projects. United States: U.S. Department of Energy.

29. Dalai, B., Dash, S.K., Singh, S.K., Swain, B.B. (2015). 1H NMR and acoustic response of binary mixtures of an organophosphorous extractant with 1-alkanols (C1–C4, C8), *J. Mol. Liq*. 208, 151-159.

30. Ehsani, I., Ehsani, A., Ucyildiz, A., Obut. A. (2022). Direct conversion of alkaline earth metal hydroxides and sulfates to carbonates in ammonia solutions. *Physicochem. Probl. Miner. Process*., 58(1), 169-180.

31. Ekberg, C., Petranikova, M. (2015). Lithium process chemistry: resources, extraction, batteries, and recycling. A. Chagnes, J. Swiatowska (Eds.), Lithium Process Chemistry: Resources, Extraction, Batteries, and Recycling, Elsevier, Amsterdam. 248-253.

32. Flexer, V., Baspineiro, C. F., and Galli, C. I. (2018). Lithium Recovery from Brines: A Vital Raw Material for green Energies with a Potential Environmental Impact in its Mining and Processing. *Sci. Total Environ*. 639, 1188–1204.

33. Gallup, D.L. (2007). Treatment of geothermal waters for production of industrial, agricultural or drinking water, *Geothermics*, 36(5), 473-483.

34. Galván-Ruiz, M., Hernández, J., Baño, L., Noriega-Montes, J., Rodríguez-García, M.E. (2009). Characterization of Calcium Carbonate, Calcium Oxide, and Calcium Hydroxide as Starting Point to the Improvement of Lime for Their Use in Construction. *J. Mater. Civ. Eng*. 21(11). 625-708.

35. Gao, Y., Duan, L., Guan, S., Gao, G., Cheng, Y., Ren, X., Wang, Y. (2017). The effect of hydrophobic alkyl chain length on the mechanical properties of latex particle hydrogels. *RSC Adv*. 7, 44673-44679.

36. Genter, A., Cuenot, N., Goerke, X., Bernd, M., Sanjuan, B., Scheiber, J. (2012. Status of the Soultz geothermal project during exploitation between 2010 and 2012. 37th Workshop on Geothermal Reservoir Engineering Stanford

University, Stanford, California, January 30 - February 1, 2012.

37. Geow, C., Tan, M., Yeap, S., Chin, N. (2021). A Review on Extraction Techniques and Its Future Applications in Industry. *Eur. J. Lipid Sci. Technol.*123(4). 2000302.

38. Goc, K., Kluczka, J., Benke, G.,Malarz, J., Pianowska, K., and Leszczyńska-Sejda, K. (2021). Application of Ion Exchange for Recovery of Noble Metals. *Minerals*. 11 (11), 1188.

39. Gregory, K, B., Vidic. R. D., Dzombak. D. A., (2011). Water Management Challenges Associated with the Production of Shale Gas by Hydraulic Fracturing. *Elements*. 7(3), 181-186.

40. Gunnarsson, I., Ívarsson, G., Sigfússon, B., Thrastarson, E. Ö., Gíslason, G. (2010). Reducing silica deposition potential in waste waters from Nesjavellir and Hellisheiði, Power Plants. Proceedings of the WGC-2010 in Bali, Indonesia.

41. Gunnlaugsson, E., Armannsson, H., Thorhallsson, S., Steingrimsson, B. (2014). Problems in geothermal operation-scaling and corrosion. Short Course VI on utilization of low and medium enthalpy geothermal resources and financial aspects of utilization, UNU-GTP and LaGeo, Santa Tecla, El Salvador, 1-18.

42. Guozhi, Z., Chen, D., Zhao, W., Zhao, H., Wang, L., Weijing. W., Qi, T.

(2016). A novel D2EHPA-based synergistic extraction system for the recovery of chromium (III). *J. Chem. Eng*. 302, 233-238.

43. Haghshenas Fatmehsari, D., Darvishi, D., Etemadi, S., Eivazi Hollagh, A.R., Keshavarz Alamdari, E., Salardini, A.A. (2009). Interaction between TBP and D2EHPA during Zn, Cd, Mn, Cu, Co and Ni solvent extraction: A thermodynamic and empirical approach, *Hydrometallurgy*, 98(1–2). 143-147.

44. Haluszczak, L. O., Rose, A. W., Kump, L. R., (2013). Geochemical evaluation of flowback brine from Marcellus gas wells in Pennsylvania, USA. *Appl. Geochem*. 28, 55–61.

45. Han, K.N., Kellar, J.J., Cross, W.M., and Safarzadeh, S. (2014). Opportunities and challenges for treating rare-earth elements, *Geosystem Eng*. 17(3), 178-194.

46. Hano, T., Matsumoto, M., Ohtake, T., Egashira, N., Hori, F. (1992). Recovery of lithium from geothermal water by solvent extraction technique. *Solvent Extra. Ion Exc*. 10(2). 195-206.

47. Harvianto, G. R., Kim, S. H., Ju, C. S. (2016). Solvent extraction and stripping of lithium ion from aqueous solution and its application to seawater. *Rare Met*. 35(12), 948-953. 144.

48. He, C., Zhang, T., Zheng, X., Li, Y., Vidic, R. (2014). Management of

Marcellus Shale Produced Water in Pennsylvania: A Review of Current Strategies and Perspectives. *Energy Technology.* Volume 2(12). 968-976.

49. He, L., Xu, W., Song, Y., Luo, Y., Liu, X., Zhao, Z. (2018). New Insights into the Application of Lithium-Ion Battery Materials: Selective Extraction of Lithium from Brines via a Rocking-Chair Lithium-Ion Battery System. *Global chall*. 2: 1700079.

50. Hem, R., Yamasaki, T., Sumida, H. (2018). Control of pH of retained water in the coastal waste disposal site. *MATEC Web Conf*. 147. 04005.

51. Hofmann, H., Babadagli, T., Zimmermann, G. (2014). Hot water generation for oil sands processing from enhanced geothermal systems: Process simulation for different hydraulic fracturing scenarios. *Appl. Energy*. 113. 524–547.

52. Hofmann, H., Zimmermann, G., Farkas, M., Huenges, E., Zang, A., Leonhardt, M., Kwiatek, G., Martinez-Garzon, P., Bohnhoff, M., Min, K., Fokker, P., Westaway, R., Bethmann, F., Meier, P., Yoon, K., Choi, J., Lee, T., & Kim, K. (2019). First field application of cyclic soft stimulation at the Pohang enhanced geothermal system site in Korea. *Geophys. J. Int*, 217(3), 926–949.

53. Ismail, A. H., Hassan, G., Sarhan, A.H. (2020). Hydrochemistry of shallow groundwater and its assessment for drinking and irrigation purposes in

Tarmiah district, Baghdad governorate, Iraq. *Groundw. Sustain. Dev.* 10, 100300.

54. Jafari, H., Abdollahi, H., Gharabaghi, M., Balesini, A. (2018). Solvent extraction of zinc from synthetic Zn-Cd-Mn chloride solution using D2EHPA: Optimization and thermodynamic studies. *Sep. Purif. Technol*. 197. 210-219.

55. Jang, E., Jang, Y., and Chung, E. (2017). Lithium recovery from shale gas produced water using solvent extraction. *J. Appl. Geochem*. 78, 343–350.

56. Jang, Y., and Chung, E. (2018). Adsorption of Lithium from Shale Gas Produced Water Using Titanium Based Adsorbent. *Ind. Eng. Chem. Res*. 57, 8381–8387.

57. Jang, Y., and Chung, E. (2019). Lithium adsorptive properties of H_2TiO_3 adsorbent from shale gas produced water containing organic compounds, *Chemosphere*. 221, 75-80.

58. Jin, Y., Ma, Y., Weng, Y., Jia, X., Li, J. (2014). Solvent extraction of Fe^{3+} from the hydrochloric acid route phosphoric acid by D2EHPA in kerosene. *J. Ind. Eng. Chem*. 20(5), 3446-3452.

59. Johnston, J. H., Borrmann, T., Rankin, D., Cairns, M., Grindrod, J. E., Mcfarlane, A. (2008). Nano-structured composite calcium silicate and some novel applications. *Curr. Appl. Phys*. 8(3-4). 504-507.

60. Joo, H., Lee, J., Yoon, J. (2020). Short Review: Timeline of the Electrochemical Lithium Recovery System Using the Spinel $LiMn_2O_4$ as a Positive Electrode. *Energies*. 13, 6235.

61. Junuzović, H., Begić, S., Selimović, A., Đozić, A., Cvrk, R., Ahmetović, M. (2019). Efficiency of Carbonate Precipitation and Removal of Copper and Nickel Ions from their Monocomponent and Two-component Aqueous Solutions. *Int. j. res. appl. sci. biotechnol*. 6(6). 11-15.

62. Kanoh, H., Ooi, K., Miyai, Y., Katoh, S. (1993). Electrochemical Recovery of Lithium Ions in the Aqueous Phase. *Sep. Sci. Technol.* 28(1-3), 643-651.

63. Karidakis, T., Agatzini-Leonardou, S., Neou-Syngouna, P. (2005). Removal of magnesium from nickel laterite leach liquors by chemical precipitation using calcium hydroxide and the potential use of the precipitate as a filler material. *Hydrometallurgy*. 76(1–2). 105-114.

64. Karmegam, U., Chidambaram, S., Prasanna, M. V., Sasidhar, P., Manikandan, S., Johnsonbabu, G., Dheivanayaki, V., Paramaguru, P., Manivannan, R., Srinivasamoorthy, K., Anandhan, P. (2011). A study on the mixing proportion in groundwater samples by using Piper diagram and Phreeqc model. *Chin. J. Geochem*, 30, 490-495.

65. Kasikowski, T., Buczkowski, R., Cichosz, M. (2008). Utilisation of synthetic

soda-ash industry by-products, *Int. J. Prod. Econ*, 112(2), 971-984.

66. Kassing, M., Jenelten, U., Schenk, J., Strube. J. (2010). A New Approach for Process Development of Plant-Based Extraction Processes. *Chem. Eng. Technol*. 33(3). 377-387.

67. Kaya, T. & Hoshan, P. (2005). Corrosion and Material Selection for Geothermal Systems. Proceedings World Geothermal Congress 2005. Antalya, Turkey, Apr. 24-29.

68. Keller, A., Hlawitschka, M.W., Bart, H.-J. (2022). Application of saponified D2EHPA for the selective extraction of manganese from spend lithium-ion batteries, *Chem. Eng. Process.: Process Intensif*. 171, 108552.

69. Khodadoust, A., Suidan, M. T., Acheson, C. M., Brenner, R. C. (1999). Remediation of soils contaminated with wood preserving wastes : crosscurrent and countercurrent solvent washing. *J. Hazard. Mater*. 64, 167-179.

70. Kihm, J., Kim, J. (2011). Geochemical characteristics of deep groundwater in the Gyeongsang-Pohang Basin, Korea. *J. Geol. Soc. Korea*, 47(2), 165-183.

71. Kim, J., Choi, H., Kim, H., Ryu, J., Lee, K. (2020). Using isotopes (strontium and radon) and microbial communities to quantify groundwater mixing influenced by anthropogenic factors at riverside area. *J. Hydrol.* 581, 12441.

72. Kim, N., Su, X., Kim, C. (2021). Electrochemical lithium recovery system through the simultaneous lithium enrichment via sustainable redox reaction. *Chem. Eng. Sci*. 420(2), 127715.

73. Kim, S., Kim, J., Kim, S., Lee, J., Yoon, J. (2018). Electrochemical lithium recovery and organic pollutant removal from industrial wastewater of a battery recycling plant. *Environ. Sci.: Water Res. Technol*. 4, 175−182.

74. Kislik, V., and Eyal, A. (2003). Competitive complexation/solvation theory of solvent extraction: general statements, acid extraction by amines, influence of active solvents and temperature. *J Chem Technol Biotechnol*. 78, 358–363.

75. Kislik, V., Eyal., A., and Hazan, B. (2003). Competitive Complexation/Solvation Theory of Solvent Extraction. III. Influence of Active Solvents on Acid Solvent Extraction by Amine Based Extractants, *Sep. Sci. Technol*. 38(8), 1681-1704.

76. Kondash, A. J., Albright, E., Vengosh, A., (2017). Quantity of flowback and produced waters from unconventional oil and gas exploration. *Sci Total Environ.* 574. 314-321.

77. Korea Institute of Geology and Mineral Resources (KIGAM). (2006). Development of deep, low-enthalpy geothermal energy. Ministry of Science and ICT.

78. Krasucka, P., Goworek, J., Kierys. A. (2016). Synthesis of the mesostructured polymer-silica composite and silicon dioxide through polymer swelling in silica precursor. *Adsorption*. 22, 663–671.

79. Kumar, P., Pournara, A., Kim, K.-H., Bansal, V., Rapti, S., and Manos, M. J. (2017). Metal-organic Frameworks: Challenges and Opportunities for Ion-Exchange/sorption Applications. *Prog. Mater. Sci*. 86, 25–74.

80. Kumari, A., Sinha, M., Sahu, S., Pandey, B. (2016). Solvent Extraction and Separation of Trivalent Lanthanides Using Cyphos IL 104, a Novel Phosphonium Ionic Liquid as Extractant, *Solvent Extr. Ion Exch*, 34:5, 469-484.

81. Kwon, S., Xie, L., Park, S., Kim, K., Min, K., Kim, K., Zhuang, L., Choi, J., Kim, H., & Lee, T. (2017). Characterization of 4.2-km-deep fractured granodiorite cores from pohang geothermal reservoir, Korea. *Rock Mechanics and Rock Engineering*, 52(3), 771–782.

82. Larriba, M., Navarro, P., García, J., Rodríguez, F. (2014). Liquid−Liquid Extraction of Toluene from n-Alkanes using {[4empy][Tf2N] + [emim][DCA]} Ionic Liquid Mixtures. *J. Chem. Eng. Data*. 59, 1692-1699.

83. Lee, D., Joo, S., Shin, D and Shin, S. (2022). Recovery of vanadium and cesium from spent sulfuric acid catalysts by a hydrometallurgical process. *Green Chem*. Volume 24(2). 1463-9262.

84. Lee, J.B and Chung, E.H. (2021). Geochemical Effect of Geothermal Water Flushing during Enhanced Geothermal Systems Operation. *J. Korean Soc. Miner. Energy Resour*. 58(3), 205-214.

85. Lee, J.B and Chung, E.H. (2022b). The Effect of Silicate Ions on the Separation of Lithium From Geothermal Fluid. *Front. Chem. Eng*. 4:741281.

86. Lee, J.B and Chung, E.H. (2022a). Lithium recovery from a simulated geothermal fluid by a combined selective precipitation and solvent extraction method, *Geothermics*, 102, 102388.

87. Lee, J.B. & Chung, E.H. (2020a). Application of geochemical modelling for hydraulic stimulation in enhanced geothermal systems, *Geosystem Eng*. 23(6), 342-350.

88. Lee, J.B. & Chung, E.H. (2020b). Lithium recovery by solvent extraction from simulated shale gas produced water – Impact of organic compounds, *J. Appl. Geochem*. 116(6). 104571.

89. Lee, S., Kim, T., Lee, T. (2011). Strontium isotope geochemistry and its geochemical implication from hot spring waters in South Korea. *Journal of Volcanology and Geothermal Research*, 208(1–2), 12-22.

90. Li, L., Deshmane, V. G., Paranthaman, M. P., Bhave, R., Moyer, B. A., Harrison, S. (2018). Lithium Recovery from Aqueous Resources and Batteries:

A Brief Review. *Johns. Matthey Technol*. 62(2), 161–176.

91. Li, X., Sengupta, T., Mohammed, K.S., Jamaani. F. (2023). Forecasting the lithium mineral resources prices in China: Evidence with Facebook Prophet (Fb-P) and Artificial Neural Networks (ANN) methods, *Resour Policy*, Volume 82, 2023, 103580.

92. Liu, B., Malekian, R., Xu, J. (2017). Groundwater Mixing Process Identification in Deep Mines Based on Hydrogeochemical Property Analysis. *Applied Science*, 7(1), 42, 1-13.

93. Liu, Y., Sohn, S., & Lee, M. (2017). Methods for the substitution of common saponification systems for the solvent extraction of REEs, *Geosystem Eng*, 20(2), 111-118.

94. Luo, J., Zhu, Y., Guo, Q., Tan, L., Zhuang, Y., Liu, M., Zhang, C., Zhu, M., Xiang, W. (2018). Chemical stimulation on the hydraulic properties of artificially fractured granite for enhanced geothermal system. *Energy*, 142, 754-764.

95. Lupi, C., Pilone, D. (2020). Effectiveness of saponified D2EHPA in Zn(II) selective extraction from concentrated sulphuric solutions, Minerals Engineering, Volume 150, 106278.

96. Maguire-Boyle, S. J. and Barron, A. R. (2014). Organic compounds in

produced waters from shale gas wells. *Environ. Sci- Proc. Imp*. 16, 2237-2248.

97. Masmoudi, A., Zante, G., Trébouet, D., Barillon, R., and Boltoeva, M. (2021). Solvent extraction of lithium ions using benzoyltrifluoroacetone in new solvents, *Sep. Purif. Technol*. 255, 117653.

98. Meshram, P. Virolainen, S. Abhilash; Sainio, T. (2022). Solvent Extraction for Separation of 99.9% Pure Cobalt and Recovery of Li, Ni, Fe, Cu, Al from Spent LIBs. *Metals*, 12, 1056.

99. Nadimi, H., Amirjani, A., Haghshenas, D., Firoozi, S., Azadmehr, A. (2014). Effect of tartrate ion on extraction behavior of Ni and Co via D2EHPA in sulfate media. Miner. Eng. 69, 177-184.

100. Naether, D.J., Slawtschew, S., Stasik, S., Engel, M., Olzog, M., Wick, L.Y., Timmis, K.N., Heipieper, H.J. (2013). Adaptation of the hydrocarbonoclastic bacterium alcanivorax borkumensis SK2 to alkanes and toxic organic compounds: a physiological and transcriptomic approach. *Appl. Environ. Microbiol*. 79 (14), 4282–4293.

101. Nardella, A., Massetti, F., Sisto, R., Tomaciello, R. (1999). Clean-up of polluted wet soils by solvent extraction. *Environ. Prog*. 18(4), 243-249.

102. Nishihama, S., Onishi, K., Yoshizuka, K. (2011). Selective Recovery Process of Lithium from Seawater Using Integrated Ion Exchange Methods. *Solvent*

Extra. Ion Exc. 29(3), 421-431.

103. Olasolo, P., Juárez, M.C., Morales, M.P., Amico, S. D´., Liarte, I.A. (2016). Enhanced geothermal systems (EGS): A review. *Renew. Sustain. Energy Rev.* 56, 133-144.

104. Owen, J., Bustin, R.M., Bustin, A.M.M. (2020). Insights from mixing calculations and geochemical modeling of Montney Formation post hydraulic fracturing flowback water chemistry. *J Petrol Sci Eng*. 195, 107589.

105. Park, Y.-M., Yeon, K.-M., and Park, C.-h. (2020). Silica Treatment Technologies in Reverse Osmosis for Industrial Desalination: A Review. *Environ. Eng. Res*. 25 (6), 819–829.

106. Park, Y., Kwon, K., Kim, N., Lee, J & Yoon, J. (2013). Change of geochemical properties of groundwater by use of open loop geothermal cooling and heating system. *J. Geol. Soc. Korea,* 49(2), 289-296.

107. Parkhurst, D. L. and Appelo, C. A. J. (1999). User's guide to PHREEQC (version 2)—A computer program for speciation, batch-reaction, one dimensional transport, and inverse geochemical calculations. US Geology Survey Water Resources Investigations Report 99-4259. Denver, Colorado, 312.

108. Patel, J. (2016). Ion exchange resins. XIII-Water-D-Ion Exchange Resins. 1-7.

109. Pauwels, H., Fouillac, C., and Criaud, A. (1992). Water-rock interactions during experiments within the geothermal Hot Dry Rock borehole GPK1, Soultz-sous-Forets, Alsace, France. *J. Appl. Geochem*. 7(3), 243-255.

110. Pawar, R., Zhang, Z., Rhoades, A,H., Blotevogel, J. and Vidic, R.D. (2022). Impact of Organic and Volatile Compounds in Produced Water from Unconventional Reservoirs on Direct Contact Membrane Distillation Permeate Quality. *ACS ES&T Water*, 2 (6), 1003-1012.

111. Pohl, A. (2020). Removal of Heavy Metal Ions from Water and Wastewaters by Sulfur-Containing Precipitation Agents. *Water Air Soil Pollut*. 231(503). 1-17.

112. Portier, S., Vuataza, F.D., Namib, P., Sanjuanc, B., Gérardd, A. (2009). Chemical stimulation techniques for geothermal wells: experiments on the three-well EGS system at Soultz-sous-Forêts, France. *Geothermics,* 4, 349-359.

113. Putera, A.D.P., Wiranda, A., Mergiana, S., Perdana, I., and Olvianas, M. (2018). Assessing silica precipitation using calcium hydroxide addition on Dieng's geothermal brine. *IOP Conf. Ser. Earth Environ. Sci.* 200. 012022.

114. Rai, S., Wasewar, K. L., Lataye, D.H., Mukhopadhyay, J., Yoo. C. K. (2013). Feasibility of red mud neutralization with seawater using Taguchi's methodology. *Int. J. Environ. Sci. Technol*.10. 305–314.

115. Rana, M., Banerjee, C., Chowdhury, P. (2021). Studies on optical signal due to oxygen efect on hydrogenated amorphous/crystalline silicon thin flms. *Appl. Phys. A.* 127:192.

116. Reyes-Serrano, A., López-Alejo, J.E., Hernández-Cortázar, M.A., Elizalde, I. (2020). Removing contaminants from tannery wastewater by chemical precipitation using CaO and $Ca(OH)_2$. *Chin. J. Chem. Eng*. 28(4). 1107-1111.

117. Riegel, M., Haist-Gulde, B. & Sacher, F. (2023). Sorptive removal of short-chain perfluoroalkyl substances (PFAS) during drinking water treatment using activated carbon and anion exchanger. *Environ Sci Eur* 35, 12.

118. Sadakane, A., Iwachido, T., and Toei, K. (1975). The extraction of alkali metal picrates with dibenzo-18-crown-6. *Bull. Chem. Soc. Jpn*. 48, 60-63.

119. Sanjuan, B., Gourcerol, B., Millot, R., Rettenmaier, D., Jeandel, E., Rombaut, A. (2022). Lithium-rich geothermal brines in Europe: An up-date about geochemical characteristics and implications for potential Li resources, *Geothermics*, Volume 101, 102385.

120. Sanjuan, B., Millot, R., Dezayes, C., and Brach, M. (2010). Main Characteristics of the Deep Geothermal Brine (5km) at Soultz-Sous-Forêts (France) Determined Using Geochemical and Tracer Test Data. *C. R. - Geosci*. 342 (7–8), 546–559.

121. Sanjuan, B., Pinault, J.L., Rose, P., Gerard, A., Brach, M., Braibant, G., Crouzet, C., Foucher, J.C., Gautier, A., Touzelet, S. (2006). Geochemical fluid characteristics and main achievements about tracer tests at Soultz-sous-Forêts(France). *EHDRA Scientific Conference*, Soultz-sous-Forêts, France. 13. hal-00773150.

122. Sanyal, S. K. & Butler, S. J. (2005). An analysis of power generation prospects from Enhanced Geothermal Systems. Proceedings of the WGC-2005 in Antalya, Turkey.

123. Scheiber, J., Nitschke, F., Seibt, A., and Genter, A. (2012). Geochemical and mineralogical monitoring of the geothermal power plant in Soultz-sous-Forets (France). In: Proceedings of the 37th workshop on geothermal reservoir engineering. 1033–1042.

124. Schill, E., Genter, A., Cuenot, N., Kohl, T. (2017). Hydraulic performance history at the Soultz EGS reservoirs from stimulation and long-term circulation tests. *Geothermics*, 70, 110-124.

125. Shen, Z., Jin, F., Zhang, Y., Wu, B., Kishita, A., Tohji, K., Kishida. H, (2009). *Ind. Eng. Chem. Res.* 48 (19), 8920-8925.

126. Shi, C., Jing, Y., Xiao, J., Wang, X., Yao, Y., Jia, Y. (2017). Solvent extraction of lithium from aqueous solution using non-fluorinated functionalized ionic

liquids as extraction agents, *Sep. Purif. Technol*, 172, 473-479.

127. Shu, B., Zhu, R., Tan, J., Zhang, S., Liang, M. (2019). Evolution of permeability in a single granite fracture at high temperature. *Fuel*, 242, 12-22.

128. Silva, A., Delerue-Matos, C., Fiuza, A. (2005). Use of solvent extraction to remediate soils contaminated with hydrocarbons. *J. Hazard. Mater*. 124, 224-229.

129. Silva, J.E, Paiva, A.P., Soares, D., Labrincha, A., Castro, F. (2005). Solvent extraction applied to the recovery of heavy metals from galvanic sludge, *J. Hazard. Mater.* B120, 113–118.

130. Sonoc, A. & Jeswiet, J. (2014). A review of lithium supply and demand and a preliminary investigation of a room temperature method to recycle lithium ion batteries to recover lithium and other materials. *Procedia CIRP*. 15. 289-293.

131. Spitzmüller, L., Goldberg, V., Held, S., Grimmer, J.C., Winter, D., Genovese, M., Koschikowski, J., Kohl, T. (2021). Selective silica removal in geothermal fluids: Implications for applications for geothermal power plant operation and mineral extraction, *Geothermics*, 95, 102141.

132. Stober, I. & Bucher, K. (2013). Geothermal Energy: From Theoretical Models to Exploration and Development, Berlin : Springer, 168.

133. Strong, L. C., Gould, T., Kasinkas, L., Sadowsky, M. J., Aksan, A., Wackett, L. P. (2014). Biodegradation in waters from hydraulic fracturing: chemistry, microbiology, and engineering. *J. Environ. Chem. Eng*. 140(5), B4013001.

134. Swain, B. (2017). Recovery and recycling of lithium: a review. *Separ. Purif. Technol*. 172, 388-403.

135. Szabó, I. and Varga, C. (2020). Finding possible pharmacological effects of identified organic compounds in medicinal waters (BTEX and phenolic compounds). *Int J Biometeorol.* 64, 989–995.

136. Tester, Jefferson W. (Massachusetts Institute of Technology); et al. (2006). The Future of Geothermal Energy – Impact of Enhanced Geothermal Systems (EGS) on the United States in the 21st Century.

137. Toba, A., Nguyen, R., Cole, C., Neupane, G., Paranthaman, M. (2021). U.S. lithium resources from geothermal and extraction feasibility, *Resour Conserv Recycl*, 169, 105514.

138. Tran, T.T and Lee, M.S. (2020). Separation of Mo(VI), V(V), Ni(II), Al(III) from synthetic hydrochloric acidic leaching solution of spent catalysts by solvent extraction with ionic liquid, *Sep. Purif. Technol*, 247, 117005.

139. Umetani, S., Maeda, Kohji., Kihara, S., Matsui., M. (1986). Solvent extraction of lithium and sodium with 4-benzoyl or 4-perfluoroacyl-5-pyrazolone and

TOPO. *Talanta*. 34(9), 779-782.

140. Urbańska, W. (2020). Recovery of Co, Li, and Ni from Spent Li-Ion Batteries by the Inorganic and/or Organic Reducer Assisted Leaching Method. *Minerals*, 10, 555.

141. Vieceli, N., Reinhardt, N., Ekberg, C., Petranikova, M. (2021). Optimization of Manganese Recovery from a Solution Based on Lithium-Ion Batteries by Solvent Extraction with D2EHPA. *Metals*. 11, 54.

142. Vikström, H., Daidsson, S., Höök. M. (2013). Lithium availability and future production outlooks. *Appl. Energy*. 110. 252-266.

143. Wang, L., Frisella, K., Srimuk, P., Janka, O., Kickelbick, G., Presser, V. (2021). Electrochemical lithium recovery with lithium iron phosphate: what causes performance degradation and how can we improve the stability?. *Sustain. Energy Fuels*. 5, 3124–3133.

144. Wang, S., Li, P., Zhang, X., Zheng, S., and Zhang, Y. (2017). SelectiveAdsorption of Lithium from High Mg-Containing Brines Using H XTiO 3 Ion Sieve. *Hydrometallurgy* 174, 21–28.

145. Warren, I. (2021). Techno-Economic Analysis of Lithium Extraction from Geothermal Brines. Golden, CO: National Renewable Energy Laboratory. NREL/TP-5700-79178.

146. Warshawsky, A., Strikovsky, A.G., Vilensky, M.Y., Jerabek, K. (2002). Interphase mobility and migration of hydrophobic organic metal extractant molecules in solvent-impregnated resins. *Sep. Purif. Technol*. 37(11), 2607–2622.

147. Westaway, R., Burnside, N. M., & Banks, D. (2020). Hydrochemistry of produced water from the pohang EGS project site, Korea: Implications for water-rock reactions and associated changes to the state of stress accompanying hydraulic fracturing of granite. Proceedings of the WGC-2020 in Reykjavik, Iceland.

148. Xu, W., Liu, D., He, L., and Zhao, Z. (2020). A Comprehensive Membrane Process for Preparing Lithium Carbonate from High Mg/Li Brine. *Membranes* 10, 371.

149. Yanagisawa, N., Sato, M., Osato, K., Yamamoto, Y., Sakura, K., Lichti, K., Mountain, B. (2020). Corrosion Test of Casing Steel at High Temperature Acid Condition. PROCEEDINGS, 45th Workshop on Geothermal Reservoir Engineering Stanford University, Stanford, California, Feb.10-12.

150. Yang, W.F., Yuan, S., Xu, Y., Xiao, Y., Fang, K.M., and Xong, B. (2003). Extraction of thorium traces from hydrochloric acid media by 1-phenyl-3-methyl-4-benzoyl- pyrazolone-5. *J. Radioanal. Nucl. Chem*. 256, 149-152.

151. Yen, F., Chang, T., Laohaprapanon, S., Chen, Y., and You, S. (2016). Recovery of Indium from LCD Waste by Solvent Extraction and the Supported Liquid Membrane with Strip Dispersion Using D2EHPA as the Extractant. *Solvent Extr. Res. Dev., Jpn*. 23(1). 63-73.

152. Zaman, H.G., Baloo, H., Pendyala, L., Singa, P.K., Ilyas, S,U., Kutty, S.R.M. (2021). Produced Water Treatment with Conventional Adsorbents and MOF as an Alternative: A Review. *Materials*, 14, 7607.

153. Zante, G., Trébouet, D., Boltoeva, M. (2020). Solvent extraction of lithium from simulated shale gas produced water with a bifunctional ionic liquid, *J. Appl. Geochem*, 123. 104783.

154. Zarrouk, S. J., Woodhurst, B. C., Morris, C. (2014). Silica scaling in geothermal heat exchangers and its impact on pressure drop and performance: Wairakei binary plant, New Zealand. *Geothermics*, 51, 445-459.

155. Zhang, H., Wen, J., Fang, Y., Zhang, S., Zeng, G. (2019). Influence of fulvic acid on Pb(II) removal from water using a post-synthetically modified MIL-100(Fe). *J. Colloid. Interf. Sci*. 551, 155-163.

156. Zhang, Q., Lin, L., Ye, W. (2018). Techniques for extraction and isolation of natural products: a comprehensive review. *Chin. Med*. 13:20.

157. Zhang, Y. & Duan, X. (2020). Chemical precipitation of heavy metals from

wastewater by using the synthetical magnesium hydroxy carbonate. *Water Sci. Technol*. 81(6). 1130-1136.

158. Zheng, T., Wang, T., Ma, R., Liu, W., Cui, F., Sun, W. (2019). Influences of isolated fractions of natural organic matter on adsorption of Cu(II) by titanate nanotubes. *Sci. Total. Environ*. 650(1), 1412-1418.

159. Zhou, Z., Liu, H., Fan, J., Liu, X., Hu, Y., Wang, Y. (2019). Selective Extraction of Lithium Ion from Aqueous Solution with Sodium Phosphomolybdate As a Coextraction Agent. *ACS Sustain Chem Eng*. 7, 8885-8892.

160. Zuo, K., Yuan, L., Wei, J., Liang, P., Huang, X. (2013). Competitive migration behaviors of multiple ions and their impacts on ion-exchange resin packed microbial desalination cell, *Bioresour. Technol*, 146, 637-642.

Appendix

A.1 Introduction

An application of the lithium recovery process to EGS sites was applied using a geochemical modelling program after implementing the Li extraction experiment from Chap. 3. A certain amount of the geothermal fluid is generally lost in EGS operation during the circulation of the fluid, and less than 10% of the fluid loss would make the long-term operation of the system possible (Clark et al., 2013; Schill et al., 2017). Therefore, in some cases, the input of new fluid such as river or lake water near the site would be required to operate the system properly. PHREEQC, a geochemical modelling computer code developed by the United States Geological Survey (USGS) that has been used extensively to predict natural hydrochemical processes in subsurface systems (Parkhurst & Appelo, 1999), was used to estimate the proper EGS operation with lithium recovery simultaneously.

By using the new solution ion concentration data due to the solvent extraction, PHREEQC was applied to estimate the proper EGS operation with lithium recovery simultaneously. PHREEQC 'MIX' code was used in many researches to figure out the proper mixing ratio of several different water samples (Karmegam et al., 2011; Liu et al., 2017). In the PHREEQC 'MIX' code, the mixing fractions (approximately mixing volumes) of each solution in the mixture is defined and each solution was multiplied by its mixing fraction (Parkhurst & Appelo, 1999; Karmegam et al., 2011). The newly formed mixture (new solution and the original geothermal water) is underdone the geochemical reactions in a given environmental condition and the PHREEQC will calculate the new composition to deduct the final solution with molar concentrations for inorganic cations and anions

(Charlton & Parkhurst., 2011; Karmegam et al., 2011). The newly formed mixture solution was recalculated and considered with the safety conditions for reusing through the EGS.

A.2 Application of the lithium recovery process to EGS sites

For an application of the lithium recovery process to EGS sites, the volume change of the geothermal fluid should be verified. It is known that a certain amount of the geothermal fluid is lost during the EGSs operation (Schill et al., 2017; Clark et al., 2013). An EGS is viable when the fluid loss is lower than 10 % for the long term (Schill et al., 2017). EGS sites such as Rosemanowes and Hijiori have high fluid loss rates over 20 % but Soultz-sous-Forêts EGS showed a relatively low fluid loss rate (Clark et al., 2013). According to Clark et al. (2013), approximately 10,000 m^3 of the initial geothermal fluid volume of 500,000 m^3 (i.e., 2 %) was lost after a year of the circulation test in Soultz-sous-Forêts EGS (Genter et al., 2012). The fluid loss is expected to increase over time so the fluid losses must be made up by introducing additional fluid to maintain the EGS efficiency (Olasolo et al., 2016; Clark et al., 2013).

The lithium recovery process in this study involves the addition of dilution water to the geothermal fluid. If the favorable condition (50 times dilution) for lithium extraction (Fig. A1 and Table A1) is applied, the amount of aqueous solution after the solvent extractions would be about 50 times that of the initial lithium recovery solution. Therefore, if 200 m^3 (0.04%) of the total geothermal fluid in Soultz-sous-Forêts EGS is pulled out for diluting (50 times) the water volume to 10,000 m^3 (2%) of the system and used for the lithium recovery so

approximately 2% (actually 2.004%) of fluid was assumed to be lost during the EGS process and lithium recovery. However, after the extraction in this study, the geothermal fluid pH decreased to 2.1 as a result of the reaction described in Equation (2.1.2). An injection of the acid solution would decrease the pH of the circulating geothermal fluid whose pH level ranges between 5.2 and 5.5 (Scheiber et al., 2012). It is reported that pH 4 or less of a fluid in the geothermal systems can cause corrosion and corrosive cracking on various types of steel pipes (Gunnlaugsson et al., 2014; Yanagisawa et al., 2020; Kaya & Hoshan., 2005). During the reinjection stage of EGS, there are problems including corrosion in surface pipelines (Axelsson, 2012).

There are various methods to neutralize the pH of fluids. Among them, mixing different solutions with different pH is an effective and economic method to control the pH (Rai et al., 2013; Hem et al., 2018). Therefore, the change in composition due to simple mixing of several fluids was calculated by a geochemical modeling program PHREEQC. The composition of solution mixtures can be predicted using the 'MIX' code in PHREEQC (Charlton & Parkhurst., 2011; Karmegam et al., 2011; Liu et al., 2017). To supply the 2% loss and control the pH of reinjecting fluid, simple mixing of fresh water, original geothermal fluid, and geothermal fluid after solvent extraction, were observed by PHREEQC.

Three types of fluids (1 – aqueous solution after lithium recovery, 2 – surface water near the site, 3 – circulating geothermal fluid) were considered for the mixing. For fluid 2, river water near Soultz-sous-Forêts EGS was used (Pauwels et al., 1992). The composition of each fluid is shown in Table A1. It was assumed that the final mixture consists of 2 % of the solution mixture (mixture of fluid 1 and fluid 2) and 98 % of the geothermal fluid (fluid 3). With different mixing ratios of

fluid 1 and fluid 2, different pH levels of the final mixture solution were determined as shown in Fig. A1.

Table A1. Chemical composition of different fluids for mixing (unit : mg/L)

	pH	Ca^{2+}	Na^{+}	K^{+}	Mg^{2+}	Li^{+}	Ba^{2+}	Sr^{2+}	Fe (Total)	$SiO_{2(aq)}$	SO_4^{2-}	Br^{-}	Cl^{-}
Fluid 1	2.1	-	696.7	65.4	-	0.8	-	-	-	-	-	3.3	108.7
Fluid 2*	7.02	12.0	3.6	2.4	1.6	-	0.28	-	-	5.4	5.4	-	6.4
Fluid 3**	5.3	7588	21340	3540	155	150	9.6	479	28.5	197	188	239	58132

*Pauwels et al. (1992), **Sceiber et al. (2012)

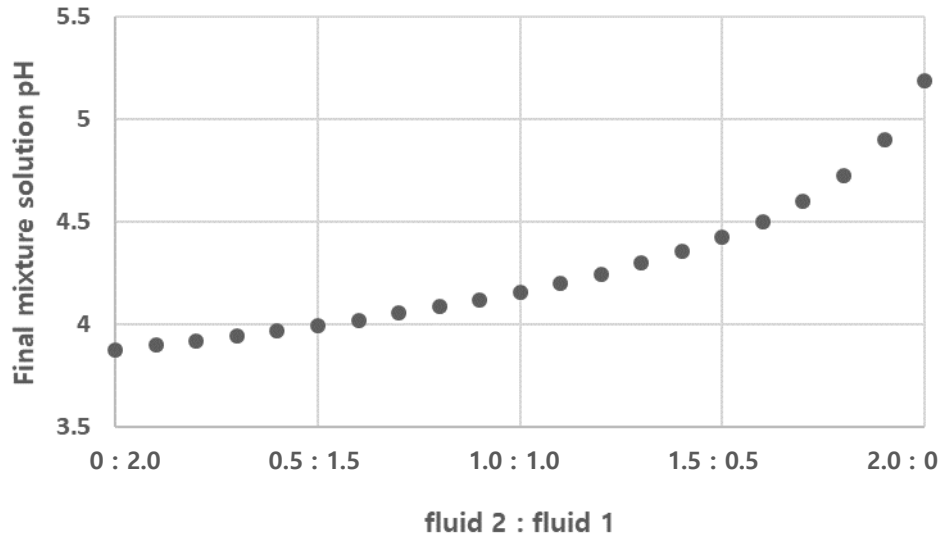

Fig. A1. Change in final mixture pH with different mixing ratios of fluid 2 and fluid 1.

When the solution after lithium extraction (fluid 1) is only mixed with geothermal fluid (fluid 3), the pH of the final mixture solution was calculated as 3.9. Considering that an acid solution of pH below 4 can cause corrosion in facilities of the EGS, surface water (fluid 2) was added to increase the pH of the injection solution. As the proportion of fluid 2 increases, the pH of the final mixture solution increased. When only the river water was used as a supplement for geothermal fluid loss, the final solution pH was calculated as 5.2 and it is within the range of the initial geothermal fluid pH.

To make the final solution pH above 4, the ratio of fluid 2 : fluid 1 should be at least 0.6 : 1.4. In PHREEQC, the geochemical reactions in the geothermal reservoir between the reservoir minerals and the pH 4.024 solution mixture of 98% geothermal fluid, 1.4 % solution after lithium extraction, and 0.6 % river water were predicted. According to André & Vuataz (2005), granite at the site consists mainly of quartz (24.2 %), K-Feldspar (23.6 %), plagioclases (42.5 %), micas (9.3 %), and small amounts of calcite (0.3 %). Using PHREEQC, molar amounts of mineral assemblages were equilibrated with the new mixed solution at the temperature of 200 ℃ and pressure of 450 atm and the solution pH slightly increased by 0.82 %. To reuse the solution of both fluid 1 and 3 to control the pH, mixing ratio of fluid 1: fluid 3 (0.6 : 1.4) shows a boundary line of pH 4.0. This represents that mixing fluid 1 higher than 0.6% and lower than 1.4% of fluid 3 from the supplying loss fluid (2%) from EGS, shows a new mixing solution with a new pH that can predict corrosion.

PHREEQC can be used extensively to predict natural hydrochemical processes in subsurface systems (Parkhurst & Appelo, 1999) like estimating the geochemical reactions precipitations or dissolutions of minerals during the

hydraulic stimulation process. In this dissertation, the PHREEQC was also used to compare the modelling results and measurements in terms of ionic concentrations of geothermal water to understand the effect of groundwater mixing in an operation of EGS.

Generally Soultz-sous-Forêts geothermal fluid has a high TDS value (approximately 100,000 mg/L) and the sum of several ions concentrations (Ca^{2+}, Mg^{2+}, Ba^{2+}, Sr^{2+}, and SiO_2) is 7,000-8,000 mg/L (Scheiber et al., 2012). The high TDS of the geothermal fluids can cause scale problems in the heat exchanger or geothermal pipes of the EGS (Zarrouk et al., 2014; Gunnarsson et al., 2010). The scale formation also induces a permeability decrease in the geothermal reservoir or inside the geothermal wells, which can result in a decline of the overall flow rate and thus lower the efficiency of the EGS process (Battistelli et al., 1995; Lee & Chung., 2021). Therefore, the treatment of such ions is necessary for a long-term operation of the EGS process (Caulk et al., 2016). The approach in this study includes two consecutive processes – precipitation and extraction. In the precipitation process, two chemical reagents ($Ca(OH)_2$ and Na_2CO_3) are used to remove more than 90 % of the total inorganic ions from the geothermal fluid. 0.62 g of $Ca(OH)_2$ were used to remove the Mg^{2+} and silicate ions and 18.6 g of Na_2CO_3 were used to remove Ca^{2+}, Ba^{2+}, and Sr^{2+} ions from 1 L geothermal fluid. The removal of Ca^{2+}, Mg^{2+}, Ba^{2+}, Sr^{2+}, and SiO_2 simultaneously helps the selective recovery of lithium and efficient operation of EGS.

The optimal condition of the dilution ratio or the TDS value of the aqueous solution after lithium recovery can be changed due to the pH isotherm experiment that was introduced in Fig. 3.5.3. By using the lower dilution ratio or high selectivity of Li, the amount of water that should be pulled out for diluting will be

less than calculated in this research. Also the usage of saponification of the extractant can also show a low pH change after solvent extraction thus the mixing ratio with river water might not be required much. Further study is needed to study the optimal condition of the lithium recovery from the geothermal water by operating the EGS simultaneously. By considering the TDS, dilution ratio, and pH changes, the simultaneous lithium recovery and EGS operation without fluid loss can be possible.

500,000 m^3 of water was injected to Soultz-sous-Forêts geothermal flowback and Li was measured approximately 150 mg/L for a long term circulation (Clark et al. 2013; Scheiber et al., 2012) and due to the solvent extraction experiment that was introduced in this dissertation, 200 m^3 (0.04%) is pulled out for diluting (50 times). Only a small amount (2%) is being mixed with the original geothermal water thus the ions including Li does not show a big change after solvent extraction process from the original geothermal water. Li that contains in a geothermal water did increase starting from 0 to 63 ppm for only 42 hours (Pauwels et al., 1992) however Li source is not infinite in the rock mass. This recovery method only shows a small amount of Li recovery thus considering the economic lifetime of EGS as 20–30 years (Tester et al., 2006), a further study is needed to consider the recovery efficiency of Li in an effective way.

A.3 PHREEQC

PHREEQC, a geochemical modelling computer code developed by the United States Geological Survey (USGS) that has been used extensively to predict natural hydrochemical processes in subsurface systems (Parkhurst & Appelo, 1999), was used to estimate the geochemical reactions precipitations or dissolutions of minerals during the hydraulic stimulation process. By comparison between modelling results and measurements in terms of ionic concentrations, the influence of formation water or bedrock groundwater mixing on the geochemical properties of flowback water can be investigated. Understanding the effect of groundwater mixing might be helpful in a successful operation of EGS.

In the EGS, a hydraulic stimulation generally is applied at the early stage of the construction to create a geothermal reservoir with high permeability. However, the stimulation also can be done during the operation of the facility (Stober & Bucher, 2013). It has been reported that the permeability of EGS geothermal reservoirs can be enhanced as hydraulic stimulation proceeds (Sanyal and Butler, 2005). Although relatively thorough studies have been conducted on the geochemical properties of the geothermal fluids used in conventional geothermal power plant systems (Bozau & Berk, 2013), no thorough studies have been conducted related to the geochemistry associated with the EGSs. For example, very few geochemical studies have been conducted during the hydraulic stimulation stage (Pauwels et al., 1992; Portier et al., 2009). During the stimulation, a large amount of the surface water is injected, and this water has significantly different physical and chemical characteristics from the groundwater due to the various types of geochemical reactions that can occur in the subsurface system (Pauwels et

al., 1992; Haluszczak et al., 2012). Such geochemical reactions are important because the efficiency of the geothermal system depends directly on the changes in permeability due to the geochemical reactions. For example, minerals can be precipitated or dissolved in the geothermal reservoir as a result of the interactions between the injected solution and the surrounding rocks under the conditions of high pressure and high temperature (Shu et al., 2019; Luo et al., 2018). PHREEQC 'MIX' code was used in many researches to figure out the proper mixing ratio of several different water samples (Karmegam et al., 2011; Liu et al., 2017). In the PHREEQC 'MIX' code, the mixing fractions (approximately mixing volumes) of each solution in the mixture is defined and each solution was multiplied by its mixing fraction (Parkhurst & Appelo, 1999; Karmegam et al., 2011). The newly formed mixture is underdone the geochemical reactions in a given environmental condition and the PHREEQC will calculate the new composition to deduct the final solution with molar concentrations for inorganic cations and anions (Charlton & Parkhurst., 2011; Karmegam et al., 2011). In this study, the ionic concentrations in the injected water and groundwater were introduced in the code with several mixing fractions in different scenarios and PHREEQC will calculate the geochemical composition of the mixture in the reservoir. PHREEQC requires input data, such as the hydrogeochemical properties or composition of the injection fluid and the mineral assemblages of the bedrock. It was reported that the injection fluid was obtained from a nearby irrigation reservoir of Pohang province, filtered to remove particles larger than 180 μm, and stored in a water tank. Water samples were collected from the water tank using 1 L polyethylene water-sample bottles. The properties of the water, including pH, temperature, and electrical conductivity (EC), were measured by a multi-meter (Orion Star A329, Thermo Fisher Scientific,

USA) at the site, and alkalinity was determined by a volumetric titration method. In addition, the characteristics of the groundwater near the Pohang province site at the depth 1,504 m were obtained from a reference (KIGAM, 2006). The subsurface of the study site (i.e., below 2.2 km) was composed of granodiorite basement rock (Kwon et al., 2017). The mineral compositions of the core samples from the granodiorite basement rock were analyzed by X-ray diffraction (XRD) analyzer, and it was reported that the granodiorite rock consisted mainly of albite (43.1%), quartz (28.6%), microcline (13.7%), muscovite (10.1%), and small amounts of calcite (2.3%) and chlorite (2.2%) (Kwon et al., 2017).

The hydrogeochemical compositions of the fluids were used as input data for the PHREEQC modelling, and the data included the ionic concentrations of Li^+, Na^+, K^+, Mg^{2+}, Ca^{2+}, Sr^{2+}, Ba^{2+}, $Fe_{(total)}$, Al^{3+}, F^-, Cl^-, Br^-, SO_4^{2-}, NO_3^-, $SiO_{2(aq)}$, CO_3^{2-}, and HCO_3^- and the mineral assemblages of the bedrock, i.e., calcite, quartz, albite, k-feldspar, k-mica, and chlorite.

Samples of the injection water were collected from the water tank and analysed. In addition, several samples of the flowback water were collected and analyzed during the release from the well to evaluate the result of the geochemical modelling (Fig. A2). Three flowback water samples (FB1, FB2, and FB3) were collected and their HRTs were 22.5, 41.75, and 86.7 hours, respectively. After the field measurement for pH, EC, and temperature, for every water sample, two sample bottles were filled, and the solution in one bottle was acidified with HCl and analyzed to determine the cation. The samples were stored at the constant temperature of 4 ℃ for chemical analysis. The collected water samples were analyzed for major inorganic cations and anions after filtering using 0.45 μm filter by inductive coupled plasma optical emission spectrometry (ICP-OES, Optima

8300, PerkinElmer, USA) and ion chromatography (IC, Dionex ICS-1100, Thermo Scientific, USA).

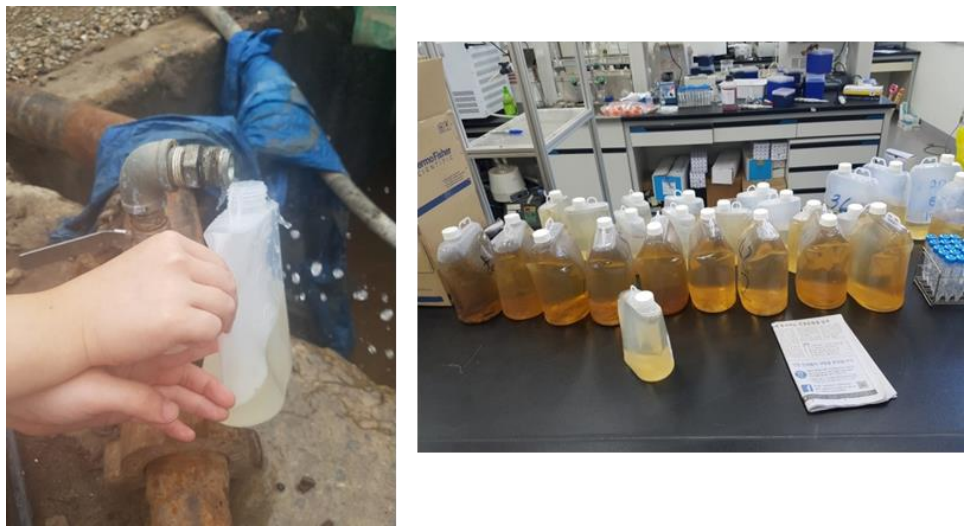

Fig. A2. Sampling injection and flowback water samples from geothermal system.

The chemical properties of the injection fluid and the groundwater near the site are summarized in Table A2. The injection water had a pH value of 7 (neutral), and major inorganic ions in the solution included Na^+, Ca^{2+}, K^+, Mg^{2+}, Cl^-, SO_4^{2-}, and HCO_3^-. The pH values of the groundwater were slightly higher than the pH of the injection water, and its electrical conductivity levels were four times higher than that of the injection fluid. Table A3 shows the physical and chemical properties of three flowback water samples. The pH levels were maintained between 6.9 and 7.3, but the electrical conductivity increased gradually as the HRT increased. As HRT increased, the concentrations of all of the major inorganic ions increased with the exception of magnesium, and the temperature of the flowback water during the measurement was kept constant at approximately 50 ℃.

Table A2. Physical and chemical properties of the injection fluid and groundwater (units: mg/L)

	Temp (℃)	EC (mS/cm)	pH	Na^+	Ca^{2+}	K^+	Mg^{2+}	Cl^-	$SiO_{2(aq)}$	$SO4^{2-}$	HCO_3^-
Injected fluid	29.5	1.10	7.1	62.2	107	9.2	35.3	163	29.0	363	68.4
Ground Water	48.1	4.61	7.7	976.0	13.7	13.0	5.6	763.0	27.1	401.0	871.5

Table A3. Physical and chemical properties of the flowback water (units: mg/L)

	Temp (°C)	EC (mS/cm)	pH	Na^{+}	Ca^{2+}	K^{+}	Mg^{2+}	Cl^{-}	$SiO_{2(aq)}$	$SO4^{2-}$	HCO_3^{-}
FB1	55.3	1.9	7.2	168.0	124.0	15.9	10.5	205.0	120.0	415.8	54.9
FB2	58.5	3.2	7.0	292.7	161.0	21.4	6.2	471.9	140.0	475.8	79.3
FB3	51.2	3.5	7.0	426.6	178.6	30.5	3.7	734.7	160.0	518.8	54.9

A.4 Modelling approach

In the geochemical model using PHREEQC, the processes of the injection and release of the fluids and the environmental or geological conditions of the site were obtained from the extant literature. Briefly, the Pohang province site had a temperature of 160 ℃ at the depth of about 4.3 km (Hofmann et al., 2019). A total of 1,756 m^3 of surface water was injected into a well for 8 days, and 1,771 m^3 of water were released from the well over a period of more than 30 days (Westaway et al., 2020; Hofmann et al., 2019). It was assumed that the water was injected into the bedrock at a depth of 4.3 km to create fractures and that the water also underwent geochemical reactions with surrounding rocks. Then, when the injection ended, the water flowed out of the well due to the pressure difference. The temperature of the geothermal reservoir varied from approximately 30 ℃ at the surface to 160 ℃ near the bedrock at the depth of 4.3 km. A gradual increase in the temperature was assumed during the injection, and the temperature of the flowback from the well was cooled to approximately 50 ℃. Fig. A3 shows the movement of the injected fluid in the modelling scenario. The hydraulic retention time (HRT) was calculated from the cumulative water volume graph in Hofmann et al. (2019).

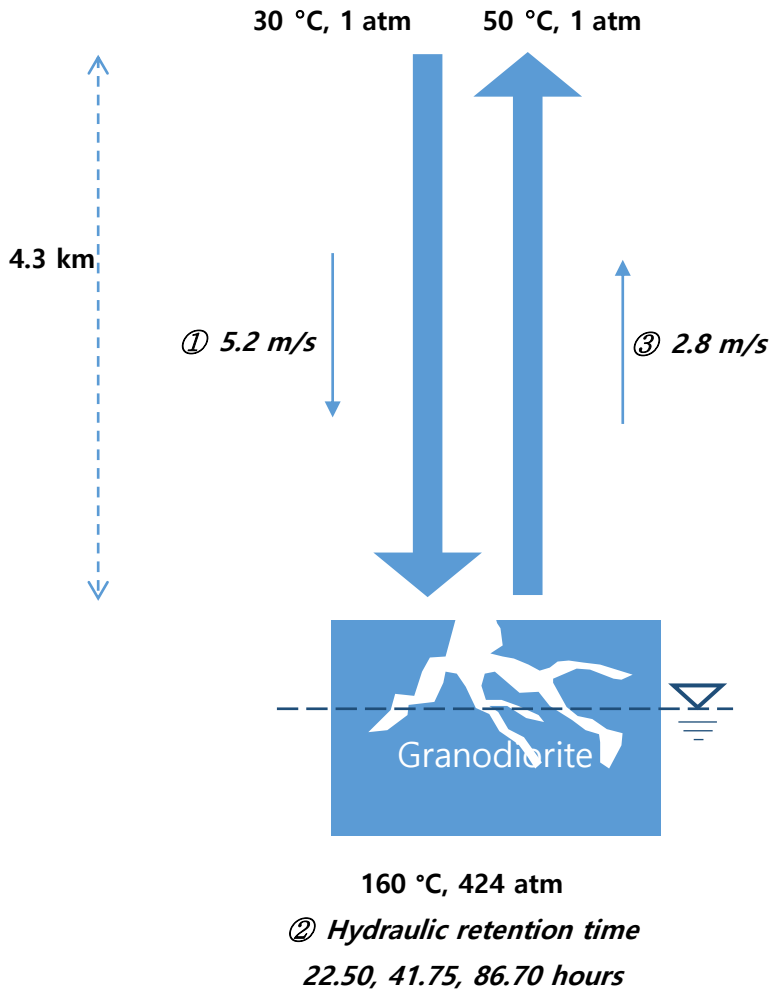

Fig. A3. Schematics of the movement of the injected fluid in the PHREEQC modelling scenario.

Since the injection water is expected to reach the bedrock, it was believed that the injected fluid was mixed with formation water or groundwater originally located inside the bedrock or nearby. Therefore, several mixing ratios between the injection water and the groundwater were tested. First, it was assumed that only the injected water stayed in the subsurface system and underwent geochemical reactions with the primary mineral assemblages of the bedrock (scenario I). Then, different mixing conditions were tested in different scenarios (i.e., 90% injection water and 10% groundwater in scenario II, 80% injection water and 20% groundwater in scenario III, 70% injection water and 30% groundwater in scenario IV, and 60% injection water and 40% groundwater in scenario V).

A.5 Groundwater mixing ratios

Fig. A4 shows the results of the geochemical modelling for FB1 which had an HRT of 22.5 hours. The error rate for chemical species *i*, Err_i, was calculated by comparing the results of the modelling output and the analytical measurements using equation (A.5.1):

$$Err_i = \frac{|C_{i,e} - C_{i,m}|}{C_{i,m}} \times 100\ \% \qquad \text{(A.5.1)}$$

$$Err_{ave} = \frac{\sum_i C_{i,m} Err_i}{\sum_i C_{i,m}} \qquad \text{(A.5.2)}$$

where $C_{i,e}$ and $C_{i,m}$ are the ionic concentrations of species *i* from the model estimation and the measurement, respectively. Also, the weighted average error rate for a scenario was calculated by Equation (A.5.2) and the calculated error rates are summarized in Table A4.

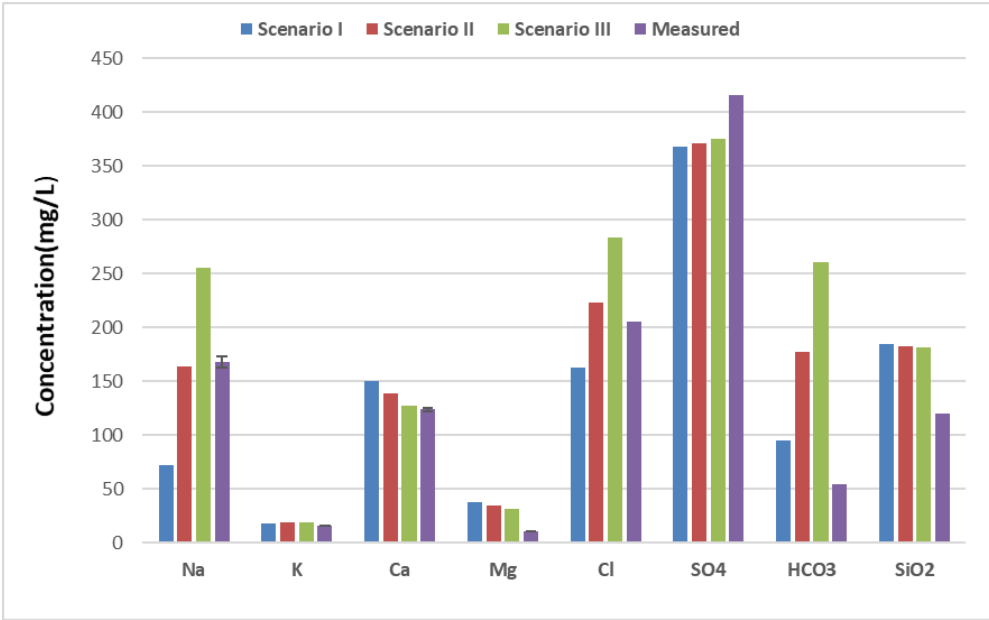

Fig. A4. FB1 major ionic concentrations through modelling and measurement.

Table A4. Error rates (%) for the FB1 modelling outputs

	E_{Na}	E_K	E_{Ca}	E_{Mg}	E_{Cl}	E_{SO4}	E_{HCO3}	E_{ave}
Scenario I (100%:0%)	57	16	21	261	21	12	73	28
Scenario II (90%:10%)	2	19	12	232	9	11	223	23
Scenario III (80%:20%)	52	21	2	204	38	10	374	44
Simple mixing (90%:10%)	9	40	22	207	9	12	143	22

Figure A4 and Table A4 shows that the estimated concentrations of some ions, such as Na and Cl in scenario II, were closer to the measurement than in other scenarios. However, for several ions, scenarios I and III provided the least error rates. Based on the average error rates, scenario II, which had the lowest error rate, provided the best estimation of FB1 among the three scenarios.

As the groundwater mixing rate increased from 0% to 20 %, some ionic concentrations increased, i.e., Na^+, K^+, Cl^-, SO_4^{2-}, and HCO_3^-, and other ionic concentrations decreased, i.e., Ca^{2+} and Mg^{2+}. These results were expected since the concentrations of Na^+, K^+, Cl^-, SO_4^{2-}, and HCO_3^- in groundwater were higher than they were in the injection water, and the concentrations of Ca^{2+} and Mg^{2+} were lower than they were in the injection water. When it was assumed that simple mixing occurred between the aqueous solution and the bedrock without any chemical reaction, the average error rate was 22%, which was slightly lower than it was for scenario II.

These results imply that a small portion of groundwater mixes with the injection fluid inside the bedrock and that the geochemical reactions between the fluid and the bedrock might be negligible for FB1.

Figure A5 and Table A5 show the results for FB2, which had an HRT value that was about twice that of FB1. Scenario III, in which the injection fluid and groundwater mixing ratio was 80% : 20%, had the lowest error rate on average. Also, when HRT was about four times that for FB1, the most appropriate mixing ratio of injection water and groundwater was 70% : 30%, as shown in Figure A6 and Table A6. This indicated that more groundwater was mixed with the injection fluid because the injection fluid stayed inside the bedrock longer.

In addition, when simple mixing is assumed, the average error rates (40% and 52% for FB2 and FB3, respectively) were greater than those in the scenarios with the same mixing rates. This implies that the likelihood of the geochemical reaction occuring is higher when the retention time of the fluid inside the bedrock is longer.

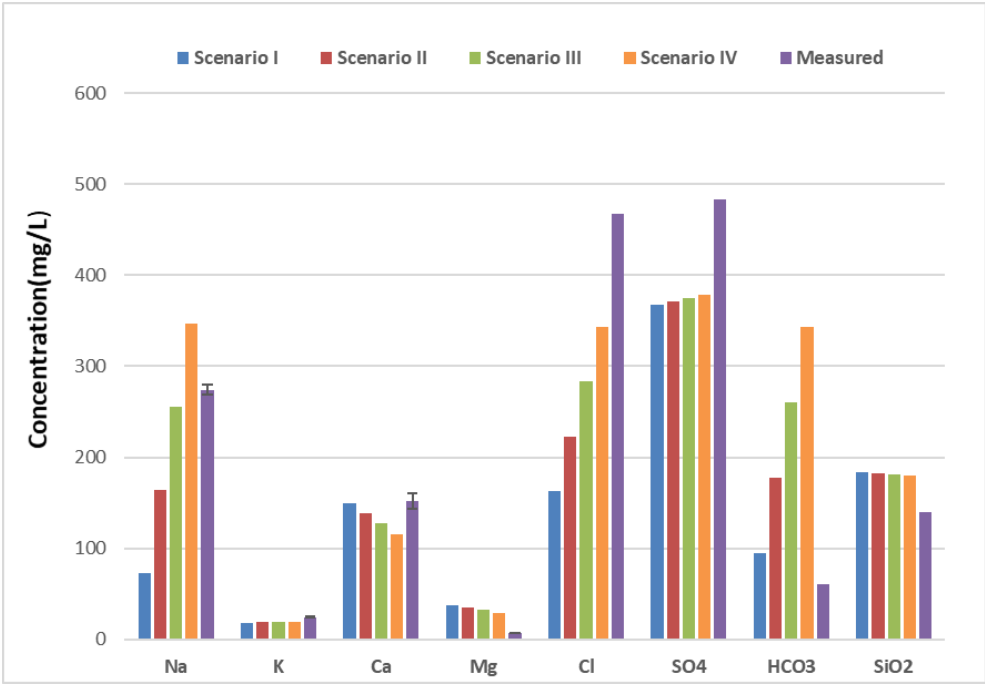

Fig. A5. FB2 major ionic concentrations through modelling and measurement.

Table A5. Error rates (%) for FB2 modelling outputs

	E_{Na}	E_{K}	E_{Ca}	E_{Mg}	E_{Cl}	E_{SO4}	E_{HCO3}	E_{ave}
Scenario I (100%:0%)	74	24	1	475	65	24	55	47
Scenario II (90%:10%)	40	22	9	430	52	23	191	43
Scenario III (80%:20%)	7	21	16	385	39	22	327	38
Scenario IV (70%:30%)	27	19	24	340	26	22	462	44
Simple mixing (80%:20%)	11	59	42	344	39	23	253	40

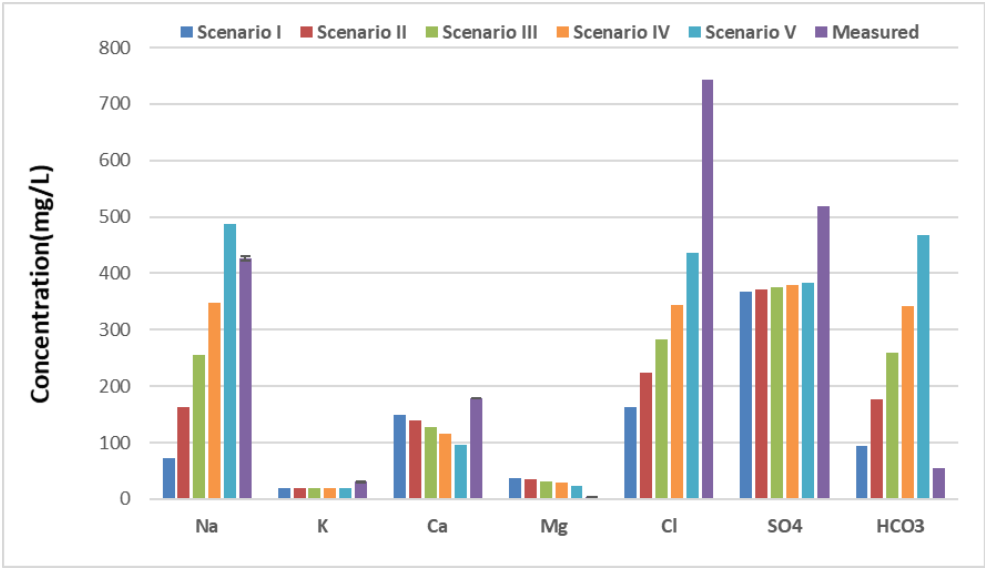

Fig. A6. FB3 major ionic concentrations through modelling and measurement.

Table A6. Error rates (%) for FB3 modelling outputs

	E_{Na}	E_{K}	E_{Ca}	E_{Mg}	E_{Cl}	E_{SO4}	E_{HCO3}	E_{ave}
Scenario I (100%:0%)	83	39	16	918	78	29	73	61
Scenario II (90%:10%)	62	38	22	838	70	28	223	58
Scenario III (80%:20%)	40	37	29	758	62	28	374	55
Scenario IV (70%:30%)	19	36	35	679	54	27	525	51
Scenario V (60%:40%)	14	36	46	549	41	26	752	53
Simple mixing (70%:30%)	21	66	56	606	54	28	442	52

Average error rates for FB1, FB2, and FB3 for the scenarios that had the lowest values (scenarios II, III, and IV, respectively) were 23%, 38%, and 51%. The fact that the error rates increased as the hydraulic retention time increased might be explained in several ways. One way is that several geochemical reactions could have occurred that were not accounted for in the PHREEQC model. Among the error rates of various chemical species, E_{Mg} and E_{HCO3} had significantly higher values. In the model, a limited number of geochemical reactions were considered because only major minerals and major ions were used to represent the bedrock and the aqueous solution. The reactions in which ions such as Mg^{2+} or HCO_3^- were involved could be neglected in the model, thereby causing discrepancies between the results of the model and the field measurements.

One of the other possibilities could be that inappropriate data were used in the model. For example, the chemical compositions and ionic concentrations in groundwater were obtained from a reference, not from the measurements of field samples. The depth of the groundwater in the reference used for this study was 1,504 m, but it was assumed in the model that the injection fluid was mixed with groundwater at a depth of 4,300 m. Table A7 shows the chemical data of groundwater in the Pohang province that is reported is several reports and journal article (KIGAM, 2006; Lee et al., 2011; Kihm & Kim., 2011). They showed significant different pH or EC values and ionic concentrations possibly due to the different locations, depths, and sampling seasons. Some of them were chosen to be used in the model in this study and the results (Table A8-A10) showed that the groundwater at the depth of 1,504 m (deepest among others) showed the lowest average error rate for each scenario. In addition, the results indicate that the modelling results is significantly influenced by the groundwater properties.

Table A7. Physical and chemical properties of several groundwater in Pohang province (units: mg/L)

Sample No.	Approximate distance from EGS site (km)	Depth (m)	Temp (℃)	EC (mS/cm)	pH	Na^+	Ca^{2+}	K^+	Mg^{2+}	Cl^-	$SiO_{2(aq)}$	$SO4^{2-}$	HCO_3^-
D-2 (200 m^3/d) [1)*]	2.23	1504	48.1	4.61	7.7	976.0	13.7	13.0	5.6	763.0	27.1	401.0	871.5
PDHS-09 [2)]	4.7	700	44.0	1.98	8.4	536.0	3.6	3.6	1.7	122	20.1	17.5	991.6
D-4 [1)]	2.23	303	28.5	1.67	8.5	353.0	3.5	3.0	0.1	276.0	14.8	0.7	448.3
I-12 [1)]	2.23	170	14.6	0.57	6.8	50.1	30.4	2.9	9.6	29.4	26.3	128.0	145.8

1) KIGAM. (2006) 2) Lee et al. (2011)

Table A8. Error rates (%) for the FB1 modelling outputs, Scenario II (90%:10%)

Sample No.	Depth (m)	E_{Na}	E_K	E_{Ca}	E_{Mg}	E_{Cl}	E_{SO4}	E_{HCO3}	E_{ave}
D-2 (200 m^3/d) 1)*	1504	2	19	12	232	9	11	223	23
PDHS-09 2)	700	29	13	11	229	23	20	236	37
D-4 1)	303	40	12	11	227	15	20	141	33
I-12 1)	170	58	12	13	236	27	17	98	35

1) KIGAM. (2006) 2) Lee et al. (2011)

Table A9. Error rates (%) for the FB2 modelling outputs, Scenario III (80%:20%)

Sample No.	Depth (m)	E_{Na}	E_K	E_{Ca}	E_{Mg}	E_{Cl}	E_{SO4}	E_{HCO3}	E_{ave}
D-2 (200 m^3/d) 1)*	1504	7	21	16	385	39	22	327	38
PDHS-09 2)	700	43	19	22	407	67	37	245	56
D-4 1)	303	55	19	22	401	61	38	114	51
I-12 1)	170	76	20	19	432	71	33	54	53

1) KIGAM. (2006) 2) Lee et al. (2011)

Table A10. Error rates (%) for the FB3 modelling outputs, Scenario IV (70%:30%)

Sample No.	Depth (m)	E_{Na}	E_K	E_{Ca}	E_{Mg}	E_{Cl}	E_{SO4}	E_{HCO3}	E_{ave}
D-2 (200 m^3/d) 1)*	1504	19	36	35	679	54	27	525	51
PDHS-09 2)	700	50	45	37	647	80	49	561	71
D-4 1)	303	63	45	37	634	74	50	278	64
I-12 1)	170	84	46	32	711	83	43	148	67

1) KIGAM. (2006) 2) Lee et al. (2011)

The piper diagram was drawn to show the hydrogeochemical types of formation water (or bedrock groundwater), injection water and flowback water using the ionic concentrations converted into the milligram equivalent percentage (meq/L%) unit. The modelling results showing the least average error rates were also plotted on a Piper trilinear diagram as shown in Figure A7. Many previous researches have used the piper diagram to identify the type of different water samples or to observe the property changes of water (Chon et al., 1999; Karmegam et al, 2011; Kim et al, 2020; Ismail et al, 2020).

The injected water in this study can be classified as the Ca-Cl water type, meanwhile the groundwater and three flowback water samples are classified as the Na-Cl water type. From FB1 to FB3, the hydraulic retention time increases and the cationic milligram equivalent percentage shows an increase for Na^{+}+K^{+} (15.5%) and decrease for Ca^{2+} (10.7%) and Mg^{2+} (4.8%). The anionic percentage of milligram equivalent shows an increase of Cl^{-} (26.3%) and decrease of SO_4^{2-} (22.6%), HCO_3^{-} (3.7%).

The result implies that a certain changes in chemical properties of flowback water occurred due to some chemical reactions.

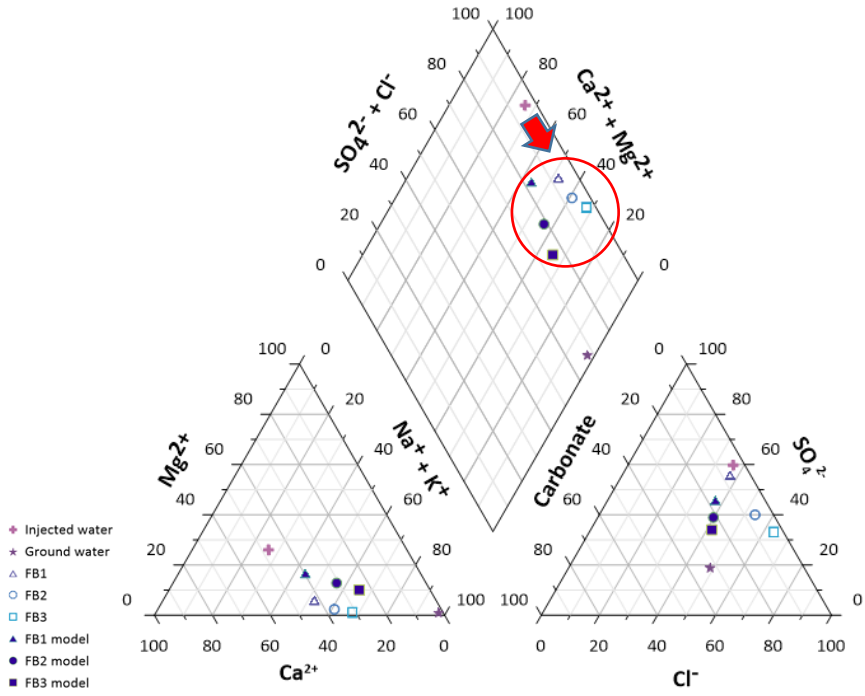

Fig. A7. Piper diagram for water samples.

FB1 modelling result shows a higher meq/L% of Mg^{2+} (10.7%) and HCO_3^- (10.1%) and a lower meq/L% of $SO4^{2-}$ (10.1%), Na^+ (8.5%), and Ca^{2+} (2.2%) compared to the measured data of FB1. In the modelling data of FB2 and FB3, the Mg^{2+} and HCO_3^- percentages were higher and Cl^-, Ca^{2+}, and Na^+ were lower than the measured data. The difference between modelling and measurement in HCO_3^- and Cl^- ions percentage increases predominantly (>20%) when the retention time is long as in case of FB3. This indicates that carbonate minerals and Mg bearing minerals might be precipitated more than predicted by a model.

According to Bam et al. (2020), a bivariate plot of $(Ca^{2+}+Mg^{2+})/(Na^++K^+)$ ratios versus the total cations can show the chemical transformations of a mixture solution such as cation exchange reaction. Vertical distances between FBs and FB models in Figure A8 implies that additional cation exchange reactions between divalent $(Ca^{2+}+Mg^{2+})$ and monovalent (Na^++K^+) cations occurred in the flowback solutions than expected by the modelling results. From FB1 to FB3, the difference between the measured data and modelling results decreases as the retention time increases.

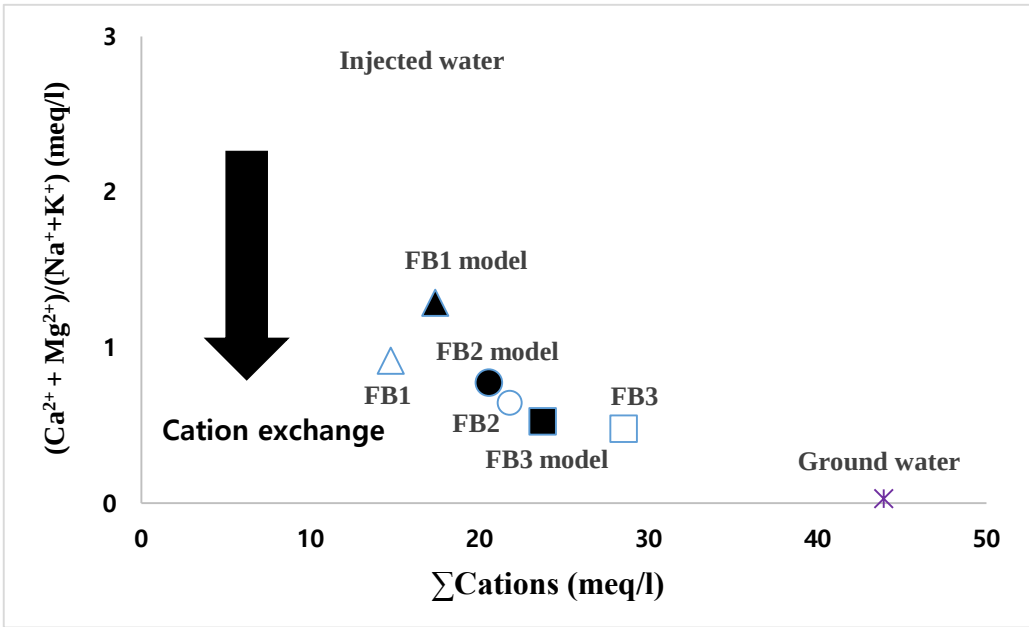

Fig. A8. Bivariate plot of $(Ca^{2+} + Mg^{2+})/(Na^{+}+K^{+})$ vs ∑Cations.

A.6 Prediction of precipitation

Precipitation or the formation of scale inside the fractures in the bedrock might prevent the successful creation of a geothermal reservoir. The saturation index (SI) in Equation (A.6.1) is a factor that is used to predict the precipitation of minerals (Parkhurst and Appelo, 1999; Park et al., 2013).

$$SI = \log\left(\frac{IAP}{K_{sp}}\right) \qquad \text{(A.6.1)}$$

Ion activity product (IAP) can be measured by the activities of the dissolved components, and the constant reaction at equilibrium (K_{sp}) can be referred by a thermodynamic data (Park et al., 2013). PHREEQC was used to calculate K_{sp} and IAP in this study. If the SI value is greater than 0 (i.e., IAP > Ksp), it means that the aqueous solution inside the bedrock is oversaturated, so the minerals can be precipitated. In contrast, if the SI value is less than 0 (i.e., IAP < Ksp), the dissolution of minerals can occur.

Using the data of flowback water samples in their own appropriate scenarios, the SI values of various minerals were obtained in the downhole condition of 160 ℃ and 424 atm. As shown in Table A12, for carbonate minerals, the SI values were slightly higher than 0 showing a slightly oversaturation and the values increases as the hydraulic retention time increases. Minerals including Mg among various silicates showed great SI values, which means the mixture is oversaturated in terms of those minerals. Especially chlorite, talc, and chrysotile showed significantly high SI values (greater than 7) and it indicates that the minerals could be precipitated inside the reservoir fractures. From FB1 to FB3, the SI values for

those minerals decreases. Silicate minerals that does not include Mg such as chalcedony, quartz, and K-feldspar showed an negative value of SI (0 > SI), except K-mica..

Considering the results in Figure A8, the carbonate minerals and Mg^{2+} bearing minerals are actually being more precipitated than being predicted by a model. By the condition of high temperature and pressure in the geothermal reservoir, many minerals can be dissolved or predicted and, in this study, it was found that carbonate minerals and minerals including Fe (goethite and hematite) and Mg (chlorite, talc, and chrysotile) were oversaturated and easy to be precipitated.

Table A11. Saturation indices of minerals

Mineral	Formula	FB1 (160 ℃, 424 atm)	FB2 (160 ℃, 424 atm)	FB3 (160 ℃, 424 atm)
Carbonate minerals	Aragonite($CaCO_3$),	1.27	1.40	1.46
	Calcite ($CaCO_3$),	1.33	1.46	1.52
	Dolomite ($Ca,Mg(CO_3)_2$)	0.62	0.91	1.05
Silicate minerals	Chalcedony (SiO_2)	-0.19	-0.19	-0.20
	Quartz (SiO_2)	-0.05	-0.05	-0.06
	K-feldspar ($KAlSi_3O_8$)	-1.37	-1.39	-1.40
	K-mica ($KAl_3Si_3O_{10}(OH)_2$)	5.41	5.35	5.31
	Chlorite(14A) ($Mg_5Al_2Si_3O_{10}(OH)_8$)	20.56	20.37	20.09
	Talc ($Mg_3Si_4O_{10}(OH)_2$)	12.50	12.40	12.24
	Chrysotile ($Mg_3Si_2O_5(OH)_4$)	7.71	7.62	7.47
	Sepiolite ($Mg_2Si_3O_{7.5}OH \cdot 3H_2O$)	1.11	1.04	0.93
Minerals including Fe	Hematite (Fe_2O_3)	14.68	14.56	14.43
	Goethite (α-$Fe^{3+}OOH$)	6.15	6.09	6.02
	$Fe(OH)_3(a)$	-2.80	-2.86	-2.92

A.7 Summary

The PHREEQC program was used to conduct the geochemical modelling of hydraulic stimulation for the creation of a geothermal reservoir in an EGS. When the modelling outputs were compared to analytical measurements, it was found that the effect of groundwater were negligible when the hydraulic retention was less than one day. However, as the injection fluid remained in the bedrock for a longer period of time, it became mixed with more groundwater. Also, considering the geochemical reactions between the injection fluid and the bedrock minerals helped to decrease the error of the model's output. Among the various inorganic ions, the magnesium and bicarbonate ions showed significantly high error rates. These error rates possibly could have been due to 1) the relatively small concentrations of those ions compared to the other ions, 2) geochemical reactions that occurred but were not in the model, or 3) inappropriate representation of the concentrations of the ions in the groundwater. In addition, it was found that the precipitation of minerals that contain Ca, Fe, and Mg should be considered when the retention time of the fluid in the bedrock is long enough. The results of this study imply that the characteristics of the groundwater near EGS sites can be important for the formation of reservoirs at these sites.

국문 초록

셰일가스 생산수 및 지열 환류수는 저류층내 지화학 반응을 통하여 주입수와는 다른 화학적 성질이 나타나며 많은 양의 TDS가 존재한다. 특히 마르셀스(Marcellus) 셰일가스 생산수 및 슐츠-수-포레(Soultz-sous-Forêts) 지열 환류수는 많은 양의 리튬이온이 존재하며 선택적으로 리튬이온을 회수하기 위하여 많은 연구가 진행 중이다.

생산수/환류수 내 리튬외에 불순물로 분류되는 유기물질 및 실리케이트 이온이 많이 들어있으며 이러한 물질들이 리튬 회수의 선택성을 낮출 가능성이 존재한다. 본 연구는 용매추출 방법을 사용하여 리튬이온을 추출하고자 하였으며 유기물질 및 실리케이트 이온들이 리튬 회수를 어떻게 방해하는지 관찰하고자 하였다. 생산수내 다른 유기물질의 종류 및 농도의 주입에 따라 리튬 회수율을 비교하였으며 지열 환류수는 실리케이트 농도에 따라 리튬 회수율을 비교하였다.

더 나아가 높은 리튬 순도를 얻기 위하여 활성탄(AC)을 이용한 흡착 및 침전제($Ca(OH)_2$ 및 Na_2CO_3)를 이용한 침전을 통하여 선택적으로 생산수/환류수 내 존재하는 유기물질, 실리케이트 이온 및 다가양이온을 제거하여 리튬의 추출률을 증가시키고자 하였다. 리튬을 선택적으로 회수할 수 있는 용매를 Cyphos IL 101 와 D2EHPA를 반응시켜 Ionic liquid를 합성하여 추출제로 사용하였으며, 25배로 희석된 생산수에 [Cyphos IL 101][D2EHPA](1M)를 추출제로 적용했을 경우 리튬 추출률이 최대 85.9 % 나타나는 것으로 밝혀졌다.

핵심어: 리튬 회수, 리튬 흡착, 전기화학, 전기화학적 리튬 회수, 배터리 재활용

학번: 2017-21273